XLPR MODELS SUBGROUP REPORT

CRACK OPENING DISPLACEMENT

PROBABILISTIC FRACTURE MECHANICS CODE

DISCLAIMER

THIS PUBLICATION WAS PREPARED AS AN ACCOUNT OF WORK JOINTLY SPONSORED BY THE ELECTRIC POWER RESEARCH INSTITUTE (EPRI) AND AN AGENCY OF THE U.S. GOVERNMENT. NEITHER EPRI NOR THE U.S. GOVERNMENT NOR ANY AGENCY THEREOF, NOR ANY EMPLOYEE OF ANY OF THE FOREGOING, MAKES ANY WARRANTY, EXPRESSED OR IMPLIED, OR ASSUMES ANY LEGAL LIABILITY OR RESPONSIBILITY FOR ANY THIRD PARTY'S USE, OR THE RESULTS OF SUCH USE, OF ANY INFORMATION, APPARATUS, PRODUCT, OR PROCESS DISCLOSED IN THIS PUBLICATION, OR REPRESENTS THAT ITS USE BY SUCH THIRD PARTY COMPLIES WITH APPLICABLE LAW.

THIS PUBLICATION DOES NOT CONTAIN OR IMPLY LEGALLY BINDING REQUIREMENTS. NOR DOES THIS PUBLICATION ESTABLISH OR MODIFY ANY REGULATORY GUIDANCE OR POSITIONS OF THE U.S. NUCLEAR REGULATORY COMMISSION AND IS NOT BINDING ON THE COMMISSION.

xLPR Models Subgroup Report

Crack Opening Displacement

xLPR-MSGR-COD Version 1.0	
Author Signature	**Date**
Rick Olson Rick Olson, Battelle Crack Opening Displacement Subgroup	03/29/16
Reviewer Signatures	**Date**
Michael Benson Michael Benson, Nuclear Regulatory Commission Member, Crack Opening Displacement Subgroup	03/28/16
Approver Signatures	**Date**
Marjorie Erickson Marjorie Erickson, PEAI xLPR Models Group Lead	04/01/16
Craig D. Harrington Craig D. Harrington, Electric Power Research Institute xLPR Code Development Lead	04/20/16

THE TECHNICAL CONTENTS OF THIS DOCUMENT WERE NOT PREPARED IN ACCORDANCE WITH THE XLPR SOFTWARE QUALITY ASSURANCE PLAN.

Revision History

Version Number	Description of Changes	Issue Date
1.0	Initial Issue	4/20/2016
	The U.S. Nuclear Regulatory Commission Office of Nuclear Regulatory Research's and the Electric Power Research Institute's xLPR Project Contacts approved an administrative update in 2021 to support public release of this document without incrementing the version number or issue date. The administrative updates included: (a) title changed from "Summary of the xLPR Version 2.0 Crack Opening Displacement (COD) Modules" to "xLPR Models Subgroup Report—Crack Opening Displacement" throughout the document, (b) cover and title pages updated accordingly, (c) disclaimer statement added, (d) notice regarding official document version records storage location during code development removed as it is no longer needed, and (e) statement that the document was not prepared in accordance with the xLPR Software Quality Assurance Plan added.	

EXECUTIVE SUMMARY

New modules for estimating the crack-opening displacements (COD) for both circumferentially (CrCOD) and axially (AxCOD) oriented through-wall cracks (TWC) have been developed as part of xLPR Version 2.0. Both the CrCOD and AxCOD models are based on the previously developed GE/EPRI method for predicting crack-opening displacements for through-wall cracked pipe, where elastic and plastic influence functions are fitted to finite element results that are functions of geometry and material properties. The total COD is the sum of the elastic and plastic contributions to COD. The CrCOD model includes the contributions to COD from tension, bending, and crack face pressure loading conditions. The AxCOD model includes the contributions to COD from internal pipe pressure and weld residual stresses. The weld residual stress contribution is handled in a somewhat simplistic manner through the inclusion of an effective pressure term to account for the weld residual stresses. The design space for the CrCOD model has been increased with respect to the original GE/EPRI solutions through the inclusion of elastic and plastic influence functions for a wider range of pipe mean radius-to-thickness ratios (R_m/t) and normalized crack sizes (θ/π).

Both COD modules assume a planar crack. Because planar cracks are assumed, the crack are an idealized representation. Actual PWSCC cracks are not planar and do not have a simple leak path for through-wall cracks. Thus, for a given leak rate, a PWSCC crack system would be more diffuse than a planar crack system. PWSCC cracks are characterized by a distributed, connected network of cracks in 3D rather than a single, idealized 2D planar crack. A model for COD of diffuse and connected (i.e. flow through porous media) set of cracks is very different from the ideal crack case used in xLPR 2.0. The effect of this assumption is to over predict crack opening displacement and the subsequently calculated leak rate. In addition, two other phenomena contribute to uncertainty in COD calculations and can be considered major contributors to xLPR uncertainty. These are the effects of Weld Residual Stress, which is unaccounted for in COD calculations and the Restraint of Pressure Induced Bending which is also unaccounted for in both COD and leak-rate calculations. Weld residual stress may open or close the crack more than is calculated by CrCOD. Unaccounted for Restraint of Pressure Induced Bending leads to over-predictions in CrCOD and subsequent leak rates.

The verification of the CrCOD and AxCOD models is documented in detail in the Software Test Results Reports (STRR) for the CrCOD and AxCOD models, respectively. The testing activities described in the STRRs are intended to verify that the requirements specified in the CrCOD and AxCOD Software Requirements Documents (SRD) are met. Within the planar crack assumptions of the COD models, the stated requirements specific to the models have been met. In addition to the model-specific requirements, the SRDs also levy requirements on the xLPR Framework regarding input/output requirements and error handling that are addressed in the Framework STP.

Validation of the CrCOD models was accomplished by comparing the predicted CODs from the CrCOD model with available experimental data from full-scale pipe experiments. In total, 36 individual through-wall cracked pipe experiments were used to validate CrCOD. These through-wall cracked pipe experiments evaluated a range of pipe sizes (4 to 42-inch nominal diameter), materials (stainless and carbon steels and their associated welds), and loading conditions (quasi-static monotonic four-point bending, combined pressure and bending, cyclic bending, dynamic bending, and combined pressure and dynamic/cyclic bending). Predicted COD values from the CrCOD model were compared with COD values obtained from the experimental data files at both crack initiation and maximum moment. On average, the CrCOD model over-predicted the experimental COD values by about 23 percent at crack initiation, i.e., the ratio of the predicted to experimental COD values was 1.23 (average) with a standard deviation of 0.75. For the maximum

moment cases, the ratio of the predicted to experimental COD values was 1.41 (average) with a standard deviation of 0.80. Part of this uncertainty can be attributed to analyzing dynamic, cyclic experiments with quasi-static, monotonic stress-strain data. If the dynamic, cyclic experiments are eliminated from the validation matrix or dynamic and/or cyclic stress-strain data are used to analyze these dynamic and/or cyclically loaded pipe experiments, the agreement between predictions and experimental data improves, somewhat.

Validation of the AxCOD models was accomplished by comparing the analytically predicted COD values from the AxCOD model with finite element results and engineering judgment, because there simply are no axial crack COD experimental data available. This validation exercise demonstrated that as long as the internal pipe pressure was less than 60 percent of the pressure at the limit load, then the AxCOD-predicted COD values agreed very well with the finite element results. Accordingly, the axial crack COD module includes a warning check to ensure that pressure is indeed less than 60 percent of the limit pressure. If not, then a warning message is issued for user interpretation and the calculations are continued with the pressure equal to 60 percent of the limit pressure. In addition, it was shown that the elastic (V_1) and plastic (h_2) influence functions determined as part of the AxCOD development process compare reasonably well with the values reported previously in the literature. Finally, it has to be noted that both CrCOD and AxCOD are rooted in identical methodologies. Accordingly, it might be expected that AxCOD would perform about the same as CrCOD, if data were available to make comparisons with experiments. The validation of the CrCOD and AxCOD models is documented in detail in the Module Validation Reports (MVR) for the CrCOD and AxCOD models, respectively.

TABLE OF CONTENTS

TABLE OF FIGURES

TABLE OF TABLES

NOMENCLATURE/LIST OF SYMBOLS

Symbols

a	Half the circumferential crack length
A	Cross sectional area of pipe
c	Half the axial crack length
c_e	Half the effective axial crack length to correct for small scale yielding assumption
E	Elastic modulus
f_1	Fitting term which is a function of the normalized crack length (θ-π)
f_2	Fitting term for tension which is a function of the strain hardening exponent (n)
f_3	Fitting term for bending which is a function of the strain hardening exponent (n)
f_4	Fitting term to empirically correct solution to best match experimental data
h_2	Plastic influence functions
I	Moment of inertia
J	Elastic plastic fracture toughness
K	Stress intensity factor
K_{in}	Stress intensity factor on the ID of the pipe
K_{out}	Stress intensity factor on the OD of the pipe
M	Bending moment
M_{app}	Applied bending moment
M_{eff}	Total effective bending moment
M_{eq}	Equivalent bending moment for plastic component of COD
M_0	Collapse moment
n	Strain hardening exponent
p	Pipe pressure
p_{CF}	Crack face pressure
p_{eff}	Effective pressure
p_L	Limit pressure
P	Axial load
P_A	Axial load due to far field force
P_{CFP}	Axial load due to crack face pressure
P_{ip}	Axial load due to internal pipe pressure
P_0	Collapse load
P_o'	Effective collapse load accounting for crack face pressure
R	Stress ratio (minimum stress/maximum stress for cyclic loading)
R	Pipe radius
R_i	Inside pipe radius
R_m	Mean pipe radius

R_o	Outside pipe radius
r_y	Plastic zone size
t	Pipe wall thickness
V_1	Elastic influence functions
x	Load category: (T) tension; (B) bending; (CFP) crack face pressure
α	Coefficient in Ramberg-Osgood relationship
β	Fitting term based on the strain hardening exponent (n)
δ	Crack opening displacement
δ^{el}	Elastic contribution to the crack opening displacement
δ^{pl}	Plastic contribution to the crack opening displacement
δ^{total}	Total crack opening displacement (sum of elastic and plastic contributions)
ε	Strain
ε_0	Reference strain
γ	Ratio of crack face pressure to internal pipe pressure (hard coded to 0.5 in code)
λ	Load ratio (ratio of load due to crack face pressure to load due to external loads and internal pipe pressure)
ρ	Normalized crack length for axial crack solutions
σ	Stress
σ_{eff}	Effective ultimate tensile strength
σ_{eff}^{∞}	Effective remote stress for axial crack solution to account for weld residual stresses
σ_f	Flow stress
σ_u	Ultimate strength
σ_y	Yield strength
σ_{WRS}	Weld residual stress
$\sigma_{WRS,avg}$	Average through thickness weld residual stress
σ_0	Reference stress
σ^{∞}	Remote stress
θ	Half the total crack angle
v	Poisson's ratio

ACRONYMS AND INITIALISMS

ASTM	American Society for Testing and Materials
COD	Crack Opening Displacement
CS	Carbon Steel
DLL	Dynamic Link Library
DMW	Dissimilar Metal Weld
FE	Finite Element
FEA	Finite Element Analysis
EPRI	Electric Power Research Institute
GE	General Electric
ID	Inside Diameter
IEEE	Institute of Electrical and Electronics Engineers
IPIRG	International Piping Integrity Research Group
LVDT	Linear Variable Differential Transformer
MVR	Module Validation Report
NRC	Nuclear Regulatory Commission
OD	Outside Diameter
PFM	Probabilistic Fracture Mechanics
RTM	Requirements Traceability Matrix
SDD	Software Design Description
SI	Système International d'Unités
SRD	Software Requirements Document
SS	Stainless Steel
STP	Software Test Plan
STRR	Software Test Results Report
TWC	Through-Wall Crack
V&V	Verification and Validation
WRS	Weld Residual Stress
xLPR	eXtremely Low Probability of Rupture

1. INTRODUCTION

The Crack-Opening Displacement (COD) Subgroup within the xLPR Models Group was charged with developing COD models for both axially and circumferentially oriented through-wall cracks (TWCs). The resultant COD values from the COD models would, in turn, be used, along with the TWC length, as part of the leak-rate analyses within the xLPR probabilistic fracture mechanics (PFM) code to establish whether or not a leaking TWC would be detected by the plant's leakage detection system. The scope of work for the COD Subgroup included the development of predictive models for COD for both circumferentially (Circumferential Through-Wall Crack Combined Tension and Bending Crack Opening Displacement Module - CrCOD) and axially (Axial Crack Opening Displacement Module - AxCOD) oriented TWCs.

The key requirements for both models are described in their respective Software Requirements Documents (SRD) [1, 2]. Table 1 lists the requirements specified in the SRD for circumferentially oriented TWCs, while Table 2 lists the requirements specified in the SRD for axially oriented TWCs.

Table 1. SRD requirements for CrCOD model

Requirement	Short Description of Requirement
RCCOD-1	Develop a software application that will calculate an estimate of the COD for a Circumferential TWC in three locations through the thickness of the pipe (Inner-Diameter (ID), mid-wall, and Outer-Diameter (OD)).
RCCOD -2	Implement the Modified GE/EPRI Circumferential TWC COD model [3, 4, and 5].
RCCOD -3	The required inputs and outputs are presented in Tables 1 and 2 in the SRD.
RCCOD-4	Input will be required in SI system of units (see Table 1 of the SRD). Additionally, the physical models will be implemented using the SI system of units.
RCCOD -5	The required list of errors and warning is shown in Table 3 in the SRD.
RCCOD -6	Develop the Circumferential TWC COD Module to be implemented as an external DLL element where the actor is the GoldSim xLPR application.
RCCOD-7	The module coding will follow the xLPR coding guidelines.
RCCOD -8*	The Framework shall call the CrCOD module whenever there is an active idealized or transitioning through-wall crack.
RCCOD -9*	If the module is called from the DLL wrapper, communication of inputs and outputs shall be conducted with explicit passing of variables.
RCCOD -10*	The Framework shall call the CrCOD subroutine with a set of inputs that are in conformance with the required units, range of validity and data types, specified in Table 1 in the SRD
RCCOD-11*	The Framework shall also accept the outputs in conformance with the required units, range of validity and data types, specified in Table 2 in the SRD.
RCCOD-12*	Upon receiving an error message from this module, the Framework shall terminate the analysis (individual realization or complete simulation, at the discretion of the Computational Group).
RCCOD-13	Develop a suite of tests that exercise all significant elements of the module.

*Framework requirement

Table 2. SRD requirements for AxCOD model

Requirement	Short Description of Requirement
RAxCOD-1	The subroutine must exhibit the software design attributes of maintainability and portability.
RAxCOD-2	The subroutine must implement best-estimate models.
RAxCOD-3	The subroutine must minimize computational resources.
RAxCOD-4	The subroutine shall be written in Fortran such that it can be compiled to a DLL
RAxCOD-5	The subroutine must follow the best practices defined in [6].
RAxCOD-6	The subroutine shall be implemented in terms of SI units, with unit conversion accomplished according to IEEE/ASTM SI 10 2010.
RAxCOD-7	The subroutine shall account for material properties through the use of Ramberg-Osgood material parameters.
RAxCOD-8	The subroutine should be valid for a range of pipe geometries.
RAxCOD-9	The subroutine should be valid for a range of crack lengths.
RAxCOD-10	The subroutine should implement a GE/EPRI model for calculating COD.
RAxCOD-11	The subroutine shall calculate COD for both linear elastic and elastic-plastic cases.
RAxCOD-12	The subroutine should account for two loading conditions: internal pressure and weld residual stress.
RAxCOD-13*	The subroutine shall output the COD at three locations along the pipe thickness. The Framework shall supply these outputs to the Crack Transition Module and/or to leak rate calculations.
RAxCOD-14*	The Framework shall call the COD module when a crack is transitioning from a surface crack to a through-wall crack, i.e., $a/t \geq 0.95$, and all subsequent time steps.
RAxCOD-15*	The Framework shall supply a through-thickness averaged hoop weld residual stress as an input for the axial crack COD subroutine. For reference, weld residual stress is not an input to the circumferential crack COD subroutine.
RAxCOD-16*	The Computational Group shall compile this subroutine as a Dynamic Link Library for incorporation into the xLPR Framework.
RAxCOD-17	Regarding input validity checking, the Module shall perform the checks and actions listed in Table 3 in the SRD.

*Framework requirement

2. THE COD MODELS

Two separate models were developed for predicting CODs; one for circumferentially oriented TWCs (CrCOD) and one for axially oriented TWCs (AxCOD). The technical basis for the CrCOD model will be discussed first, followed by a similar discussion for the AxCOD model. For an in-depth discussion of the technical bases behind these models the reader is referred to the Software Design Description (SDD) for each model [7, 8].

The CrCOD model is based on the GE/EPRI methodology [9, 10, 11] for estimating the COD of a TWC in a pipe subjected to combined tension and bending loads. The GE/EPRI method separates the COD into elastic and plastic contributions, see Equation 1.

$$\delta^{total}=\delta^{el}+\delta^{pl} \qquad \text{(Eqn. 1)}$$

GE/EPRI solutions are given for pure bending, pure tension, and combined loading cases. However there are known limitations associated with the use of the GE/EPRI method for predicting the COD, most notably limitations associated with how the methodology handled the combined load case, i.e., combined tension and bending, and limitations on the design space, e.g., R_m/t values were limited to values between 10 and 20 and θ/π values were limited to values less than or equal to 0.5. To overcome some of these limitations, as part of the xLPR Version 1.0 development process, a blended solution for COD was developed. This blended solution used a mixture of the pure GE/EPRI tension solution and pure GE/EPRI bending solution.

For the blended solution used for xLPR Version 1.0, a single value of COD was provided for a prescribed loading condition, which was then applied uniformly at every location through the thickness of the pipe. Furthermore, the xLPR Version 1.0 circumferential TWC COD module, CALC_COD, also had all of the same restrictions and limitations of the GE/EPRI solution on which it was based. Differences between the Version 1.0 COD model and that used for Version 2.0 include:

(1). The Version 1.0 method was only valid for normalized crack length values (θ/π) of 0.5 or less, whereas Version 2.0 includes solutions for θ/π up to 0.9 . For cases where the crack length is more than 90 percent of the pipe circumference, the $\theta/\pi = 0.90$ solution is used.

(2). The Version 1.0 method was only valid for mean radius-to-thickness ratios (R_m/t) of 10 to 20, whereas Version 2.0 includes solutions for R_m/t values of 2 to 20. Again, for cases were the R_m/t values are outside this range, the solutions for R_m/t of 2 or 20 are used.

(3). The pressure on the crack face was not accounted for in the Version 1.0 COD calculations.

Recognizing the limitations of the CALC_COD blended solution, important requirements were levied against a replacement module to add more fidelity to the COD calculations:

(1). The module must provide COD at the inner surface of the pipe, at the mid-thickness of the pipe and at the outer surface so that a better estimate of the leak rate can be made. Tapering of the opening or expansion of the opening will both affect leak rate.

(2). The module must consider cracks as small cracks and large cracks. In xLPR, TWCs start very small and are grown to rupture. Accordingly, the COD must be calculated for any possible crack size.

(3). The module must consider a wide range of pipe geometries.

(4). The module must consider the full spectrum of loads that drive COD and it must also consider proper interaction between the loading modes.

As part of the xLPR Version 2.0 development process, a new circumferential crack COD model was developed (CrCOD). The new methodology satisfies the following constraints:

(1). The solution would be obtained using a GE/EPRI-like scheme [9, 10, 11].
(2). The axial load due to internal pipe pressure and crack face pressure would be applied concurrently.
(3). The crack face pressure is proportional to the internal pipe pressure.
(4). The crack face pressure is applied uniformly across the pipe wall thickness.
(5). The moment is applied subsequent to the axial forces (internal pressure, crack face pressure, and external axial load), whereas the pressure and bending loads were assumed to be applied concurrently in the Version 1.0 version (CALC_COD).
(6). The solution provides the COD at three locations through the pipe wall thickness: the inner diameter, the mid-wall thickness location, and the outer diameter at the crack centerline.
(7). The design space for normalized crack length values (θ/π) is 0.05 to 0.9.
(8). The design space for mean radius-to-thickness ratio (Rm/t) is 2 to 20.
(9). The design space for the Ramberg-Osgood exponent (n) is 2 to 10.
(10). The boundary conditions for the model consist of the pipe ends being free to rotate.

The CrCOD development process consisted of fitting a continuum analytical solution to a set of discrete finite element COD results by adhering to the following steps:

(1). For a wide range of pipe geometries, material conditions, and crack sizes; determine the COD solutions at the inner diameter, mid-thickness, and outer diameter locations at the crack center-line for a TWC in a cap-ended pipe under multiple loadings, including axial loading due to internal pressure, crack face pressure, and an applied bending moment.

(2). Use a GE/EPRI solution methodology to develop elastic and plastic influence functions and modifications using a failure surface theory and fracture mechanics plastic zone theory.

(3). Assume a Ramberg-Osgood material representation for an isotropic, homogeneous material. Modifications will be made to the solutions to obtain a better match to the large-displacement theory results from the finite element analyses.

(4). Finite element modeling using ABAQUS with 3D continuum 20-node brick elements with half-symmetry.

(5). Loads consist of axial load due to internal pressure; pressure evenly distributed on the crack face; and applied bending moment. Boundary conditions consist of symmetry on the crack plane, restraint of free body motion, and continuum distributing constraint

(i.e., distributed loads, not constrained degrees of freedom) on the free-end of the pipe.

(6). The design space consists of the following independent variables:

a. Mean radius–to–thickness ratios (R_m/t) of 2, 5, 10, and 20
b. Normalized crack length ratios (θ/π) of 0.05, 0.10, 0.25, 0.50, 0.75, and 0.90
c. Material properties: linear elastic plus elastic-plastic with strain hardening exponents (n) of 2, 3, 5, 7, and 10. Note, the Ramberg-Osgood coefficient (α) was arbitrarily set to 1.0 for the determination of the influence functions.

(7). Use ABAQUS, Python Scripts, and EXCEL VBA to complete and synthesize analyses.

(8). Review contour plots for acceptability of mesh, review pipe deformation for validity checks, complete pipe-independent size (i.e. variation in pipe diameters) analyses to ensure size independence of results.

(9). Use FORTRAN 90/95 to code the modified GE/EPRI equations with fitting functions using fracture mechanics plastic zone theory for combined tension and bending solutions.

(10). Using a subset of the COD data available from past pipe fracture experimental programs, verify and validate the continuum solution code from #9.

(11). Iterate steps 9 and 10 for empirical fitting functions

2.1 The Circumferential COD Model

2.1.1 An Overview of the GE/EPRI Method

As mentioned previously, the GE/EPRI method uses the theory of superposition to calculate the total COD as the sum of the elastic and the plastic contributions of COD, see Equation 1. The total elastic COD is the linear sum of the elastic COD values determined for each of the applicable load categories, i.e., tension, bending, and crack face pressure. The individual components of the elastic COD are provided in Equation 2, where the elastic influence functions (V1) are expressed in tabular form as a function of the normalized crack length (θ/π) and pipe mean radius to wall thickness ratio (Rm/t).

$$\delta_{(x)}^{el} = \frac{4a}{E}\sigma_{(x)}^{\infty} V_{1(x)}\left(\frac{\theta}{\pi}, \frac{R_m}{t}\right) \qquad \text{(Eqn. 2)}$$

In Equation 2 the subscript *(x)* represents a given load category.

Thus, to obtain the total elastic COD, the following sum is used.

$$\delta_{(total)}^{el} = \frac{4a}{E}\left[\sigma_{(T)}^{\infty} V_{1(T)} + \sigma_{(B)}^{\infty} V_{1(B)} + \sigma_{(CFP)}^{\infty} V_{1(CFP)}\right] \qquad \text{(Eqn. 3)}$$

where the subscripts, T, B, and CFP correspond to the tension, bending, and crack face pressure loading contributions, respectively.

In order to calculate the plastic component of COD, the GE/EPRI method provides Equation 4 for the calculation of the plastic COD due to bending and Equation 5 for the calculation of the plastic COD due to tension [10, 11].

$$\delta_{(B)}^{pl} = \alpha \varepsilon_o a h_2^B \left(\frac{\theta}{\pi}, n, \frac{R_m}{t}\right) \left(\frac{M}{M_o}\right)^n \quad \text{(Eqn. 4)}$$

$$\delta_{(T)}^{pl} = \alpha \varepsilon_o a h_2^T \left(\frac{\theta}{\pi}, n, \frac{R_m}{t}\right) \left(\frac{P}{P_o}\right)^n \quad \text{(Eqn. 5)}$$

In turn, Equation 6 shows the total plastic component of COD per the GE/EPRI method

$$\delta_{(total)}^{pl} = \delta_{(T)}^{pl} + \delta_{(B)}^{pl} \quad \text{(Eqn. 6)}$$

2.1.2 An Overview of the Finite Element Model Used to Develop the CrCOD Module

Using the ABAQUS solver, finite element analyses were conducted [12, 13] to determine elastic influence functions (V1-functions) and plastic influence functions (h2-functions) for the analytical formulas required for the calculation of COD. Figure 1 through Figure 3 provide schematics of the geometrical features and loading of a typical through-wall cracked pipe.

2.1.3 Elements and Meshes

The elements used for the analysis were three-dimensional, quadratic order, continuum brick elements with reduced integration. The ABAQUS designation for this type of element is C3D20R, where “C” means continuum, “3D” means three-dimensional, “20” means 20 nodes per element, and “R” indicates reduced integration. Figure 4 through Figure 6 show a typical mesh used for these analyses.

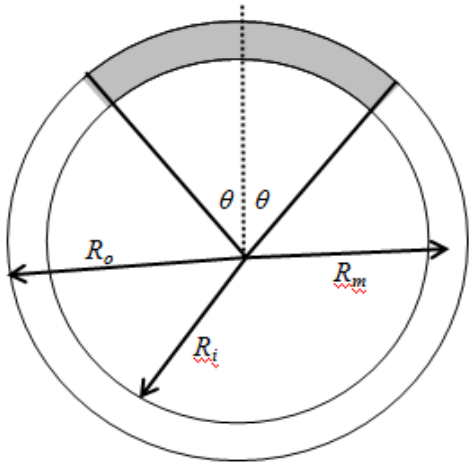

Figure 1. Idealized through-wall crack

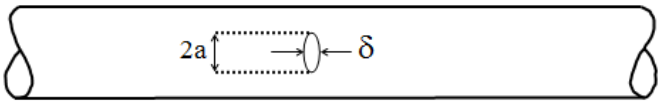

Figure 2. Circumferential through-wall crack in a pipe

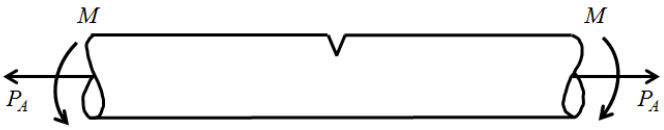

Figure 3. Cracked pipe under tension and bending

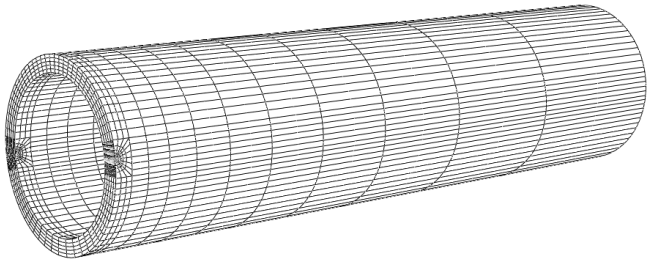

Figure 4. Typical mesh used in finite element analysis (FEA)

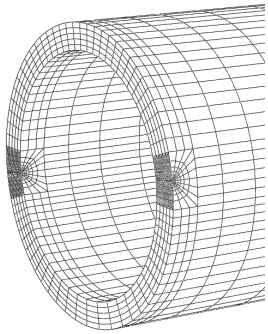

Figure 5. Through-thickness mesh

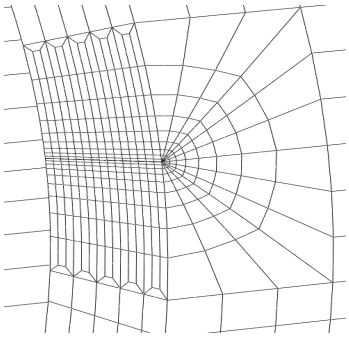

Figure 6. Keyhole spider mesh at crack tip

2.1.4 Boundary Conditions

The pipe was oriented such that the long axis was in the z-axis of the global Cartesian coordinate system. The half-length of the pipe was four times the outer diameter of the pipe. The crack was oriented at the center of the pipe such that one of the two crack faces was modeled with symmetry in the z-direction yielding a half-symmetry model. Three boundary conditions were required: (1) symmetry in the z-direction at the center of the pipe, (2) an anchor point on the symmetry plane to prohibit free-body motion, and (3) a rotation boundary condition to prohibit torsional free-body rotation. Figures 7 through 9 show typical boundary conditions for the analyses performed.

It should be noted that the pipe is symmetric at the crack mid-plane in the length direction, but this symmetry condition was not used in these analyses due to the limitation of mixing coordinate systems with different boundary conditions in ABAQUS. Additionally, any future work, such as restraint changes and weld residual stress, will use the same models and may not have this inherent symmetry.

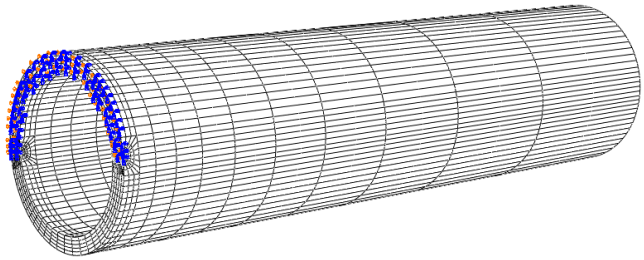

Figure 7. Half-length symmetry boundary condition; the non-cracked ligament

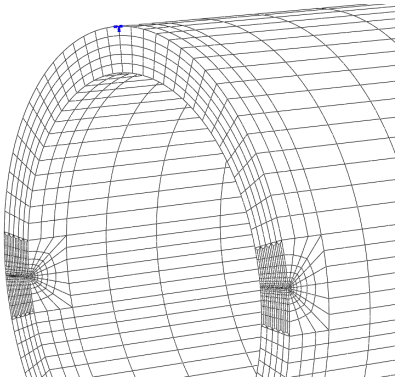

Figure 8. Anchor point free-body motion boundary condition in the center of the non-cracked ligament

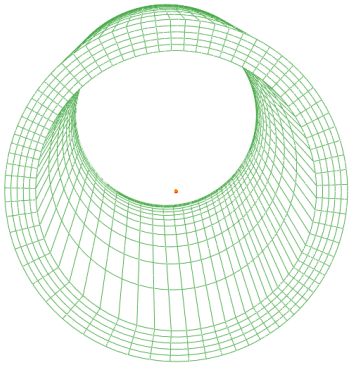

Figure 9. Rotation boundary condition at non-cracked end of the pipe at the reference point on the pipe centerline

2.1.5 Constraints

Initially, a kinematic coupling constraint was used to apply the axial load and the bending moment via a reference node at the non-cracked end of the pipe. However, inspection of results revealed that this constraint was not behaving as required. This was determined to be a limitation in the ABAQUS constraints, which provides a means to constrain displacements, rather than providing a means to distribute forces.

Thus, based on the information provided in Reference [13], a continuum distributed coupling constraint was applied to the non-cracked end of the pipe to allow for the proper force transmission and proper pipe-end shape development, when axial loads and bending moments were applied. Figure 10 displays the implementation of this constraint in the finite element (FE) model.

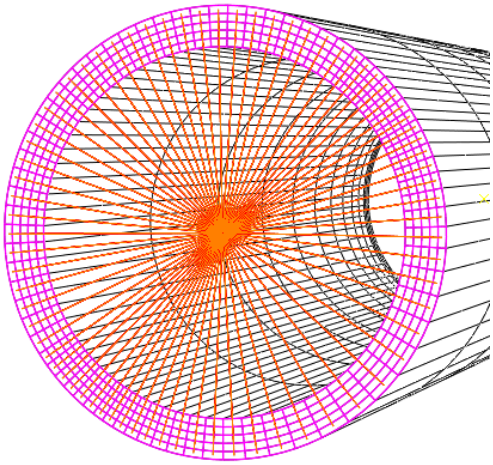

Figure 10. Continuum distributed coupling constraint at the non-cracked pipe end

2.1.6 Application of Forces

Three types of forces are required to be applied during the analyses conducted in this study. These forces are an axial load to simulate a cap-ended pipe subjected to internal pipe pressure, a crack face pressure, and a bending moment.

Axial stress was required to be applied to the finite element model in order to emulate a capped-end pipe. The application of stress in the axial direction was accomplished by applying a concentrated force to a reference node at the non-cracked end of the pipe in conjunction with the constraint previously discussed. To simulate the pressure on the crack face of a cracked pipe, a pressure force was applied uniformly to the crack surface in the finite element model. The application of the bending moment was accomplished by applying a concentrated moment to the reference node at the non-cracked end of the pipe in conjunction with the constraint previously discussed.

2.1.7 Follower Force Assumption

For the analyses conducted during this study, one of the assumptions for the boundary condition for the pipe end was that it was “free to rotate”. Because the pipe ends are free, the pressure in the pipe causes an eccentric load at the crack plane, so the cracked pipe rotates. Because the pipe rotates during the analysis, the applied axial force does not always act along the z-axis, but rather, acts normal to the pipe end. ABAQUS provides a method to automatically keep the force normal to the pipe end, which is called a “follower force.” This method was invoked during the analyses for the application of both pressure and moment. It should be noted that only a small change was seen when using this assumption, possibly due to the small strain assumption discussed in the next sub-section.

2.1.8 Small Displacement (Small Strain) Assumption

For the development of an elastic plus plastic solution to the COD problem, the stress-strain field around the crack tip must exhibit contained plasticity (i.e. small scale yielding). This assumption is also true for other elastic-plastic theory such as that by Hutchinson, Rice and Rosengren (HRR theory) [14, 15] for elastic-plastic fracture toughness. The HRR solutions are predicated on contained plasticity, which assumes the elastic-plastic fracture toughness value (J) is valid to calculate the stress-strain field around the crack tip. Thus, for the analyses conducted during this study, a small strain assumption is made. In practical terms, this means that the term NLGEOM (Non-Linear GEOMetry) is not invoked in ABAQUS [16].

2.1.9 Material Properties

Because, in theory, the analytical solution should work for any material that behaves in accordance with the Ramberg-Osgood plasticity model, Equation 7, the material properties chosen for the analyses were arbitrary. Table 3 provides the values for both the elastic and plastic material properties used in the analyses.

$$\varepsilon = \frac{\sigma}{E} + \alpha \frac{\sigma_o}{E} \left(\frac{\sigma}{\sigma_o} \right)^n \qquad \text{(Eqn. 7)}$$

Table 3. Material properties used in ABAQUS FEA

Material Constant	Value	Units
E	206.843	GPa
α	1.0	unitless
σ_o	344.7	MPa
υ	0.3	mm/mm
n	analysis dependent	unitless

2.1.10 Independent Analysis Cases

A large number of independent finite element runs were conducted to determine the values of the COD influence functions (V1 and h2) The four variables changed during these independent analyses were the pipe diameter (914.4, 406.4, 114.3 mm), the mean pipe radius to wall thickness ratio, Rm/t, (initially 5, 10, 20), the normalized crack length, θ/π, (0.05, 0.10, 0.25, 0.50, 0.75, 0.90), and the strain hardening exponent, n, (Linear Elastic, 2, 3, 5, 7, 10). Each case was required to be run for each determination of the various influence functions (i.e. elastic tension, elastic bending, elastic crack face pressure, etc.). Additionally, once the initial runs were completed and the results synthesized, the xLPR COD Subgroup judged that influence functions for the ratio of mean pipe radius to pipe wall thickness (Rm/t) of 2 were also required. Thus, one diameter (914.4 mm) was chosen with the crack length to pipe circumference ratios (θ/π) and strain hardening exponents (n) listed previously to determine the influence functions for mean pipe radius to pipe wall thickness ratio (Rm/t) of 2.

2.1.11 Development of the Elastic Influence Functions

Based on the use of continuum elements for the finite element analyses (FEA), the elastic crack opening displacement (COD) can be separated into independent categories based on load type. The total elastic COD is the linear sum of the values determined for each of these load categories, i.e., tension, bending, and crack face pressure. The base-equation for each one of these independent categories was shown in Equation 2 previously, where the far-field stresses for those equations are defined in Equations 8 through 10. It should be noted that an assumption of thin shell theory was used in the analysis. Because COD is measured in the FEA analysis at three locations across the thickness, it has been judged that this assumption only affects the values of the influence functions and does not introduce error into the analysis. The assertion that the thin shell assumption has no impact is sustained by the fact that the analysis, which uses the thin-shell assumption, matches the FEA which makes no assumption on thin or thick behavior.

$$\sigma_{(T)}^{\infty} = \frac{pR_i^2}{2R_m t} + \frac{P_A}{A} \qquad \text{(Eqn. 8)}$$

$$\sigma_{(B)}^{\infty} = \frac{MR_m}{I} \qquad \text{(Eqn. 9)}$$

$$\sigma^{\infty}_{(CFP)} = p_{CF} \quad \text{(Eqn. 10)}$$

For linear-elastic analyses, the material response is given in Equation 11. The elastic modulus used for the analyses was given previously in Table 3.

$$\varepsilon = \frac{\sigma}{E} \quad \text{(Eqn. 11)}$$

For reference, Table 4 provides the elastic influence function (V_1) for the GE/EPRI results provided in Reference 10. Based on FEA conducted as part of this effort Table 5 through Table 8 were generated to provide the fitting coefficients V_1 for each radius-to-thickness ratio of interest at various locations through the pipe wall. Comparing the results from Table 4 for the original GE/EPRI solutions for a R_m/t ratio of 20 with the results from Table 5 for this new analysis for a R_m/t ratio of 20 at the mid-wall thickness location, shows that the agreement in the elastic influence functions for both tension and bending are within approximately 1.0 percent of each other, for cases where there are common normalized crack lengths, i.e., θ/π ratios of 0.25 and 0.5. Thus, as a result of this agreement, there is a measure of confidence that the models and elastic influence functions for CrCOD are correctly formulated.

Based on the information provided in Table 5 through Table 8 [17], the elastic influence functions for the tension case and the crack face pressure case are nearly equivalent (within 0.5%, in most cases). Thus, the tension stress solution and the crack face pressure stress solution can be linearly combined. The equation for linear combination of stresses can be written as Equation 12.

$$\sigma^{\infty}_{(T)} = \frac{pR_i^2}{2R_m t} + \frac{P_A}{A} + p_{CF} \quad \text{(Eqn. 12)}$$

Thus, the total elastic crack opening displacement can be rewritten as Equation 13.

$$\delta^{el}_{(total)} = \frac{4a}{E}\left[\sigma^{\infty}_{(T)} V_{1(T)} + \sigma^{\infty}_{(B)} V_{1(B)}\right] \quad \text{(Eqn. 13)}$$

Table 4. GE/EPRI V_1 functions for shell elements with R_m/t = 20 [10]

Category	Theta-over-Pi Ratio			
	0.0625	0.125	0.25	0.50
(T)	1.144	1.530	2.922	11.089
(B)	1.141	1.510	2.753	8.727

Table 5. V_1 for R_m/t = 20 from this study

Category	Theta-over-Pi Ratio – OD					
	0.05	0.10	0.25	0.50	0.75	0.90
(T)	1.2245	1.5624	3.2048	11.396	95.002	1312.1
(B)	1.2327	1.5563	3.0270	8.9909	56.560	679.25
(CFP)	1.2227	1.5584	3.1922	11.353	94.648	1308.6
	Theta-over-Pi Ratio – Mid Thickness					
(T)	1.0930	1.3576	2.9518	11.109	93.668	1295.6
(B)	1.0918	1.3470	2.7820	8.7435	55.733	670.68
(CFP)	1.0916	1.3541	2.9403	11.067	93.320	1292.2
	Theta-over-Pi Ratio – ID					
(T)	0.9693	1.1541	2.6986	10.823	92.334	1279.1
(B)	0.9587	1.1390	2.2537	8.4958	54.906	662.11
(CFP)	0.9679	1.1511	2.6881	10.782	91.991	1275.7

Table 6. V_1 for R_m/t = 10 from this study

Category	Theta-over-Pi Ratio- OD					
	0.05	0.10	0.25	0.50	0.75	0.90
(T)	1.1729	1.3952	2.5350	8.8007	73.475	655.30
(B)	1.1967	1.4033	2.4011	6.9105	43.496	340.23
(CFP)	1.1708	1.3917	2.5252	8.7681	73.210	653.61
	Theta-over-Pi Ratio – Mid-Thickness					
(T)	1.0460	1.2075	2.2540	8.3394	71.421	638.96
(B)	1.0461	1.2004	2.1264	6.5475	42.235	331.69
(CFP)	1.0448	1.2045	2.2454	8.3385	71.163	637.31
	Theta-over-Pi Ratio – ID					
(T)	0.9505	1.0267	1.9728	7.9372	69.366	622.61
(B)	0.9267	1.0044	1.8514	6.1839	40.974	323.15
(CFP)	0.9488	1.0241	1.9652	7.9079	69.115	621.01

Table 7. V1 for Rm/t = 5 from this study

Category	Theta-over-Pi Ratio – OD					
	0.05	**0.10**	**0.25**	**0.50**	**0.75**	**0.90**
(T)	1.1829	1.3144	2.1218	6.9346	55.118	267.57
(B)	1.2465	1.3547	2.0347	5.4311	32.531	139.93
(CFP)	1.1816	1.3112	2.1138	6.9100	54.930	233.92
	Theta-over-Pi Ratio – Mid-Thickness					
(T)	1.0094	1.1226	1.8243	6.3598	52.138	254.46
(B)	1.0126	1.1207	1.7304	4.9535	30.719	133.01
(CFP)	1.0077	1.1198	1.8174	6.3372	51.960	253.84
	Theta-over-Pi Ratio – ID					
(T)	0.9384	0.9593	1.5287	5.7830	49.155	241.33
(B)	0.8814	0.9150	1.4282	4.4747	28.905	126.07
(CFP)	0.9373	0.9571	1.5230	5.7625	48.988	240.75

Table 8. V_1 for $R_m/t = 2$ from this study

Category	Theta-over-Pi Ratio – OD					
	0.05	0.10	0.25	0.50	0.75	0.90
(T)	1.3215	1.3662	1.9147	5.6589	30.141	73.746
(B)	1.5527	1.5428	1.9484	4.5506	18.256	39.976
	Theta-over-Pi Ratio – Mid-Thickness					
(T)	0.9601	1.0514	1.5451	4.8237	26.558	65.478
(B)	0.9759	1.0704	1.5052	3.8300	16.018	35.398
	Theta-over-Pi Ratio – ID					
(T)	0.8243	0.8630	1.1958	3.9894	22.974	57.207
(B)	0.6741	0.7314	1.0822	3.1118	13.780	30.821

With the elastic influence functions provided in Table 5 through Table 8, along with the available FEA, a preliminary validation of the results was completed. Figure 11 through Figure 15 show the results of the validation. Comparisons to previously published data are also shown, when data are available. The analytical model shown in Equation 13 was used for the comparisons.

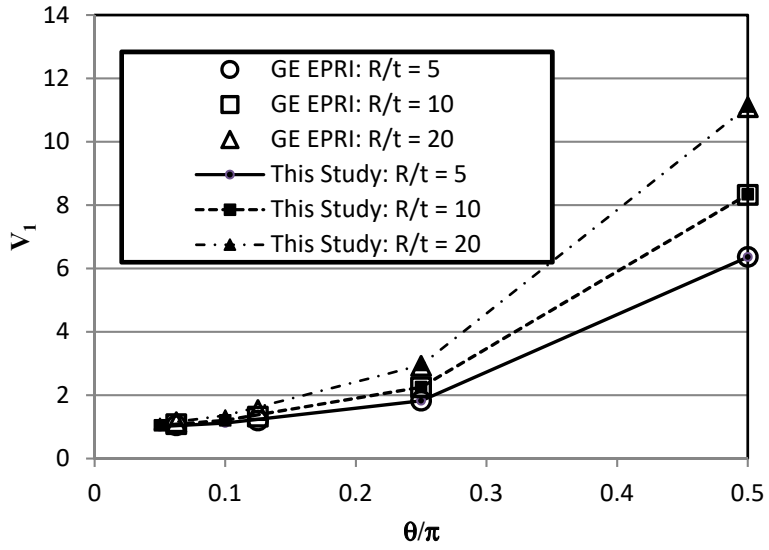

Figure 11. Comparison between the elastic influence functions for tension $V_{1(T)}$ from this study and the GE/EPRI $V_{1(T)}$ functions [10]

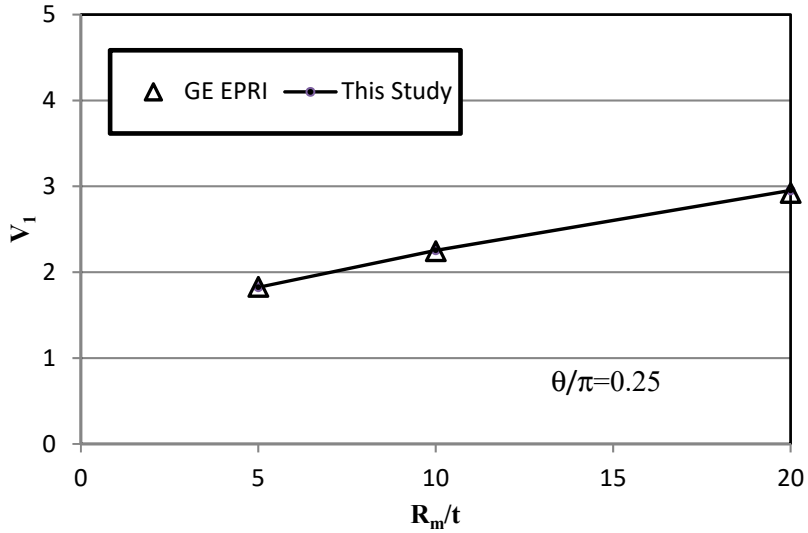

Figure 12. A second comparison between the elastic influence functions for tension developed as part of this program and those developed as part of the GE/EPRI program [10]

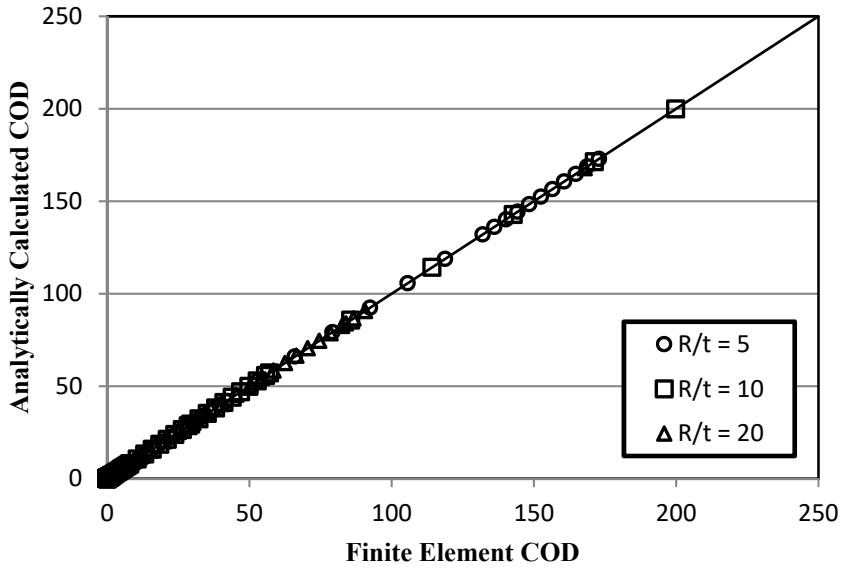

Figure 13. Analytical versus FEA COD results at the inside pipe surface under linear-elastic loading for a pipe with an outside diameter of 406.4 mm (16 inches)

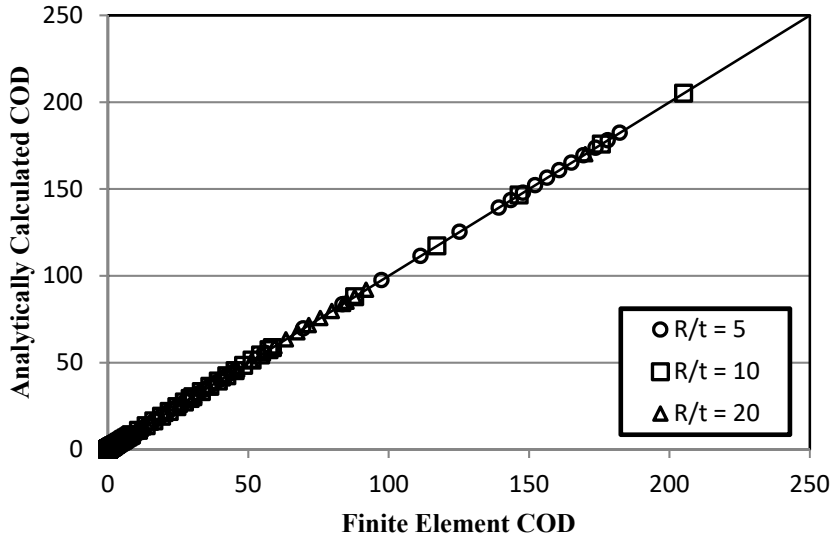

Figure 14. Analytical versus FEA COD results at the mid-thickness location under linear-elastic loading for a pipe with an outside diameter of 406.4 mm (16 inches)

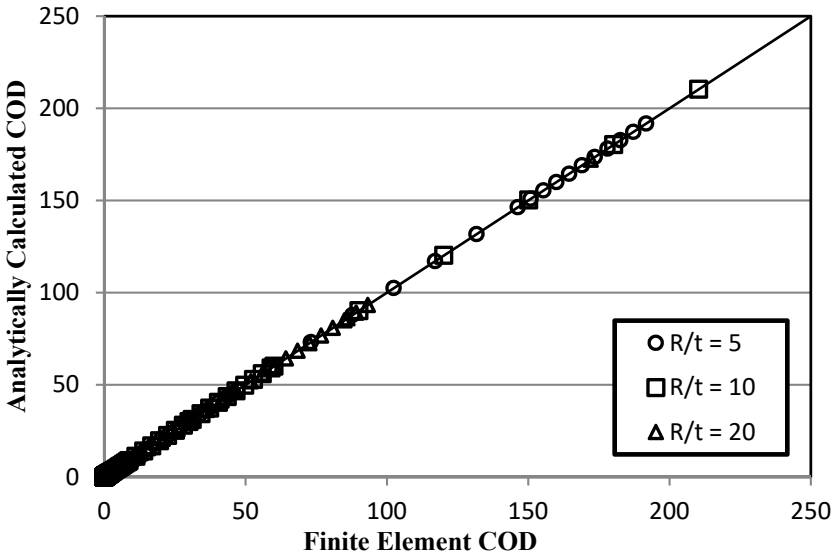

Figure 15. Analytical versus FEA COD results at the outside pipe surface under linear-elastic loading for a pipe with an outside diameter of 406.4 mm (16 inches)

2.1.12 Development of the Plastic Influence Functions

Recall that the application of the theory of superposition requires the total COD to be the sum of the elastic contribution to COD and the plastic contribution to COD, as shown in Equation 1. Once an elastic-plastic finite element analysis is completed, the results provide the total COD value. From the elastic solutions, Equation 13 provides the elastic contribution to the total COD. Thus, Equation 1 can be rewritten as Equation 14 in order to obtain the plastic contribution to COD.

$$\delta^{pl} = \delta^{total} - \delta^{el} \qquad \text{(Eqn. 14)}$$

While the GE/EPRI formulation requires the calculation of an effective crack length to be used in the elastic portion of the solution [10], this study did not make that assumption. The end use of these equations will be for inclusion in the xLPR Framework, where the user will not know the stress state prior to the analyses, nor will the stress state remain constant throughout a given analysis. Thus, the elastic portion and the plastic portion of COD must be based on the physical crack size.

Pure Bending Plastic Solution

The small strain theory method used to determine the plastic influence functions for bending, h_2^B, involves solving the finite element problem at an applied moment such that the elastic contribution is small compared to the plastic contribution. For these analyses, a moment equivalent to four times the collapse moment shown in Equation 15, was used (i.e. M=4M0, where M0 is the collapse moment). Equation 14 was applied to the specific bending solution to develop Equations 16 and 17, consistent with the form of Equation 4 at $M/M_0 = 4$.

$$M_o = 4\sigma_o R_m^2 t\left[cos\left(\frac{\theta}{2}\right) - \frac{1}{2}sin(\theta)\right] \quad \text{(Eqn. 15)}$$

$$\delta_{(B)}^{pl}\Big|_{M=4M_o} = \delta_{(B)}^{Total}\Big|_{M=4M_o}^{FEA} - \delta_{(B)}^{el}\left(\frac{R_m}{t}, \frac{\theta_e}{\pi}\right)\Big|_{M=4M_o}^{Analytical} \quad \text{(Eqn. 16)}$$

$$h_2^B = \frac{\delta_{(B)}^{pl}\Big|_{M=4M_o}}{\alpha\varepsilon_o a(4^n)} \quad \text{(Eqn. 17)}$$

Table 9 through Table 11 provide the plastic influence functions for the different locations through the pipe wall thickness (ID, mid-thickness, and OD) for the pure bending solution as a function of mean radius–to–thickness ratio (Rm/t), normalized crack length (θ/π), and strain hardening exponent (n).

A preliminary validation of the results was completed. Figure 16 through Figure 21 show examples of the results obtained during this preliminary validation. Comparisons to previously published data are shown, when such data are available. Figure 19 through Figure 21 are included to show solution independence of absolute pipe size. Differences in results are small and are attributed to three factors: (1) shell elements were used in the GE and Rahman analyses versus continuum elements in this analyses (Young analysis in Figure 16 through Figure 18); (2) this analyses assumed a thin shell behavior with an average stress used to calculate the COD at three locations across the thickness of pipe; and (3) the h-functions are an asymptotic solution and are dependent on the collapse moment or collapse load ratio. For all results analyzed, the results are judged to be within acceptable error.

Table 9. Plastic Influence function, h_2^B at ID surface for bending loading

R_m/t	θ/π	n=2	n=3	n=5	n=7	n=10
2	**0.05**	3.665	3.943	4.006	3.806	3.300
	0.10	3.407	3.489	3.223	2.789	2.103
	0.25	2.622	2.216	1.505	1.023	5.800E-01
	0.50	1.872	1.241	6.054E-01	3.226E-01	1.328E-01
	0.75	6.412E-01	2.510E-01	4.065E-02	6.952E-03	5.288E-04
	0.90	1.673E-02	1.456E-03	2.329E-05	7.772E-07	1.214E-08
5	**0.05**	5.113	5.718	6.358	6.544	6.288
	0.10	4.458	4.756	4.820	4.558	3.915
	0.25	3.862	3.469	2.672	2.077	1.449
	0.50	3.155	2.275	1.310	0.844	0.475
	0.75	2.188	1.306	0.539	0.247	0.082
	0.90	0.185	0.036	1.64E-03	8.60E-05	1.15E-06
10	**0.05**	5.410	6.213	7.268	7.823	7.924
	0.10	5.084	5.608	6.064	6.084	5.633
	0.25	5.403	5.032	4.062	3.300	2.475
	0.50	4.525	3.307	1.973	1.350	0.844
	0.75	3.377	2.222	1.142	0.670	0.329
	0.90	0.883	0.289	0.032	3.44E-03	1.21E-04
20	**0.05**	5.723	6.754	8.305	9.349	10.041
	0.10	6.146	7.080	8.184	8.603	8.343
	0.25	7.915	7.474	6.111	5.037	3.882
	0.50	6.530	4.755	2.881	2.044	1.369
	0.75	4.620	3.127	1.711	1.090	0.610
	0.90	2.750	1.340	0.330	8.28E-02	9.89E-03

Table 10. Plastic Influence function, h_2^B at mid-thickness for bending loading

R/t	θ/π	n=2	n=3	n=5	n=7	n=10
2	**0.05**	4.805	5.157	5.243	4.961	4.266
	0.10	4.586	4.562	4.083	3.461	2.563
	0.25	3.491	2.868	1.896	1.274	7.183E-01
	0.50	2.272	1.489	7.188E-01	3.816E-01	1.568E-01
	0.75	7.426E-01	2.901E-01	4.691E-02	8.019E-03	6.097E-04
	0.90	1.917E-02	1.667E-03	2.660E-05	8.855E-07	1.384E-08
5	**0.05**	5.707	6.335	6.951	7.082	6.750
	0.10	5.410	5.617	5.498	5.102	4.321
	0.25	4.628	4.077	3.059	2.337	1.607
	0.50	3.451	2.461	1.403	0.901	0.506
	0.75	2.315	1.380	0.569	0.261	0.087
	0.90	0.195	0.037	1.72E-03	9.00E-05	1.20E-06
10	**0.05**	6.145	6.927	7.882	8.348	8.381
	0.10	6.114	6.582	6.890	6.780	6.175
	0.25	6.164	5.643	4.445	3.555	2.630
	0.50	4.742	3.441	2.041	1.393	0.870
	0.75	3.471	2.283	1.173	0.688	0.338
	0.90	0.906	0.297	3.26E-02	3.53E-03	1.24E-04
20	**0.05**	6.632	7.662	9.144	10.116	10.731
	0.10	7.307	8.237	9.236	9.519	9.061
	0.25	8.610	8.014	6.434	5.246	4.008
	0.50	6.681	4.847	2.929	2.076	1.390
	0.75	4.684	3.169	1.734	1.104	0.618
	0.90	2.790	1.350	0.334	8.38E-02	1.00E-02

Table 11. Plastic Influence function, h_2^B at OD surface for bending loading

R_m/t	θ/π	n=2	n=3	n=5	n=7	n=10
2	**0.05**	7.889	7.882	7.399	6.700	5.555
	0.10	6.489	6.117	5.162	4.241	3.063
	0.25	4.398	3.538	2.291	1.527	8.570E-01
	0.50	2.669	1.736	8.319E-01	4.405E-01	1.807E-01
	0.75	8.437E-01	3.291E-01	5.317E-02	9.085E-03	6.906E-04
	0.90	2.161E-02	1.877E-03	2.989E-05	9.930E-07	1.552E-08
5	**0.05**	7.041	7.481	7.820	7.769	7.275
	0.10	6.502	6.572	6.222	5.673	4.738
	0.25	5.388	4.678	3.442	2.595	1.763
	0.50	3.743	2.646	1.495	0.957	0.537
	0.75	2.442	1.454	0.599	0.274	0.091
	0.90	0.205	0..039	1.81E-03	9.50E-05	1.25E-06
10	**0.05**	7.068	7.764	8.559	8.916	8.859
	0.10	7.174	7.576	7.730	7.488	6.723
	0.25	6.917	6.247	4.825	3.808	2.785
	0.50	4.959	3.575	2.109	1.437	0.897
	0.75	3.566	2.343	1.203	0.706	0.347
	0.90	0.929	0.304	3.34E-02	3.62E-03	1.27E-04
20	**0.05**	7.589	8.605	10.002	10.898	11.429
	0.10	8.467	9.393	10.289	10.436	9.778
	0.25	9.301	8.552	6.756	5.455	4.134
	0.50	6.833	4.939	2.976	2.108	1.411
	0.75	4.748	3.212	1.756	1.119	0.626
	0.90	2.820	1.370	3.38E-01	8.49E-02	1.01E-02

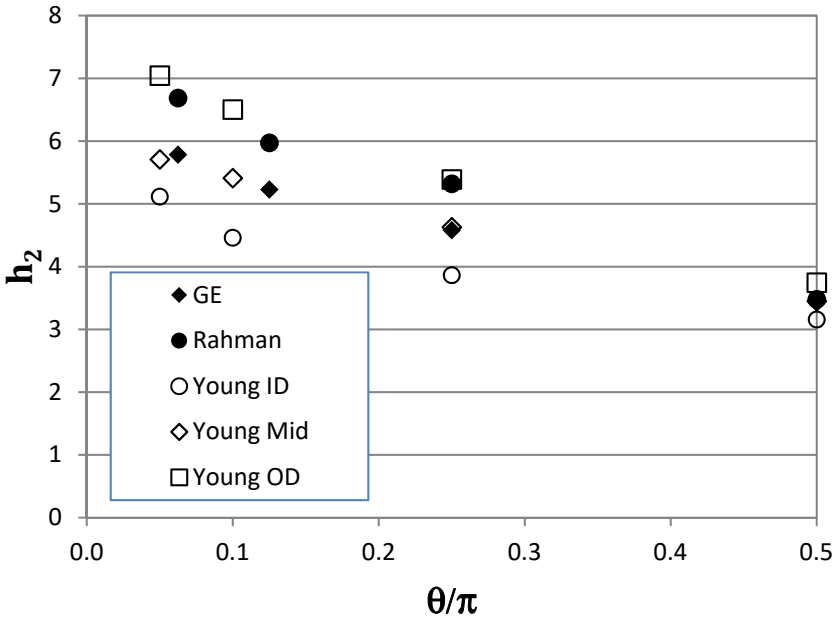

Figure 16. Pure bending results for $R_m/t = 5$ and n =2 [10, 18]

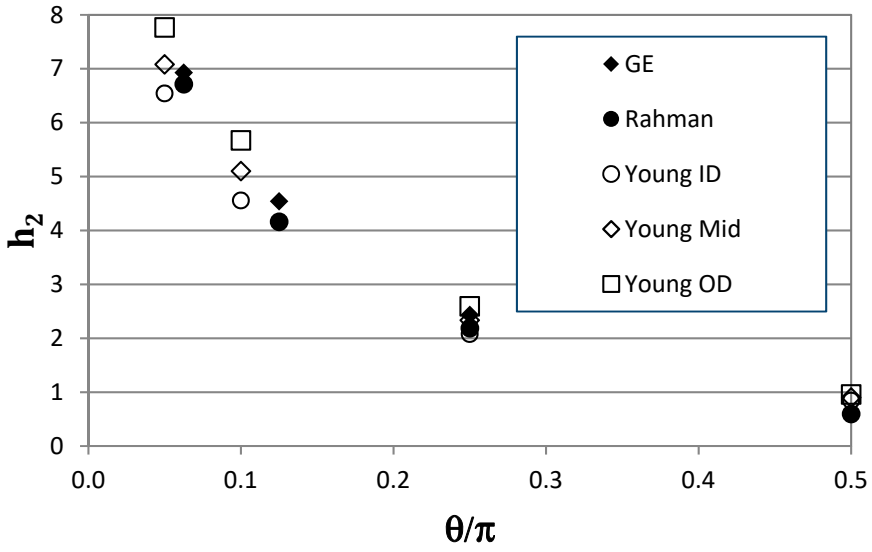

Figure 17. Pure bending results for $R_m/t = 5$ and n = 7 [10, 18]

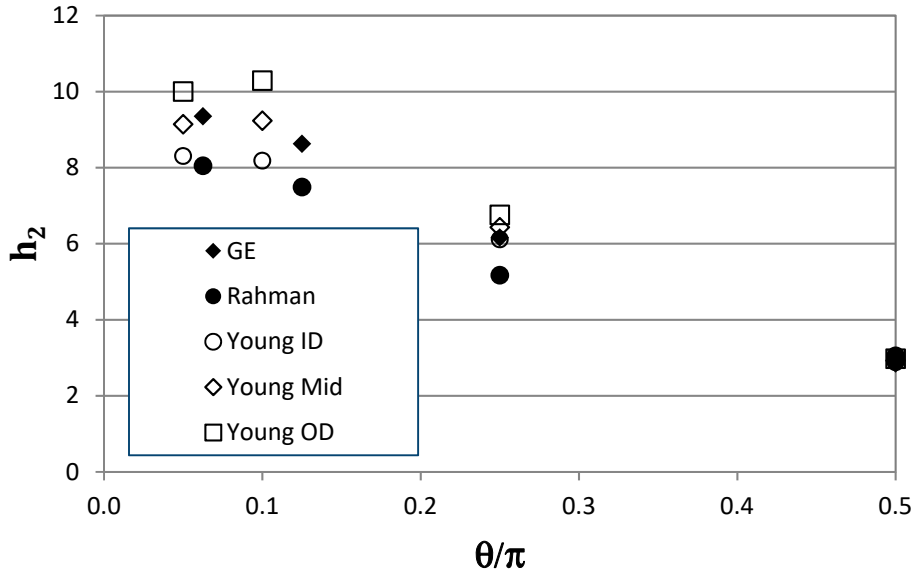

Figure 18. Pure bending results for $R_m/t = 20$ and $n = 5$ [10, 18]

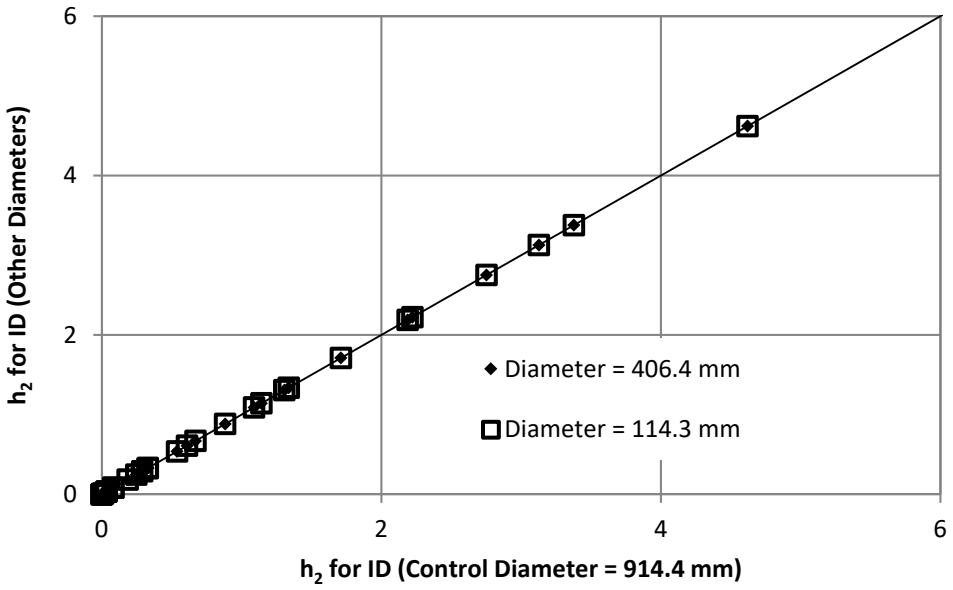

Figure 19. Comparison of plastic influence-functions (h_2) at ID surface for pure bending from base case to cases with other pipe diameters

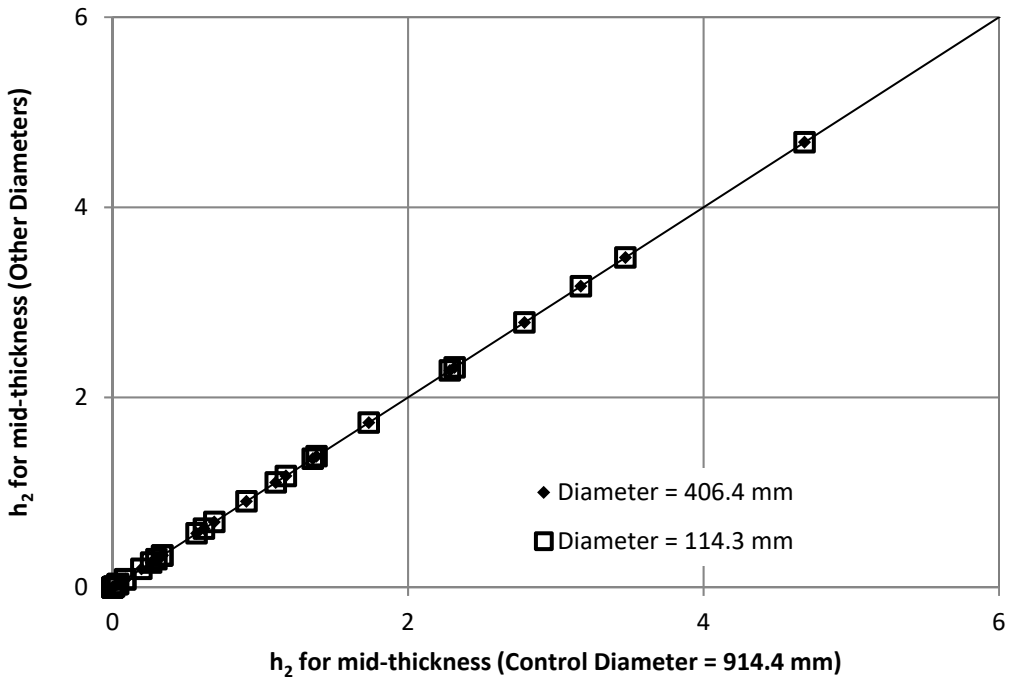

Figure 20. Comparison of plastic influence-functions (h_2) at mid-thickness location for pure bending from base case to cases with other pipe diameters

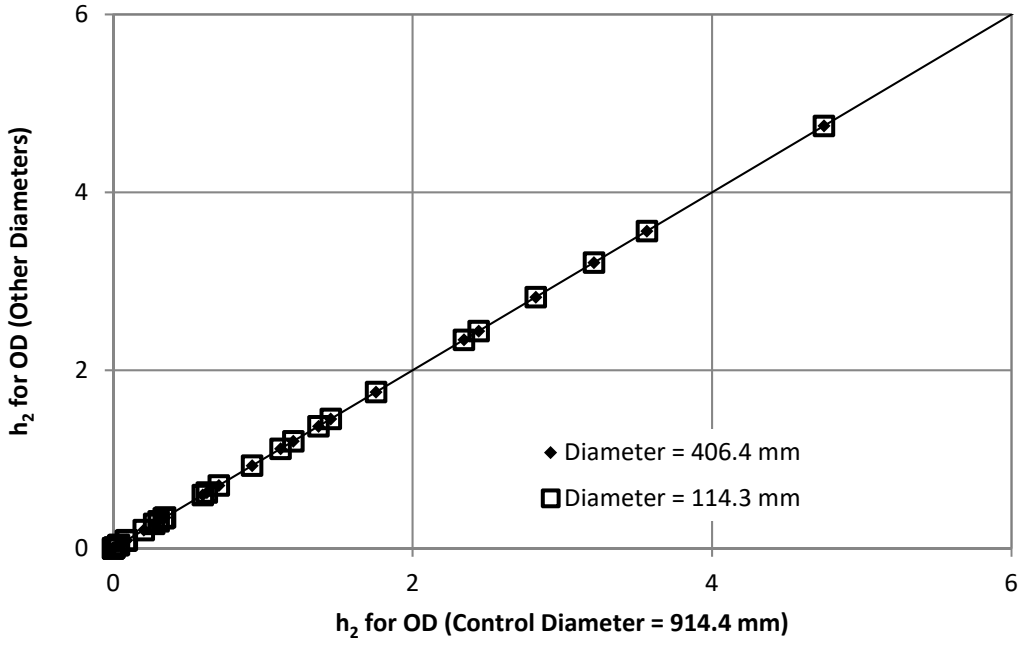

Figure 21. Comparison of plastic influence-functions (h_2) at OD surface for pure bending from base case to cases with other pipe diameters

Pure Tension Plastic Solution

Again, the small strain theory method used to determine the plastic influence functions, h_2^T, involves solving the finite element problem at a tension such that the elastic contribution is small compared to the plastic contribution. For these analyses, a tension equivalent to either eight or ten times the collapse tension, shown in Equation 18, was used (P=g*P_o; where g=8 or 10). Equation 14 was applied to the specific tension solution to develop Equations 19 and 20, consistent with the form of Equation 5 at $P/P_0 = g$.

$$P_o = 2\sigma_o R_m t\left\{\pi - \theta - 2sin^{-1}\left[\frac{1}{2}sin(\theta)\right]\right\} \quad \text{(Eqn. 18)}$$

$$\delta_{(T)}^{pl}\Big|_{P=gP_o} = \delta_{(T)}^{Total}\Big|_{P=gP_o}^{FEA} - \delta_{(T)}^{el}\left(\frac{R_m}{t}, \frac{\theta_e}{\pi}\right)\Big|_{P=gP_o}^{Analytical} \quad \text{(Eqn. 19)}$$

$$h_2^T = \frac{\delta_{(T)}^{pl}\Big|_{P=gP_o}}{\alpha\varepsilon_o a(g^n)} \quad \text{(Eqn. 20)}$$

Table 12 through

Table 14 provide the plastic influence functions for the different locations through the pipe wall thickness (ID, mid-thickness, and OD) for the pure tension solution as a function of mean pipe radius–to–thickness ratio (R_m/t), normalized crack length (θ/π), and strain hardening exponent (n).

Table 12. Plastic influence function, h_2^T, at the ID surface for tension loading

R_m/t	θ/π	n=2	n=3	n=5	n=7	n=10
2	**0.05**	3.390	3.723	3.993	3.950	3.697
	0.10	3.121	3.258	3.245	3.001	2.469
	0.25	2.318	2.034	1.399	9.455E-01	5.257E-01
	0.50	1.542	9.641E-01	4.301E-01	2.086E-01	7.430E-02
	0.75	5.704E-01	2.061E-01	3.110E-02	5.134E-03	3.605E-04
	0.90	1.613E-02	1.249E-03	1.075E-05	1.189E-07	1.735E-10
5	**0.05**	4.029	4.484	5.046	5.246	5.236
	0.10	3.463	3.763	4.031	3.970	3.583
	0.25	3.152	2.930	2.260	1.722	1.183
	0.50	2.482	1.708	0.962	0.602	0.482
	0.75	1.911	1.093	0.440	0.195	0.099
	0.90	0.171	0.028	8.06E-04	2.40E-05	2.10E-07
10	**0.05**	4.088	4.669	5.507	5.943	6.099
	0.10	3.834	4.309	4.881	5.043	4.817
	0.25	4.330	4.139	3.314	2.610	1.905
	0.50	3.460	2.399	1.411	0.948	0.574
	0.75	2.950	1.886	0.927	0.561	0.263
	0.90	0.821	0.245	2.37E-02	2.34E-03	7.12E-05
20	**0.05**	4.254	4.992	6.162	6.926	7.641
	0.10	4.585	5.373	6.444	6.930	6.814
	0.25	6.261	6.051	4.874	3.858	2.873
	0.50	4.858	3.344	1.997	1.384	0.906
	0.75	3.989	2.628	1.469	0.925	0.496
	0.90	2.581	1.193	2.74E-01	5.70E-02	2.97E-03

Table 13. Plastic influence function, h_2^T, at the mid-thickness location for tension loading

R_m/t	θ/π	n=2	n=3	n=5	n=7	n=10
2	**0.05**	3.766	4.136	4.470	4.456	4.158
	0.10	3.618	3.763	3.709	3.394	2.758
	0.25	2.931	2.500	1.660	1.102	6.061E-01
	0.50	1.834	1.133	4.999E-01	2.416E-01	8.593E-02
	0.75	6.578E-01	2.372E-01	3.575E-02	5.901E-03	4.144E-04
	0.90	1.866E-02	1.454E-03	1.268E-05	1.422E-07	2.105E-10
5	**0.05**	4.252	4.741	5.330	5.537	5.476
	0.10	4.066	4.329	4.494	4.349	3.861
	0.25	3.728	3.385	2.533	1.893	1.179
	0.50	2.692	1.832	1.022	0.638	0.509
	0.75	2.019	1.154	0.464	0.206	0.106
	0.90	0.180	0.030	8.49E-04	2.60E-05	2.15E-07
10	**0.05**	4.542	5.121	5.911	6.315	6.401
	0.10	4.562	5.010	5.486	5.549	5.199
	0.25	4.906	4.599	3.586	2.778	1.999
	0.50	3.610	2.484	1.453	0.975	0.590
	0.75	3.030	1.936	0.998	0.576	0.270
	0.90	0.842	0.251	2.43E-02	2.40E-03	7.35E-05
20	**0.05**	4.888	5.634	6.766	7.484	8.140
	0.10	5.432	6.225	7.230	7.613	7.331
	0.25	6.782	6.454	5.101	3.994	2.948
	0.50	4.856	3.400	2.026	1.403	0.919
	0.75	4.043	2.663	1.489	0.937	0.503
	0.90	2.614	1.209	2.77E-01	5.78E-02	3.02E-03

Table 14. Plastic influence function, h_2^T, at the OD surface for tension loading

R_m/t	θ/π	n=2	n=3	n=5	n=7	n=10
2	**0.05**	5.431	5.604	5.642	5.429	4.912
	0.10	4.708	4.683	4.374	3.888	3.088
	0.25	3.579	2.984	1.926	1.261	6.868E-01
	0.50	2.123	1.300	5.694E-01	2.745E-01	9.755E-02
	0.75	7.449E-01	2.683E-01	4.041E-02	6.668E-03	4.682E-04
	0.90	2.100E-02	1.635E-03	1.426E-05	1.597E-07	2.364E-10
5	**0.05**	5.019	5.387	5.184	5.935	5.764
	0.10	4.776	4.967	4.994	4.741	4.145
	0.25	4.300	3.838	2.803	2.063	1.375
	0.50	2.900	1.955	1.081	0.673	0.535
	0.75	2.128	1.215	0.488	0.216	0.111
	0.90	0.189	0.031	8.92E-04	2.70E-05	2.38E-07
10	**0.05**	5.134	5.662	6.366	6.714	6.715
	0.10	5.312	5.728	6.103	6.062	5.584
	0.25	5.477	5.055	3.856	2.946	2.093
	0.50	3.756	2.569	1.495	1.002	0.606
	0.75	3.111	1.987	1.024	0.591	0.277
	0.90	0.863	0.257	2.50E-02	2.46E-03	7.43E-05
20	**0.05**	5.557	6.299	7.383	8.050	8.645
	0.10	6.279	7.078	8.019	8.294	7.848
	0.25	7.300	6.856	5.328	4.131	3.023
	0.50	5.055	3.455	2.055	1.422	0.931
	0.75	4.096	2.698	1.508	0.949	0.509
	0.90	2.647	1.224	2.81E-01	5.85E-02	3.05E-03

With the plastic influence functions for pure tension shown in Table 12 through Table 14, along with the available FEA, a preliminary validation of the results was completed. Figure 22 through Figure 24 show examples of the results obtained during this preliminary validation. Comparisons to previously published data are shown, when such data are available. Figure 25 through Figure 27 are included to show solution independence of absolute pipe size. Differences in results are small and are attributed to three factors: (1) shell elements were used in the GE analyses versus continuum elements in this analysis (Young analyses in Figure 22 through Figure 24); (2) this analysis assumed a thin shell behavior with an average stress used to calculate the COD at three locations across the thickness of the pipe; and (3) the h_2-functions are an asymptotic solution and are dependent on the collapse moment or collapse load ratio. For all results analyzed, the results are judged to be within acceptable error.

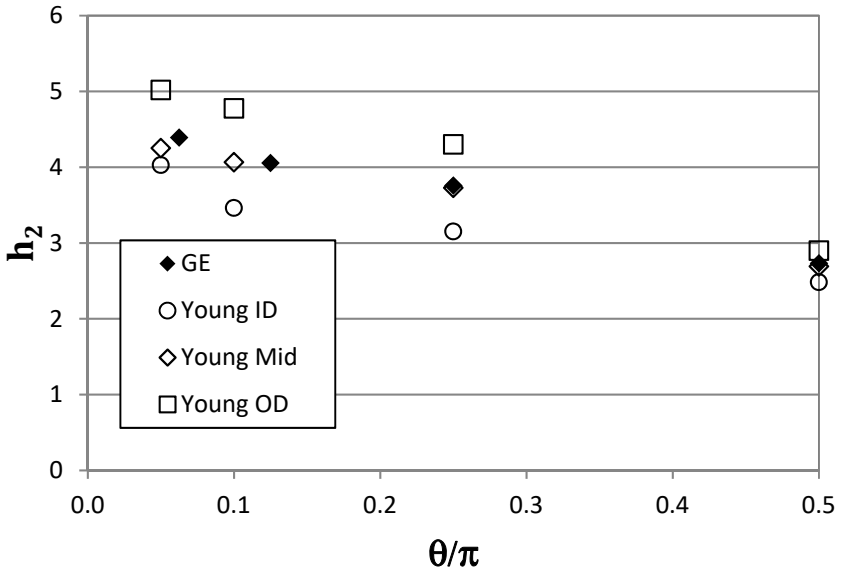

Figure 22. Pure tension results for $R_m/t = 5$ and $n = 2$ [10]

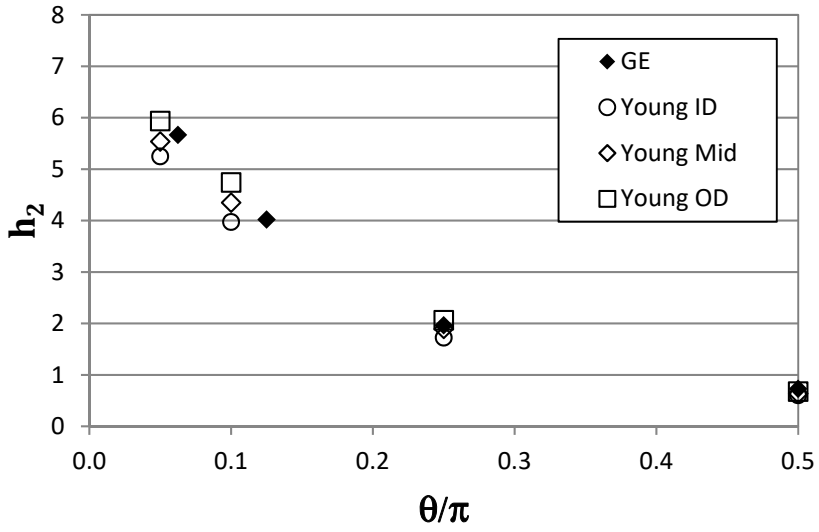

Figure 23. Pure tension results for $R_m/t = 5$ and $n = 7$ [10]

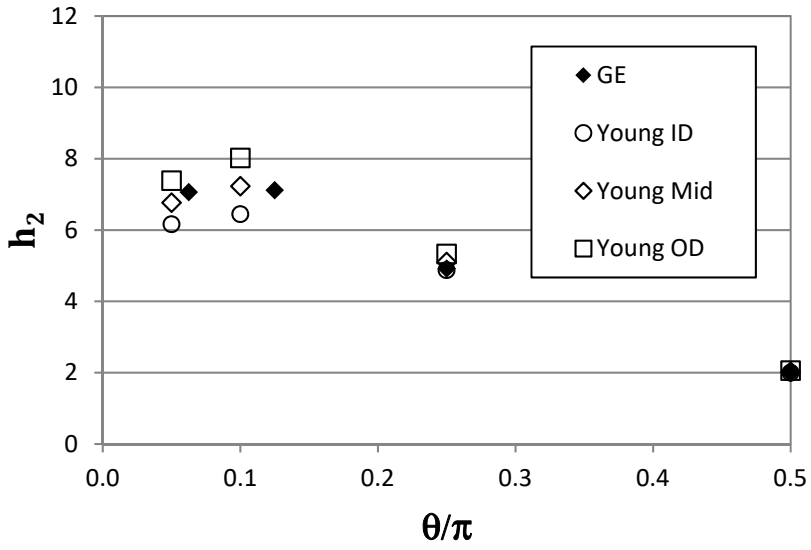

Figure 24. Pure tension results for $R_m/t = 20$ and $n = 5$ [10]

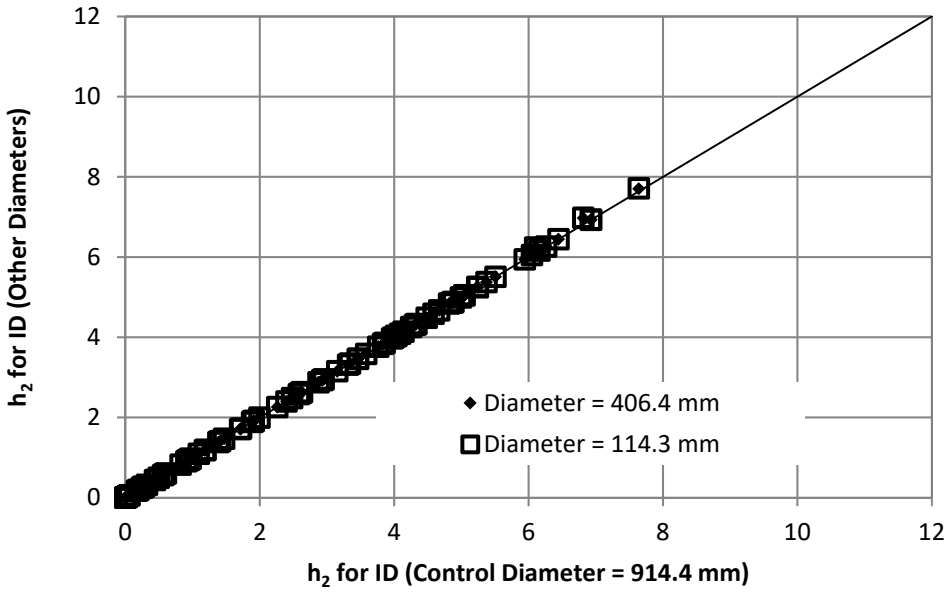

Figure 25. Comparison of plastic influence-functions (h_2) at ID surface for pure tension from base case to cases with other pipe diameters

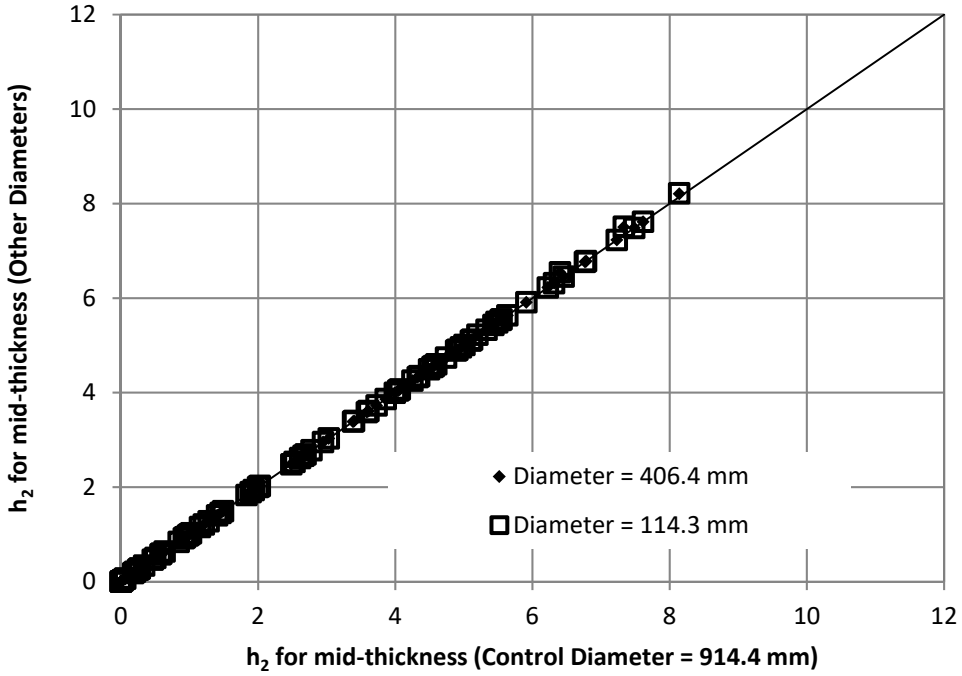

Figure 26. Comparison of plastic influence-functions (h_2) at ID surface for pure tension from base case to cases with other pipe diameters

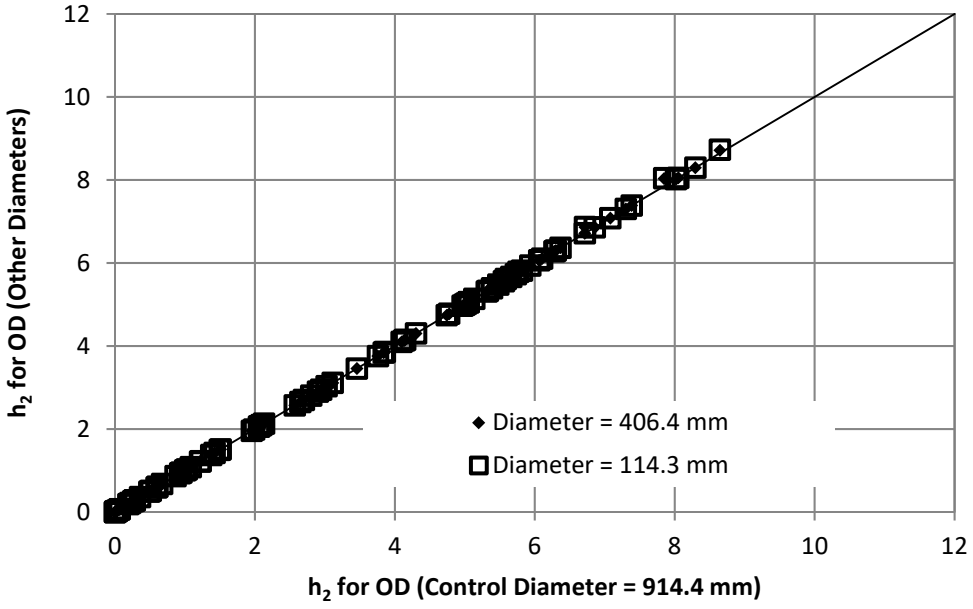

Figure 27. Comparison of plastic influence-functions (h_2) at ID surface for pure tension from base case to cases with other pipe diameters

2.1.13 Inclusion of Crack Face Pressure – Plastic Failure-Surface Solution

Under a combined loading condition, a failure surface must be defined such that the sum of the component load ratio is unity at the failure surface. To accomplish this for axial loading of a pipe with a TWC with loading due to both internal pipe pressure (with the assumption of a capped-end) and crack face pressure, the failure surface shown in Equation 21 was assumed. Because both the internal pressure and the crack face pressure are applied in the same nominal orientation, a linear superposition of loads (not stress) is proposed as shown in Equation 21. The limit load, P_0, (i.e. the load at which the uncracked ligament becomes a fully plastic hinge) for a pipe with a through-wall crack under axial load is given in Equation 18.

$$\frac{P_{CFP}}{P_o} + \frac{P_{ip}}{P_o} = 1 \qquad \text{(Eqn. 21)}$$

Because the crack face pressure is equal to the internal pressure (p) on the inner diameter of the pipe and zero on the outer diameter of the pipe, a first order approximation was made such that the crack face pressure is equal to a fraction of the internal pressure (γ). The far-field stress value to calculate the elastic COD is provided in Equation 22. The effective loads on the pipe can then be expressed as Equations 23 and 24 with the assumption of no externally applied axial loads.

$$\sigma_{(T)}^{\infty} = \frac{pR_i^2}{2R_m t} + \frac{P_A}{A} + p_{CF} = \frac{pR_i^2}{2R_m t} + \frac{P_A}{A} + \gamma p \qquad \text{(Eqn. 22)}$$

$$P = p\pi R_i^2 + \frac{P_A}{A} \qquad \text{(Eqn. 23)}$$

$$P_{CFP} = p_{cf}(2\theta)R_m t = 2\gamma p\theta R_m t \qquad \text{(Eqn. 24)}$$

To mimic the behavior in a nuclear power plant piping system, an assumption was made that the internal pressure and the crack face pressure were applied concurrently, such that the load ratio given in Equation 25, i.e., crack face pressure to internal pressure, is constant for a given crack size and pipe geometry. Therefore, Equation 21 can then be rewritten as shown in Equation 26.

$$\lambda = \left(\frac{P_{CFP}}{P_{ip}}\right) \qquad \text{(Eqn. 25)}$$

$$\frac{\lambda P_{ip}}{P_o} + \frac{P_{ip}}{P_o} = 1 \qquad \text{(Eqn. 26)}$$

Thus, using the failure surface approach, the load ratio, λ, and the load due to the internal pressure, P_{ip}, an effective limit load expression is derived and shown in Equations 27 and 28.

$$\frac{P_o'\lambda + P_o'}{P_o} = 1 \qquad \text{(Eqn. 27)}$$

$$P_o' = \frac{P_o}{1+\lambda} \quad \text{(Eqn. 28)}$$

Recall, the GE/EPRI formulation for the analytical COD equations separates the elastic and plastic solutions, as shown in Equation 1. If we assume the axial load comes from the internal pressure on an end-capped pipe with a TWC, the equation for the plastic component of COD due to pure tension is Equation 29. Based on the concurrent load arguments, Equation 29 can be recast as Equation 30.

$$\delta_{(T)}^{pl} = \alpha\varepsilon_o a h_2^T \left(\frac{P}{P_o}\right)^n \quad \text{(Eqn. 29)}$$

$$\delta_{(T+CFP)}^{pl} = \alpha\varepsilon_o a h_2^{T+CFP} \left(\frac{P_{ip}}{P_o'}\right)^n = \alpha\varepsilon_o a h_2^{T+CFP} \left[\frac{P(1+\lambda)}{P_o}\right]^n \quad \text{(Eqn. 30)}$$

To satisfy continuity when the crack face pressure is zero (i.e., $\gamma = 0$), Equation 30 must collapse to Equation 29. To complete the transition due to the constraint of continuity, the plastic influence function, h_2^{T+CFP}, must be equal to h_2^T. Thus, with continuity invoked, Equation 30 is rewritten as Equation 31.

$$\delta_{(T+CFP)}^{pl} = \alpha\varepsilon_o a h_2^T \left[\frac{P(1+\lambda)}{P_o}\right]^n \quad \text{(Eqn. 31)}$$

While the plastic COD solution is provided in Equation 31, the elastic solution was given by Equation 13 and can be rewritten as Equation 32. The initial theoretical combined elastic-plastic solution (for small strain, small displacement theory) for concurrently loaded TWCs with tension due to internal pressure and crack face pressure is provided in Equation 33.

$$\delta_{(T+CFP)}^{el} = \frac{4a}{E}\left[\sigma_{(T)}^{\infty} V_{1(T)}\right] = \frac{4a}{E}\left[\left(\frac{pR_i^2}{2R_m t} + \frac{P_A}{A} + \gamma p\right) V_{1(T)}\right] \quad \text{(Eqn. 32)}$$

$$\delta_{(T+CFP)}^{total} = \frac{4a}{E}\left[\left(\frac{pR_i^2}{2R_m t} + \frac{P_A}{A} + \gamma p\right) V_{1(T)}\right] + \alpha\varepsilon_o a h_2^T \left[\frac{P(1+\lambda)}{P_o}\right]^n \quad \text{(Eqn. 33)}$$

Because there are differences between long through-wall cracks and short through-wall cracks, mainly consisting of the in-plane rotation under pressure, two adjustments are required to the small strain, small displacement theoretical analytical solution. The first adjustment is a fitting term (f_1) which is a function of the normalized crack length. The application of the fitting function is shown in Equation 34, with a definition provided in Equation 35. It should be noted that Equation 34 reduces to the standard tension solution in the absence of crack face pressure. The second adjustment is due to the way the analytical solutions for the GE/EPRI model are derived (i.e. under the small strain, small displacement assumption). Finite element calculations using large displacement theory, which should provide closer approximations to reality, versus calculations using small displacement theory, show larger rotations of the capped-end. Thus, a second fitting term, based on the strain hardening parameter (n), is required for a reduction in error between

the analytic model and the large displacement theory finite element model. The second fitting function adjustment is shown in Equations 36 and 37 and implemented in Equation 38.

$$\delta_{(T)}^{total} = \frac{4a}{E}\left[\left(\frac{pR_i^2}{2R_m t} + \frac{P_A}{A} + \gamma p\right)V_{1(T)}\right] + \alpha\varepsilon_o a h_2^T \left[\frac{P(1+\lambda f_1)}{P_o}\right]^n \quad \text{(Eqn. 34)}$$

$$f_1 = 3 - 3\left(\frac{\theta}{\pi}\right) + \left(\frac{\theta}{\pi}\right)^2 \quad \text{(Eqn. 35)}$$

$$\beta = 0.0425(n-1) - 0.00325(n-1)^2 \quad \text{(Eqn. 36)}$$

$$f_2 = 1 + \beta \quad \text{(Eqn. 37)}$$

$$\delta_{(T)}^{total} = \left\{\frac{4aV_{1(T)}}{E}\left[f_2\left(\frac{pR_i^2}{2R_m t} + \gamma p\right) + \frac{P_A}{A}\right] + f_2\alpha\varepsilon_o a h_2^T \left[\frac{P(1+\lambda f_1)}{P_o}\right]^n\right\} \quad \text{(Eqn. 38)}$$

While the second fitting function, Equation 37, is currently based only on the strain hardening behavior of the material, it should be noted that this is only for the assumption of a free-ended boundary condition.

2.1.14 Combined Axial Load due to Internal Pressure with an Applied Bending Moment

While Equation 38 provides the results for a cap-ended pipe with axial load due to internal pressure and crack face pressure, the subsequent application of a bending moment is discussed in this section. If Equation 38 is recast into the elastic and plastic portions, the result is shown in Equation 39.

$$\delta_{(T)}^{total} = \frac{4a}{E}\left[\left(\frac{f_2 pR_i^2}{2R_m t} + \frac{P_A}{A} + f_2\gamma p\right)V_{1(T)}\right] + \alpha\varepsilon_o a h_2^T f_2 \left[\frac{P(1+\lambda f_1)}{P_o}\right]^n \quad \text{(Eqn. 39)}$$

As discussed earlier for the axial load solution, an adjustment is required for the bending moment to correct for the difference between small strain solutions and large strain behavior. This correction is shown in Equation 40. Because elastic stresses can be added linearly, the total elastic COD is then given by Equation 41; and, the plastic COD due to tension is given in Equation 42.

$$f_3 = 1 + 2\beta \quad \text{(Eqn. 40)}$$

$$\delta^{(el)} = \frac{4a}{E}\left[\left(\frac{f_2 pR_i^2}{2R_m t} + \frac{P_A}{A} + f_2\gamma p\right)V_{1(T)} + f_3\frac{M_{app}R_m}{I}V_{1(B)}\right] \quad \text{(Eqn. 41)}$$

$$\delta_{(Tension)}^{(pl)} = \alpha\varepsilon_o a h_2^T f_2 \left[\frac{P(1+\lambda f_1)}{P_o}\right]^n \quad \text{(Eqn. 42)}$$

A concept of equivalent moment is now introduced. This equivalent moment is the moment required to obtain the same plastic COD implied by Equation 42. For reference, the limit moment, M_0, (i.e., the moment at which the uncracked ligament becomes a fully plastic hinge) for a pipe with a through-wall crack under moment loading is given in Equation 43, and the plastic COD due to bending is given by Equation 43a. The equivalent moment is then determined by equating the bending and tension plastic COD's and recasting it as Equation 44.

$$M_o = 4\sigma_o R_m^2 t\left[cos\left(\frac{\theta}{2}\right) - \frac{1}{2}sin(\theta)\right] \quad \text{(Eqn. 43)}$$

$$\delta_{(Bending)}^{(pl)} = \alpha\varepsilon_o a h_2^B f_3 \left[\frac{M}{M_o}\right]^n \quad \text{(Eqn. 43a)}$$

$$M_{eq} = M_o \left[\frac{\delta_{(Tension)}^{(pl)}}{f_3\alpha\varepsilon_o a h_2^B}\right]^{(1/n)} \quad \text{(Eqn. 44)}$$

Once the equivalent moment is determined for the plastic COD due to tension, a total effective moment can be calculated using Equation 45. Equation 46 provides the final total COD solution using the form of the GE/EPRI method.

$$M_{eff} = M_{eq} + M_{app} \quad \text{(Eqn. 45)}$$

$$\delta^{total} = \frac{4a}{E}\left[\left(\frac{f_2 p R_i^2}{2R_m t} + \frac{P_A}{A} + f_2 p\gamma\right)V_{1(T)} + f_3\frac{M_{app}R_m}{I}V_{1(B)}\right] + f_3\alpha\varepsilon_o a h_2^B\left[\frac{M_{eff}}{M_o}\right]^n \quad \text{(Eqn. 46)}$$

2.1.15 Preliminary Verification

The elastic influence functions and the plastic influence functions along with Equation 46 were coded in Fortran subroutines (CrCOD_v2_R140318.f90). As part of a preliminary validation, a driver program was written to exercise the subroutines with various pipe geometry values, material property values, and load conditions. Linear interpolation was used to calculate the influence functions for the different R_m/t, θ/π, and n values. The results of these comparisons are presented in the following subsections and lead to an additional correction term.

2.1.15.1 xLPR Version 1.0 Routine

Comparisons of the COD calculation subroutines from the xLPR Version 1.0 code, CALC_COD, were made to the FEA non-linear analyses used in the development of the Version 2.0 COD model. Because the subroutines from Version 1.0 neglected crack face pressure, the FEA for these comparisons did not include crack face pressure. The GE/EPRI solutions from References

10 and 11 had a limited range for the normalized crack length, i.e., θ/π less than or equal to 0.5. Figure 28 shows the results of the xLPR Version 1.0 code compared with non-linear FEA within this range of normalized crack lengths. If confined to this design space, the results from the analytic solution appear to be representative of the FEA solutions.

Figure 29 shows the results of COD comparisons between CALC_COD and FEA with a larger range of normalized crack lengths including values of 0.75 and 0.90. Once the CALC_COD from xLPR Version 1.0 code exceeds the original GE/EPRI design space, the results become non-representative of the FEA results. This phenomenon is not acceptable for probabilistic analyses, where the analysis space may yield normalized crack lengths greater than 0.5. As noted previously, the design space for the *xLPR Version 2.0* COD module, CrCOD, was increased to include normalized crack lengths (θ/π) up to 0.90.

2.1.15.2 Revised xLPR Routine (xLPR Version 2.0 Routine)

Results from the current analytical solutions (CrCOD) were compared to FEA results. Two sets of FEA results were used in the analysis. The FEA results shown in Figure 30 are the same results used to compare against the xLPR Version 1.0 results and contained no crack face pressure. For the CrCOD analysis comparison to these results, gamma was set equal to zero. As shown in Figure 30, the CrCOD fitted elastic and plastic functions are reasonable, when compared to the FEA.

A second set of FEA results were generated which contained crack face pressure equal to half the internal pipe pressure. Results from CrCOD using gamma equal to 0.5 were compared to these FEA results. Again, as shown in Figure 31, the results are reasonable when compared with the FEA results.

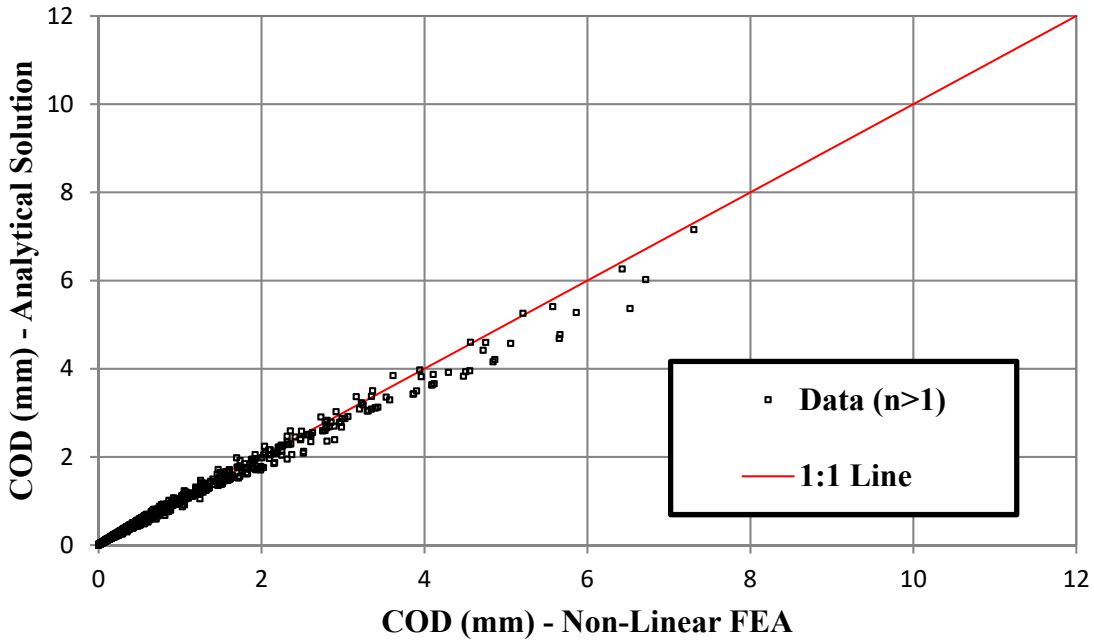

Figure 28. COD without crack face pressure (γ = 0) of xLPR Version 1.0 CALC_COD versus non-linear FEA for normalized crack lengths (θ/π) of 0.05 to 0.50

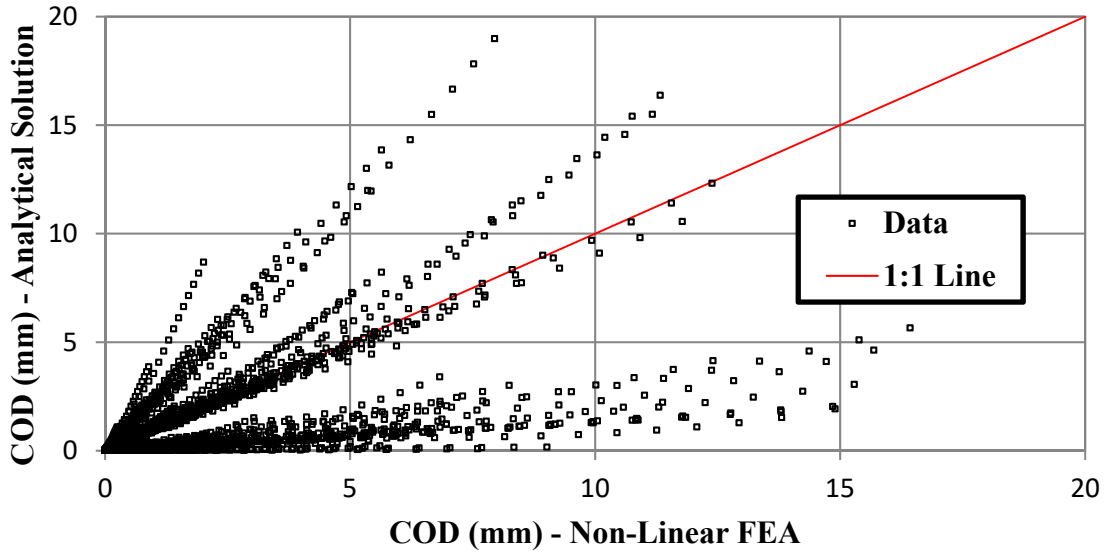

Figure 29. COD without crack face pressure (γ = 0) of xLPR Version 1.0 CALC_COD versus non-linear FEA for normalized crack lengths (θ/π) of 0.05 to 0.90

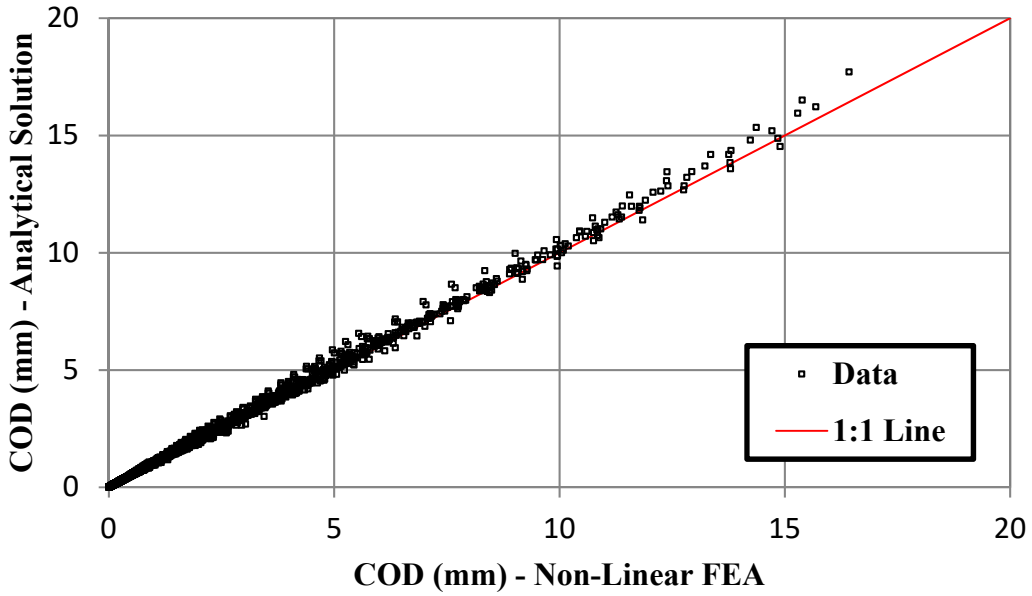

Figure 30. COD without crack face pressure (γ = 0) of xLPR Version 2.0 versus non-linear FEA for normalized crack lengths (θ/π) of 0.05 to 0.50

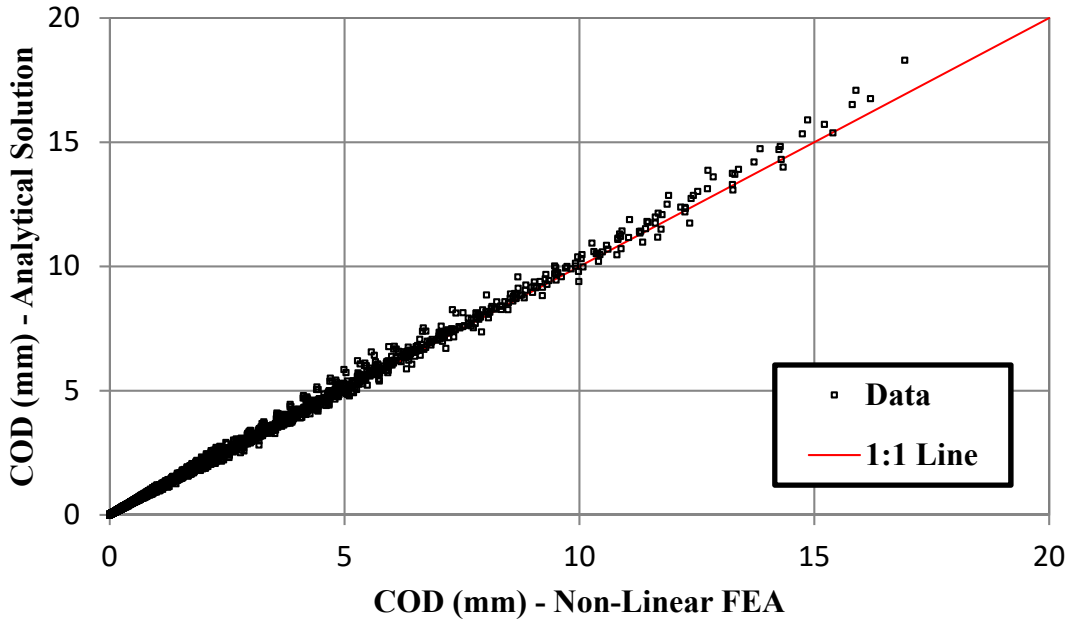

Figure 31. COD with crack face pressure (γ = 0.5) of xLPR Version 2.0 versus non-linear FEA for normalized crack lengths (θ/π) of 0.05 to 0.50

2.1.16 Empirical Correction to Test Data

While preliminary comparison of the analytical equations to non-linear FEA show good agreement, this section focuses on the results of preliminary validation of the analytical solutions to a small set of experimental results. A suite of experiment results ranging from pure tension to pure bending to tension plus bending was used for comparison. Table 15 provides the data set used for this preliminary validation. The information for these specimens was obtained from the Pipe Fracture Database [19].

Table 15. Characteristics of the circumferential through-wall cracked pipe experiments used in the preliminary validation of the CrCOD model (Version 2.0)

Specimen ID	Units	4131-1	4121-1	4111-6	1.1.1-24	4111-2	1.1.1-26	1-8
Base Material	-	304 SS	304 SS	A516 Gr70 / CS	SA 333 Gr6 / CS	A155-KC60 / CS	316L SS	A106 Gr-B CS
Weld	-	No	No	No	Yes	No	No	No
OD	(mm)	166.4	168.1	910.1	612.0	711.0	106.2	399.3
Wall	(mm)	13.4	12.9	72.84	31.3	23.6	8.3	26.2
θ/π	-	0.370	0.386	0.370	0.079	0.37	0.244	0.120
Temperature	(C)	287.8	287.8	287.8	287.8	287.8	21	287.8
Internal Pressure	(MPa)	17.235	Increasing	0	0	0	0	15.5
Gamma	-	0	0	0	0	0	0	1.0
R_m/t	-	5.71	6.02	5.75	9.28	14.6	5.9	7.12
Yield Strength	(MPa)	139.0	139.0	210.0	229.0	231.0	254.0	216.5
Ultimate Strength	(MPa)	450.0	450.0	510.0	525.0	544.0	532.0	506.1
alpha	-	9.69	9.69	2.07	2.14	1.15	5.50	2.37
n	-	3.13	3.13	5.20	4.36	5.55	4.76	4.03
E	(GPa)	182.9	182.9	206.3	200.0	206.3	157.5	206.3
σ_f	(MPa)	294.5	294.5	360.0	377.0	387.5	393.0	361.1
M_o (flow stress)	(N-mm)	3.48E7	N/A	6.93E9	3.46E9	1.63E9	1.82E7	1.05E9
P_o (flow stress)	(N)	6.20E5	5.63E5	N/A	N/A	N/A	N/A	8.46E6
Span (Inner)	(mm)	1220	N/A	3350	3350	3350	610	3350
Span (Outer)	(mm)	3200	N/A	11580	11580	11580	1524	11580
R_o	(mm)	83.2	84.1	455.1	306.0	355.5	53.1	199.7
R_m	(mm)	76.5	77.6	418.6	290.4	343.7	49.0	186.6
R_i	(mm)	69.8	71.2	382.2	274.7	331.9	44.8	173.5
Test Type*	-	FP + 4B	IP	4B	4B	4B	4B	FP + 4B

* IP–Increasing Pressure; FP–Fixed Pressure; 4B–4 Point Bend

One of the focus areas for this preliminary validation was the equations for the collapse load and collapse moment shown in Equations 47 and 48, respectively. While these equations are commonly considered the equations at which the entire uncracked ligament for a circumferential TWC in a pipe achieves some significant level of plastic deformation, the value of stress (σ_x) used in this equation is more ambiguous. Other researchers in References 20 and 21 have completed similar investigations. Based on this ambiguity, two values of stress were investigated for each experiment. For homogeneous pipe sections, these values coincided with either the yield stress

or the flow stress of the material at the experimental test temperature. For welded sections of pipe, these values coincided with either the yield stress or the flow stress of the pipe base-material at the experimental test temperature.

$$P_o = 2\sigma_x R_m t\left\{\pi - \theta - 2sin^{-1}\left[\frac{1}{2}sin(\theta)\right]\right\} \quad \text{(Eqn. 47)}$$

$$M_o = 4\sigma_x R_m^2 t\left[cos\left(\frac{\theta}{2}\right) - \frac{1}{2}sin(\theta)\right] \quad \text{(Eqn. 48)}$$

Using Equations 47 and 48, the COD values are then calculated using Equation 46. For the sensitivity analysis, Equation 49 shows the definition of the effective ultimate tensile strength. This effective ultimate tensile strength was used to vary the flow stress calculated in Equation 50.

$$\sigma_{eff} = \sigma_y + x\left(\sigma_u - \sigma_y\right) \quad \text{(Eqn. 49)}$$

$$\sigma_x = \frac{\sigma_y + \sigma_{eff}}{2} \quad \text{(Eqn. 50)}$$

Thus, when x=1, Equation 49 reduces to the ultimate tensile strength and Equation 50 reduces to the traditional flow stress which is the average of the yield and ultimate strengths. When x=0 in Equation 49, Equation 50 reduces to the yield strength. Based on the observation of the sensitivity study for Experiment 4131-1 (Figure 32), an approximate value for x of 0.25 was investigated. In addition, a second investigation was completed with an alternate form for flow stress, Equation 51, and a value for f_4 of 1.15 was used as shown in Equation 52.

$$\sigma_x = f_4\sigma_y \quad \text{(Eqn. 51)}$$

Figure 33 through Figure 39 show the results of the analyses when these alternative forms of flow stress were used. A review of the analysis results and engineering judgment suggests that Equations 51 and 52 should be used as an experimental correction factor, rather than a modification to the yield stress to provide the best estimate of COD. Thus Equation 52 provides the empirical correction to the COD formulation.

$$f_4 = 1.15 \quad \text{(Eqn. 52)}$$

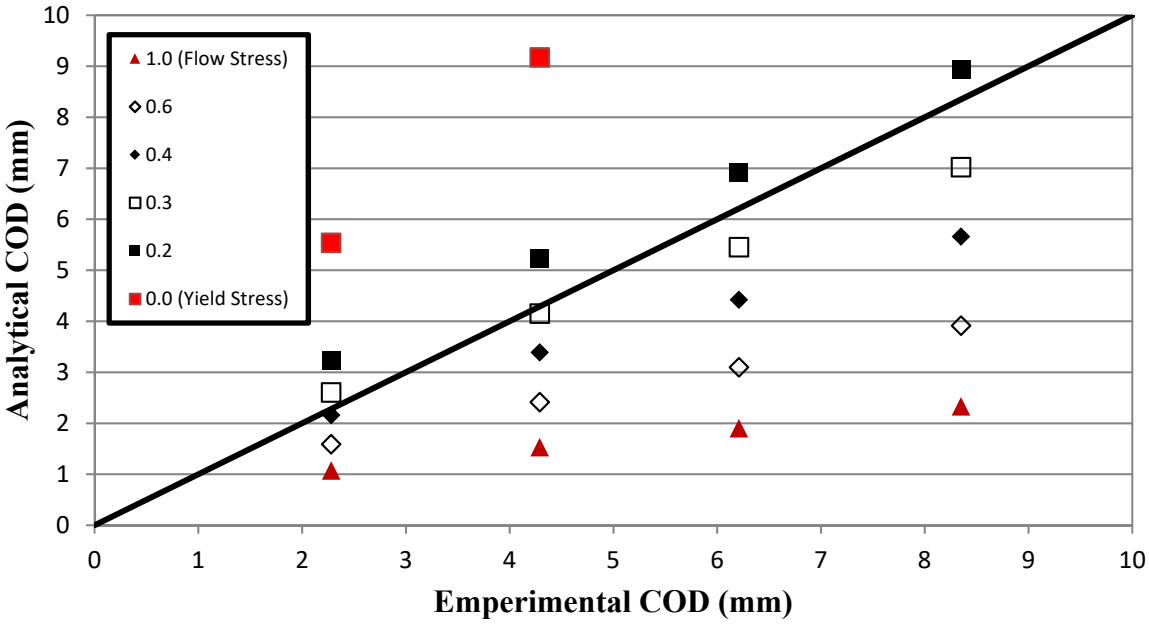

Figure 32. Experiment 4131-1 sensitivity analysis on "x" from Equation 49

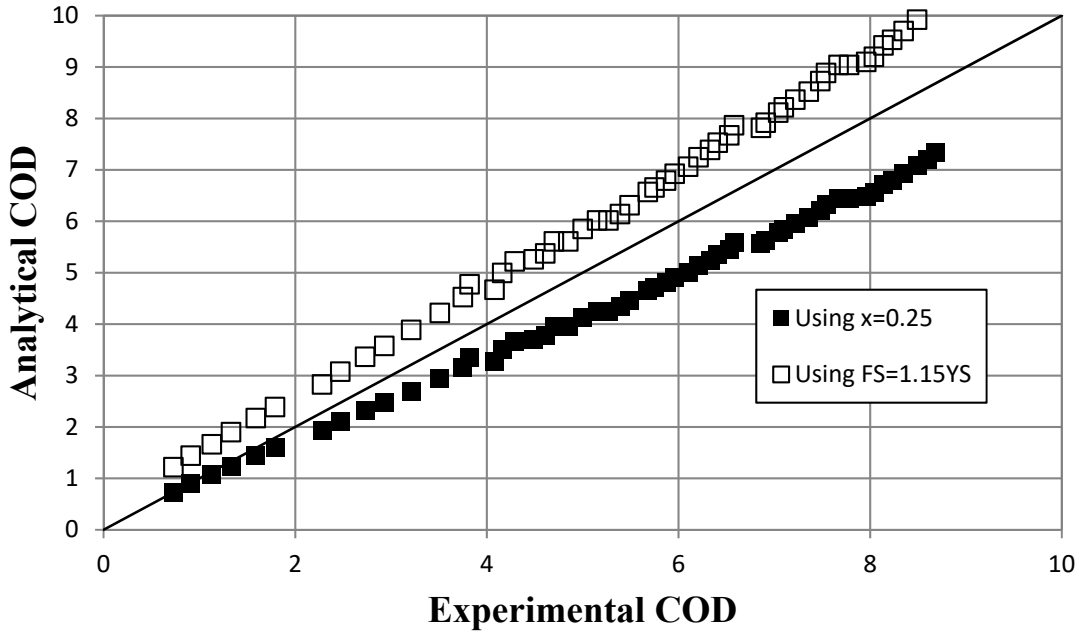

Figure 33. Experiment 4131-1 alternative flow stress forms

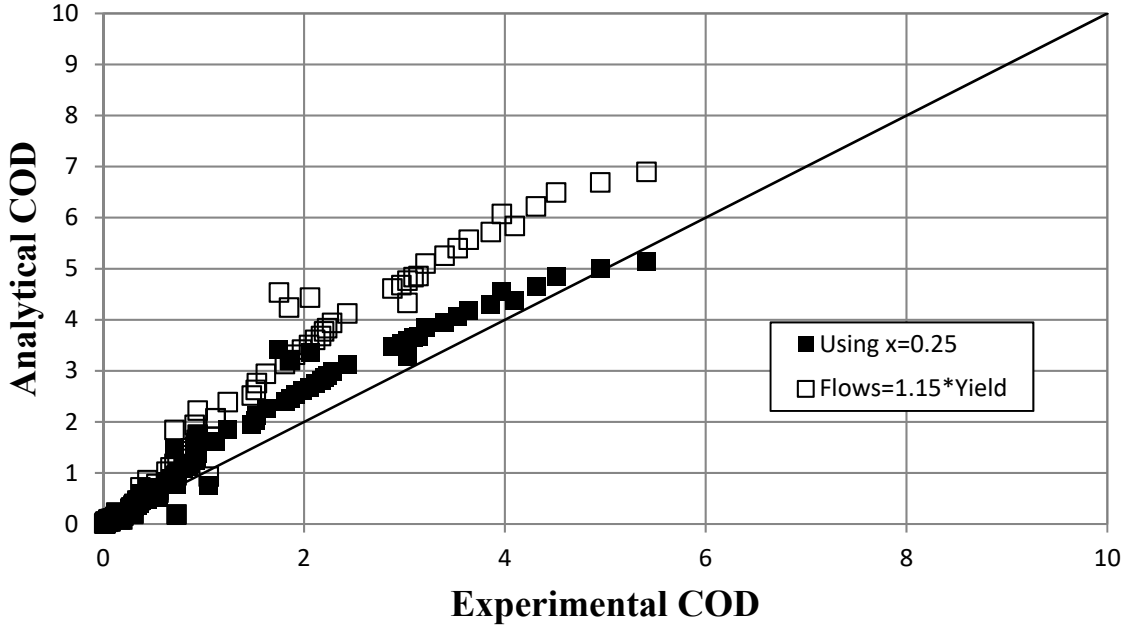

Figure 34. Experiment 4121-1 alternative flow stress forms

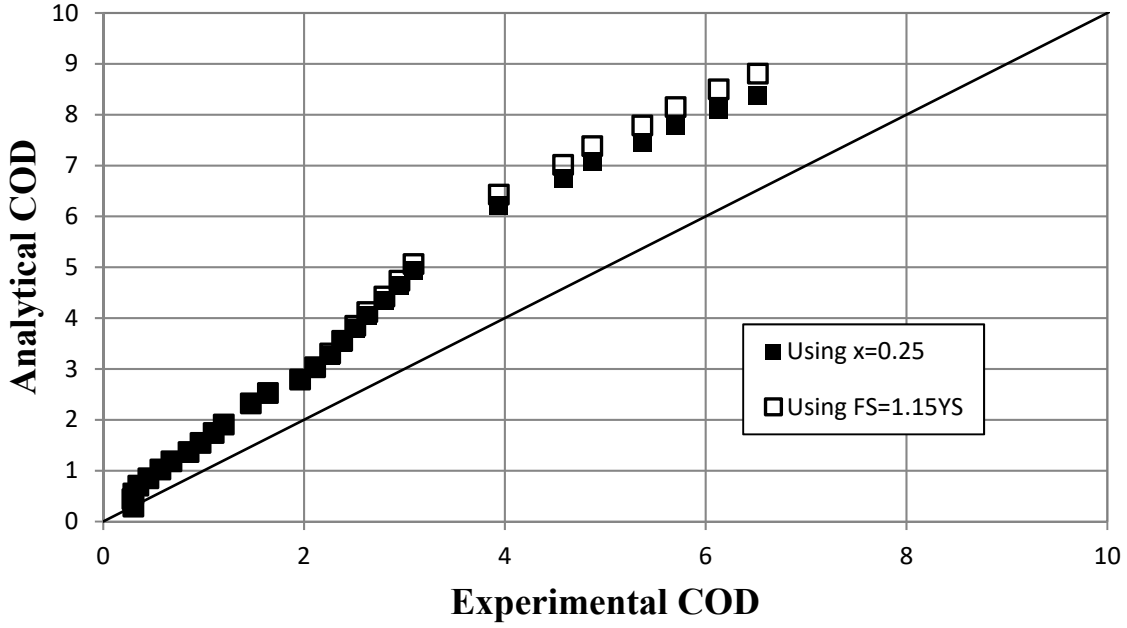

Figure 35. Experiment 4111-6 alternative flow stress forms

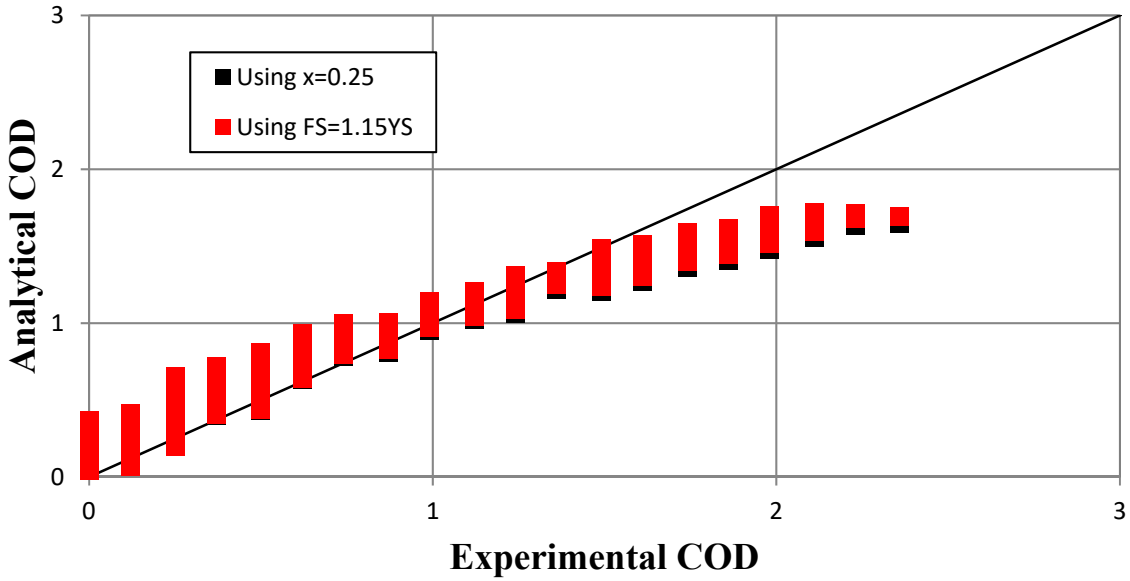

Figure 36. Experiment 1.1.1.24 alterative flow stress forms

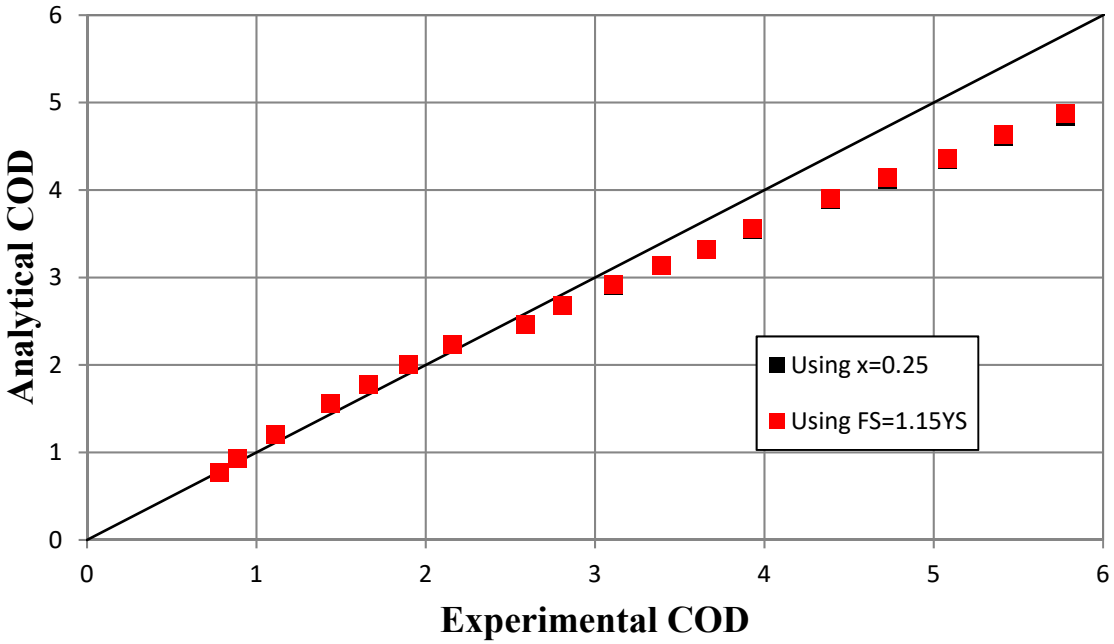

Figure 37. Experiment 4111-2 alternative flow stress forms

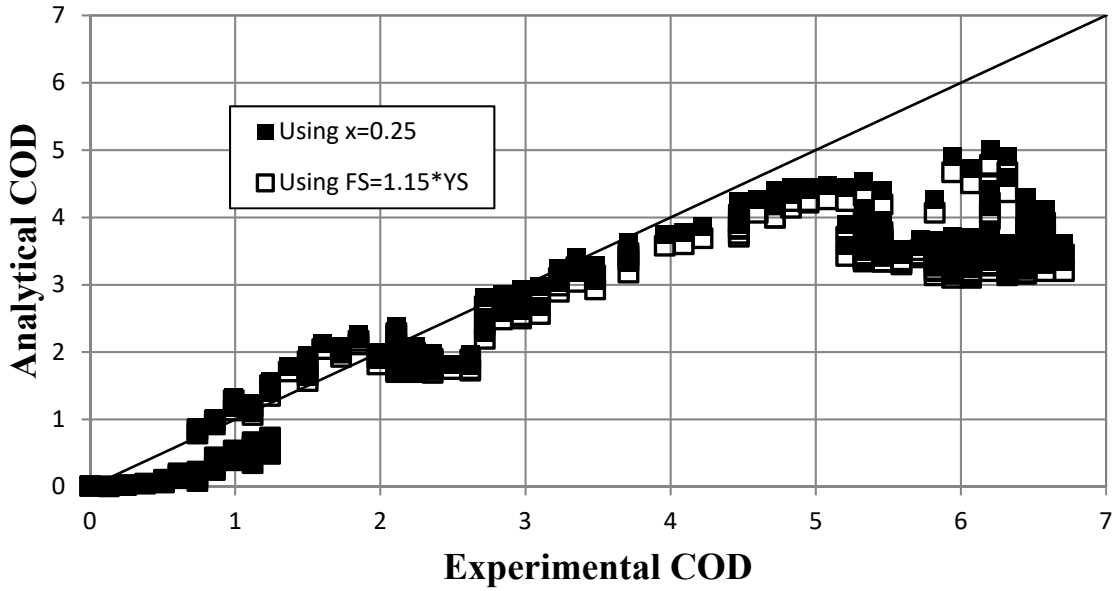

Figure 38. Experiment 1.1.1.26 alternative flow stress forms

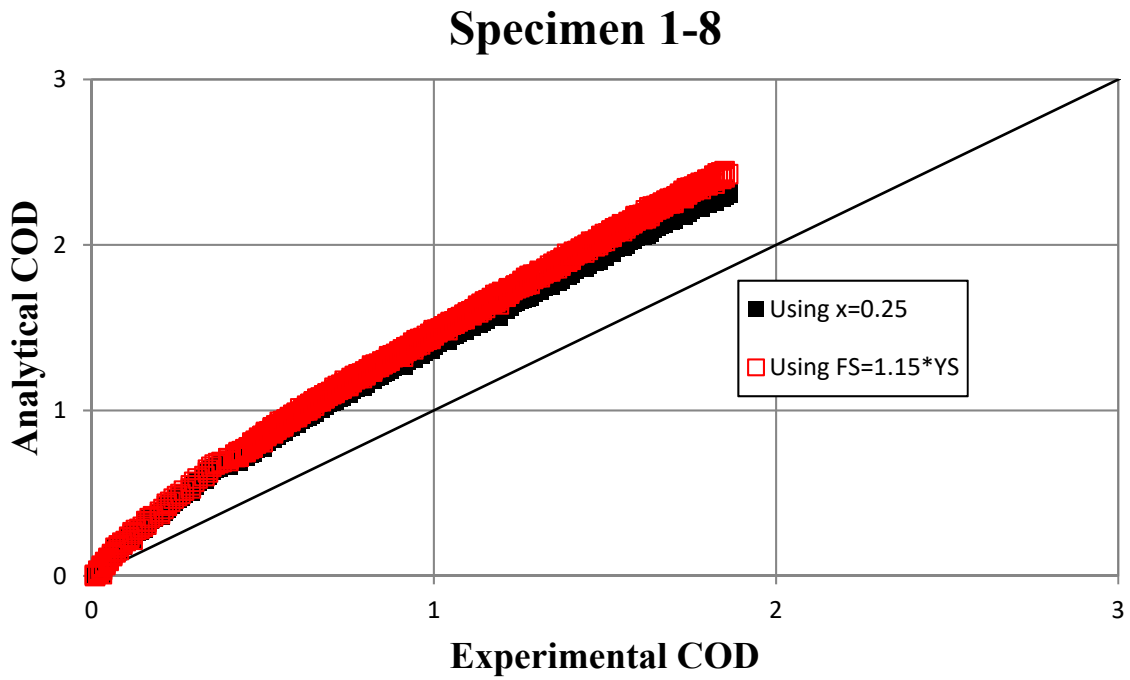

Figure 39. Experiment 1-8 alternative flow stress forms

2.1.17 Final Equations

The final equations used in the xLPR Version 2.0 CrCOD subroutine are summarized as Equations 53 through 68.

While preliminary validation of the analytical equations to non-linear FEA has been provided in previous sections, this section focuses on the results. Based on these equations, Figure 40 shows the final results of the preliminary validation.

$$\sigma_o = \sigma_y \quad \text{(Eqn. 53)}$$

$$M_o = 4\sigma_o R_m^2 t\left[cos\left(\frac{\theta}{2}\right) - \frac{1}{2}sin(\theta)\right] \quad \text{(Eqn. 54)}$$

$$P_o = 2\sigma_o R_m t\left\{\pi - \theta - 2sin^{-1}\left[\frac{1}{2}sin(\theta)\right]\right\} \quad \text{(Eqn. 55)}$$

$$P = \frac{P_A}{A} + \pi R_i^2 p \quad \text{(Eqn. 56)}$$

$$\gamma = \frac{p_{cf}}{p} = 0.5 \quad \text{(Eqn. 57)}$$

(Note: 0.5 is hardcoded into the software)

$$P_{CFP} = 2\gamma p\theta R_m t \quad \text{(Eqn. 58)}$$

$$\lambda = \frac{P_{CFP}}{P} \quad \text{(Eqn. 59)}$$

$$f_1 = 3 - 3\left(\frac{\theta}{\pi}\right) + \left(\frac{\theta}{\pi}\right)^2 \quad \text{(Eqn. 60)}$$

$$\beta = 0.0425(n-1) - 0.00325(n-1)^2 \quad \text{(Eqn. 61)}$$

$$f_2 = 1 + \beta \quad \text{(Eqn. 62)}$$

$$f_3 = 1 + 2\beta \quad \text{(Eqn. 63)}$$

$$f_4 = 1.15 \quad \text{(Eqn. 64)}$$

$$\delta_{(Tension)}^{(pl)} = \left(\frac{1}{f_4}\right)^n \alpha\varepsilon_o a h_2^T f_2 \left[\frac{P(1+\lambda f_1)}{P_o}\right]^n \quad \text{(Eqn. 65)}$$

$$M_{eq} = f_4 M_o \left[\frac{\delta_{(Tension)}^{(pl)}}{f_3 \alpha\varepsilon_o a h_2^B}\right]^{(1/n)} \quad \text{(Eqn. 66)}$$

$$M_{eff} = M_{eq} + M_{app} \quad \text{(Eqn. 67)}$$

$$\delta^{total} = \left\{\frac{4a}{E}\left[\left(\frac{f_2 p R_i^2}{2R_m t} + \frac{P_A}{A} + f_2 p\gamma\right)V_{1(T)} + f_3 \frac{M_{app} R_m}{I} V_{1(B)}\right] + \left(\frac{1}{f_4}\right)^n f_3 \alpha\varepsilon_o a h_2^B \left[\frac{M_{eff}}{M_o}\right]^n\right\} \quad \text{(Eqn. 68)}$$

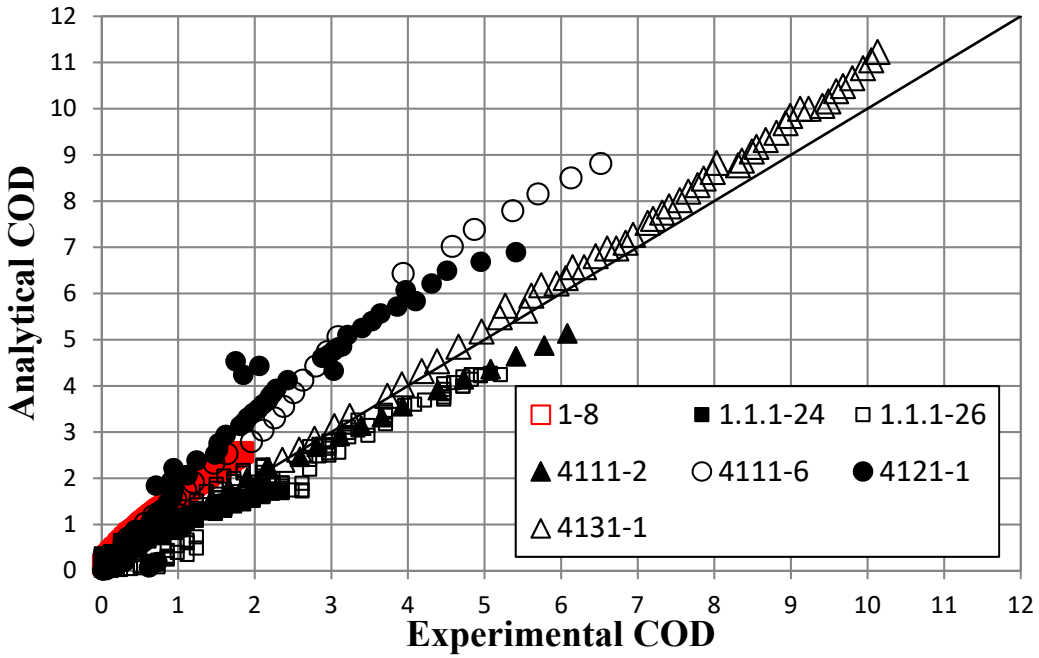

Figure 40. Final results from preliminary validation of xLPR Version 2.0 of the CrCOD model

2.2 AxCOD Model

As was the case for the CrCOD model, the approach for estimating COD for axially oriented cracks relies upon the so-called "GE/EPRI methodology", where fully-elastic and fully-plastic solutions are developed based upon finite element modeling. The resulting equations provide a computationally-efficient method to estimate the finite element solution, and hence, axial crack COD in a pipe.

2.2.1 Axial Crack COD Model

The geometry and loading conditions for the axial crack COD model developed here are illustrated in Figure 41. The finite element models upon which the methodology is based did not include weld residual stress (WRS) as a loading condition. The method of accounting for WRS is an approximation and is described in Section 2.2.2.

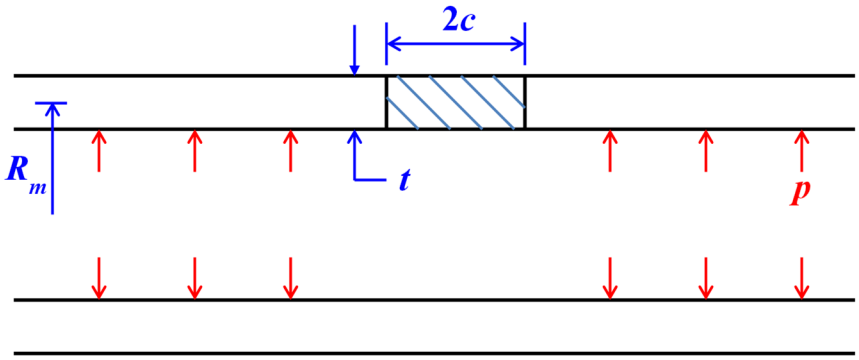

Figure 41. Geometry and loading conditions assumed for axial crack COD model

Material properties are characterized according to the Ramberg-Osgood relationship as defined previously in Equation 7.

The elastic solution for axial COD, δ^{el}, is given by:

$$\delta^{el} = \frac{4}{E}\sigma^{\infty} c V_1 \qquad \text{(Eqn. 69)}$$

where, E is the elastic modulus, $\sigma^{\infty} = (pR_m)/t$ is the remote stress for Mode I crack opening, c is half the axial crack length, and V_1 is the elastic influence function [22]. The fully-plastic COD solution, δ^{pl}, is given by:

$$\delta^{pl} = \alpha \varepsilon_0 c h_2 \left[\frac{p}{p_L}\right]^n \qquad \text{(Eqn. 70)}$$

where h_2 is the plastic influence function, p is the internal pipe pressure, and p_L is the limit pressure, see Equation 71 [22].

$$p_L = \frac{2}{\sqrt{3}}\sigma_y\left(\frac{t}{R_m}\right)\frac{1}{\sqrt{1+0.34\rho+1.34\rho^2}} \quad \text{(Eqn. 71)}$$

In Equation (71), σ_y is the yield stress, R_m is the pipe mean radius, t is the pipe wall thickness, and $\rho = c/\sqrt{R_m t}$ [22] is the normalized crack length for the axial crack. The total COD, δ^{total}, is given by:

$$\delta^{total} = \delta^{el} + \delta^{pl} \quad \text{(Eqn. 72)}$$

The V_1 and h_2 parameters were determined based upon finite element models. V_1 is a function of R_m/t and the normalized crack length, ρ. The h_2 parameter is a function of R_m/t, n, and ρ. It should be noted that these parameters are not functions of Ramberg-Osgood parameters ε_0, σ_0, and α.

Table 16 shows a matrix of the finite element models created to develop the appropriate V_1 and h_2 functions for application in the xLPR CALC_AxCOD_V2 subroutine.

To check that the procedures for finding the V_1 function are correct, the case for $R_m/t = 5$ is compared with Kim's solution [22] in Figure 42. Because of differences in how Kim et al. defined the □∞ term, it is expected that there will be a factor of 2.22 difference between Kim and AxCOD. Looking at Figure 42, we, indeed, find that the Kim data is 2.22 times the AxCOD Mid V data.

Table 16. Analysis matrix for determining axial crack COD influence functions V1 and h2

R/t	*ρ*	*n*
2	0.5	2, 3, 5, 7, and 10
	1	2, 3, 5, 7, and 10
	2	2, 3, 5, 7, and 10
	3	2, 3, 5, 7, and 10
5	0.5	2, 3, 5, 7, and 10
	1	2, 3, 5, 7, and 10
	2	2, 3, 5, 7, and 10
	3	2, 3, 5, 7, and 10
10	0.5	2, 3, 5, 7, and 10
	1	2, 3, 5, 7, and 10
	2	2, 3, 5, 7, and 10
	3	2, 3, 5, 7, and 10

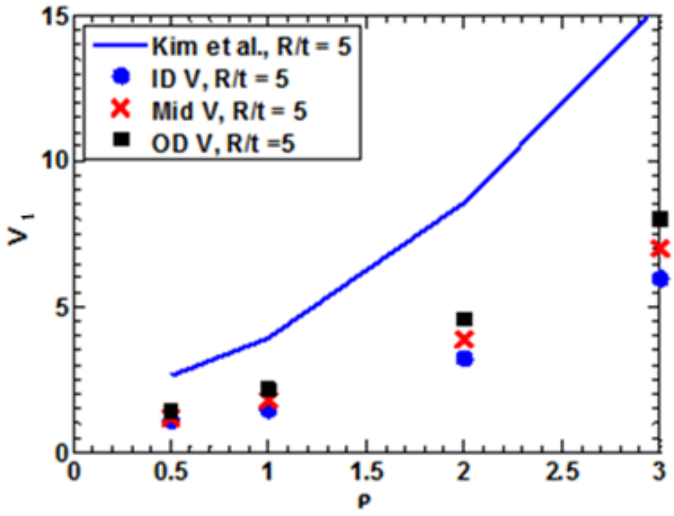

Figure 42. Comparison of elastic influence function V_1 between Kim [22] and this study as a function of normalized crack length (ρ) for $R_m/t = 5$

Figure 43 and Figure 44 show the plastic influence function for axial cracks, h_2, versus normalized pressure for two values of *n (n = 2 and n = 10)* and R_m/t = 5. The asymptotic behavior indicates that the model has become fully plastic (i.e., the elastic strains are negligible everywhere in the body). The value of p/p_L required to reach the fully-plastic solution changes with the *n* value. For the *n* = 10 case, the finite element results can become unstable at high values of internal pressure.

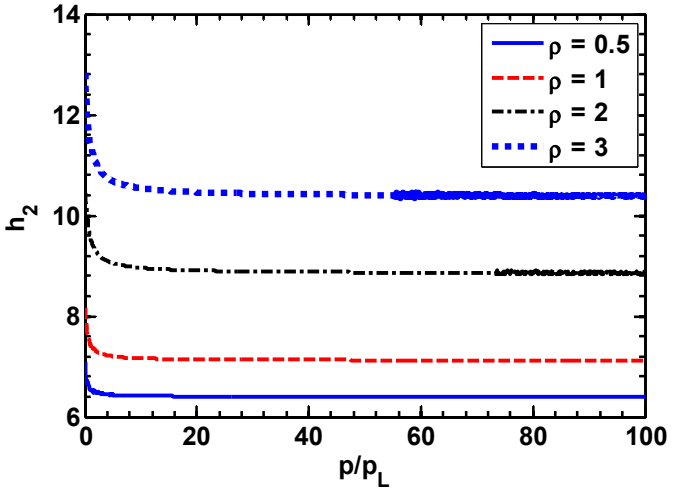

Figure 43. Plastic influence function h_2 on the OD surface as a function of internal pipe pressure for $R_m/t = 5$ and n = 2

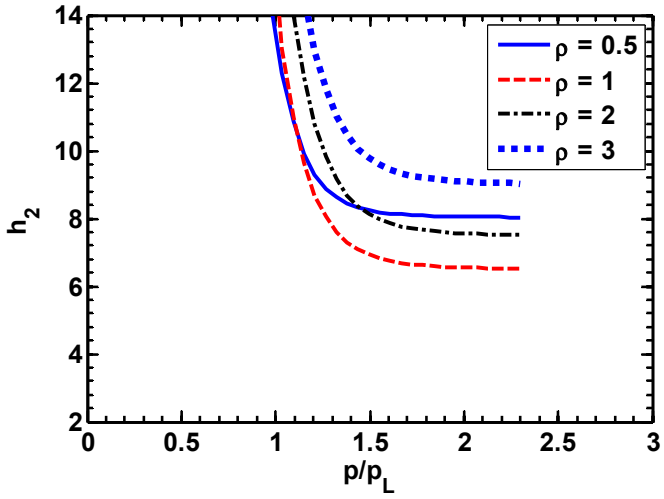

Figure 44. Plastic influence function h_2 on the OD surface as a function of internal pipe pressure for $R_m/t = 5$ and $n = 10$

Figure 45 thru Figure 47 compare the current h_2 results and the h_2 values from the previous work of Kim *et al.* [22]. The results of this work show reasonable agreement with the previous solutions.

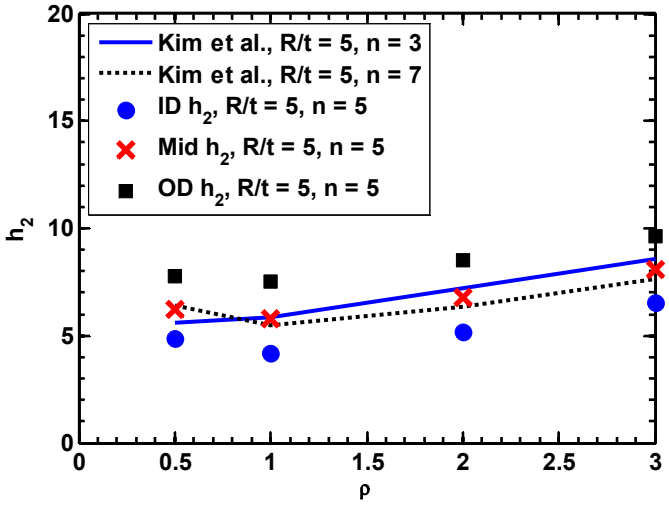

Figure 45. Comparison of h_2 results from this study versus h_2 results from Kim [22] for $R_m/t = 5$ and $n = 5$

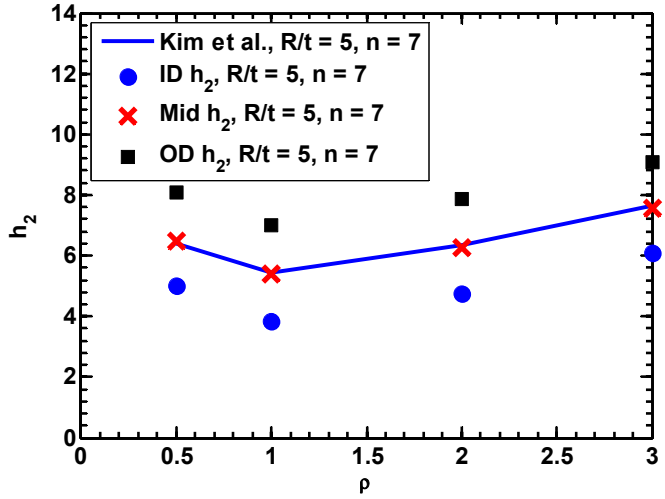

Figure 46. Comparison of h_2 results from this study versus h_2 results from Kim [22] for $R_m/t = 5$ and $n = 7$

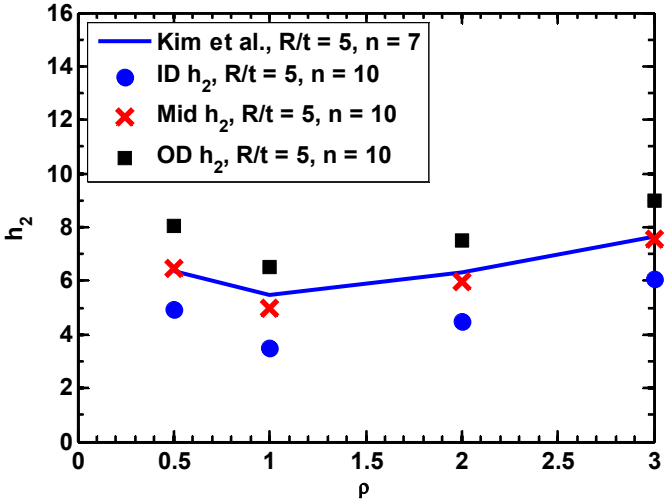

Figure 47. Comparison of h_2 results from this study versus h_2 results from Kim [22] for $R_m/t = 5$ and $n = 10$

Table 17 through

R_m/t	ρ	V_1	h_2 (n=2)	h_2 (n=3)	h_2 (n=5)	h_2 (n=7)	h_2 (n=10)
2	**0.5**	1.163	4.712	5.136	5.576	5.614	5.227
	1	1.742	5.201	5.362	5.140	4.600	3.823
	2	3.667	6.199	5.831	4.996	4.261	3.401
	3	6.207	6.977	6.300	5.133	4.193	3.101
5	**0.5**	1.204	5.133	5.656	6.245	6.487	6.443
	1	1.786	5.546	5.849	5.781	5.376	4.983

	2	3.893	7.178	7.262	6.801	6.276	5.979
	3	6.976	8.802	8.653	8.058	7.558	7.543
10	**0.5**	1.215	5.226	5.767	6.267	6.455	7.094
	1	1.799	5.619	5.940	5.722	5.133	5.123
	2	3.959	7.502	7.727	7.222	6.646	8.168
	3	7.208	9.478	9.611	9.276	8.966	8.386

Table 19 list the V_1 and h_2 values developed for each R_m/t, ρ, n, and through-thickness location.

Table 17. Axial crack influence functions for the ID surface

R_m/t	ρ	V_1	h_2 (n=2)	h_2 (n=3)	h_2 (n=5)	h_2 (n=7)	h_2 (n=10)
2	**0.5**	1.081	3.913	4.013	4.099	4.024	3.677
	1	1.400	3.687	3.715	3.488	3.074	2.516
	2	2.910	4.608	4.271	3.614	3.071	2.431
	3	5.035	5.459	4.921	3.996	3.258	2.403
5	**0.5**	1.078	4.211	4.527	4.891	5.015	4.932
	1	1.467	4.096	4.257	4.174	3.844	3.508
	2	3.225	5.595	5.601	5.163	4.730	4.489
	3	5.966	7.269	7.082	6.544	6.106	6.076
10	**0.5**	1.082	4.311	4.683	5.030	5.155	5.580
	1	1.496	4.214	4.406	4.195	3.743	3.675
	2	3.314	5.909	6.055	5.584	5.099	6.237
	3	6.225	7.903	7.996	7.630	7.360	6.856

Table 18. Axial crack influence functions for the mid-thickness location

R_m/t	ρ	V_1	h_2 (n=2)	h_2 (n=3)	h_2 (n=5)	h_2 (n=7)	h_2 (n=10)
2	**0.5**	1.163	4.712	5.136	5.576	5.614	5.227
	1	1.742	5.201	5.362	5.140	4.600	3.823
	2	3.667	6.199	5.831	4.996	4.261	3.401
	3	6.207	6.977	6.300	5.133	4.193	3.101
5	**0.5**	1.204	5.133	5.656	6.245	6.487	6.443
	1	1.786	5.546	5.849	5.781	5.376	4.983
	2	3.893	7.178	7.262	6.801	6.276	5.979
	3	6.976	8.802	8.653	8.058	7.558	7.543
10	**0.5**	1.215	5.226	5.767	6.267	6.455	7.094

	1	1.799	5.619	5.940	5.722	5.133	5.123
	2	3.959	7.502	7.727	7.222	6.646	8.168
	3	7.208	9.478	9.611	9.276	8.966	8.386

Table 19. Axial crack influence functions for the OD surface

R_m/t	ρ	V_1	h_2 (n=2)	h_2 (n=3)	h_2 (n=5)	h_2 (n=7)	h_2 (n=10)
2	**0.5**	1.405	6.350	6.914	7.472	7.495	6.959
	1	2.166	6.988	7.230	6.960	6.268	5.229
	2	4.485	7.967	7.505	6.468	5.534	4.413
	3	7.438	8.576	7.759	6.320	5.157	3.825
5	**0.5**	1.403	6.399	7.062	7.791	8.078	8.034
	1	2.139	7.123	7.541	7.512	6.982	6.519
	2	4.589	8.856	8.962	8.486	7.883	7.513
	3	8.009	10.400	10.249	9.625	9.059	9.012
10	**0.5**	1.384	6.305	6.966	7.587	7.845	8.660
	1	2.120	7.087	7.531	7.292	6.568	6.603
	2	4.615	9.149	9.400	8.907	8.215	10.218
	3	8.201	11.052	11.264	10.937	10.610	9.931

2.2.2 Weld Residual Stress

Because the finite element models used in this study did not include WRS as a loading condition, an effective pressure was introduced as an approximate method to account for WRS on COD. Future versions of xLPR may include improved methods to account for this effect. The requested WRS input is the through-thickness average of the WRS distribution, $\sigma_{WRS,avg}$. This value is added to the remote hoop stress due to internal pressure to calculate an effective remote stress, σ_{eff}^{∞}, as in Equation 73.

$$\sigma_{eff}^{\infty} = \frac{pR_m}{t} + \sigma_{WRS,avg} \qquad \text{(Eqn. 73)}$$

An effective pressure is then calculated, according to Equation 74.

$$p_{eff} = \frac{\sigma_{eff}^{\infty} t}{R_m} \qquad \text{(Eqn. 74)}$$

This effective pressure is then supplied to Equations 69 and 70.

2.2.3 Small-Scale Yielding Correction

Reference [22] discusses application of the small-scale yielding correction as in Equation 75.

$$c_e = c + \varphi r_y$$

$$\varphi = \frac{1}{1 + \left({}^{p}/_{p_l}\right)^2} \qquad \text{(Eqn. 75)}$$

$$r_y = \frac{1}{2\pi}\left(\frac{n-1}{n+1}\right)\left(\frac{K}{\sigma_y}\right)^2$$

where, c_e is half the effective crack length, r_y is the plastic zone size, K is the stress intensity factor, and σ_y is the yield stress. COD with the correction is calculated by Equation 76,

$$\delta = \frac{4}{E}\sigma^{\infty} c_e V_1(c_e) + \alpha\varepsilon_0 c h_2(n)\left[\frac{p}{p_L}\right]^n \qquad \text{(Eqn. 76)}$$

Figure 48 shows a comparison of finite element results and the present COD model calculations from this study without the small-scale yielding correction, while Figure 49 shows the comparison with the small-scale yielding correction.

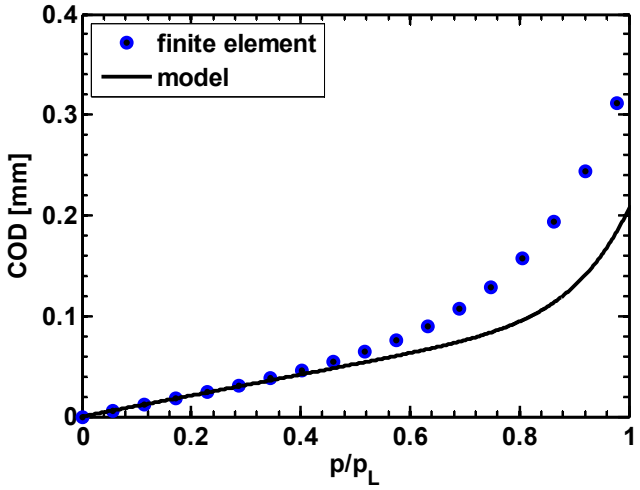

Figure 48. Finite element and model comparison at mid-thickness location without small-scale yielding correction for R_m/t =5 and n = 5

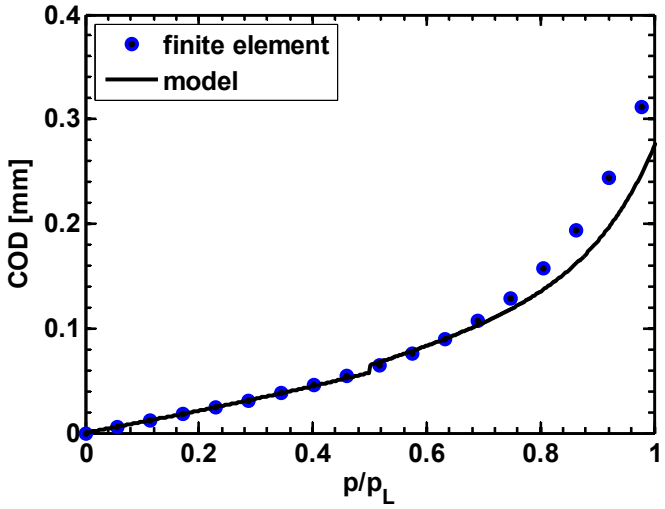

Figure 49. Finite element and model comparison at mid-thickness location with small-scale yielding correction for R_m/t =5 and n = 5

The agreement between the model and the finite element results improved with the implementation of the small scale yielding correction, for the case shown. The *n* = 2 case did not require the small-scale yielding correction. The model developed here predicts the finite element results well up to p/p_L = 0.6, as shown in Figure 49. As such, the axial crack COD module includes a warning check to ensure that p/p_L > 0.6 is not allowed.

2.2.4 Stress Intensity Factor Solution

Equation 75 requires a stress intensity factor solution to estimate the plastic zone size. The stress intensity factor solution for through-wall axial cracks in cylinders from the SINTAP solution [23] was implemented here. This solution provides the *K* values at two locations through the pipe thickness: the inner diameter location (K_{in}) and the outer diameter location (K_{out}). The procedure implemented in the axial crack COD module (AxCOD) uses the average of those two values as an estimate of the effective value. K_{in} and K_{out} are given by Equations 77 and 78, respectively,

$$K_{in} = \sigma^{\infty}\sqrt{\pi c}[G1(\rho) - g1(\rho)] \quad \text{(Eqn. 77)}$$

$$K_{out} = \sigma^{\infty}\sqrt{\pi c}[G1(\rho) + g1(\rho)] \quad \text{(Eqn. 78)}$$

where, *G*1 and *g*1 are given in Equations 79 and 80, respectively.

$$G1(\rho) = \sqrt{1 + 0.7044\rho + 0.8378\rho^2} \quad \text{(Eqn. 79)}$$

$$g1(\rho) = -0.035211 + 0.39394\rho - 0.20036\rho^2 + 0.028085\rho^3 \quad \text{(Eqn. 80)}$$

$$-0.0018763\rho^4 + \frac{3.912 - \ln(R_m/t)}{1.6094}(0.01566 - 0.05202\rho$$

$$+0.0381\rho^2 - 0.012782\rho^3 + 0.001246\rho^4)$$

The final value of the Mode I stress intensity factor, *K*, used in this work is given by Equation 81.

$$K = \frac{K_{in} + K_{out}}{2} \qquad \text{(Eqn. 81)}$$

3. MODULE DEVELOPMENT

3.1 Module Requirements

The specific requirements for the CrCOD and AxCOD modules were generated as part of the development process for the CrCOD SRD [1] and the AxCOD SRD [2] and are provided in tabular form in Table 1 and Table 2. The two sets of requirements were developed independently and thus vary somewhat due to the differences in crack driving forces (i.e., bending and axial stresses versus hoop stress). However, the computational approach and coding structures for these two modules are very similar. Those requirements appended with an asterisk at the end (i.e., RCCOD-8* thru RCCOD-12* and RAxCOD-13* thru RAxCOD-16*) are Framework interface or integration requirements. These requirements relate to the interfacing of the CrCOD or AxCOD module with the overhead DLL wrapper, the xLPR Computational Framework, the Inputs Database, or other Models Group modules, such as the Crack Growth or Leak Rate modules.

In addition, the CrCOD and AxCOD modules use the following interfaces:

- They receive information on pipe geometry from the Inputs Database
- They receive material property information from the Inputs Database
- They receive information on crack geometry from the Computational Framework
- They receive information on applied loads from the Inputs Database
- They output COD at the inner diameter, mid-thickness, and outer diameter locations to the Framework for subsequent use in leak rate calculations.
- The Framework performs actions based on error or warning flags provided by the modules
  - Errors should terminate the current simulation realization
  - Warnings should be logged for user interpretation.

3.2 Module Inputs and Outputs

The specific input and output variables used by the CrCOD Module are described in Table 20 and Table 21, respectively**.** Table 22 specifies a list of errors (the current simulation realization should terminate) and warnings (a log of the warning should be maintained for subsequent user interpretation)**.** The module relies on the xLPR Framework to sample any random variables and pass them to the module as input arguments.

Table 20. CrCOD module input parameters

Input Variable Name	Type	Description	Units	Value	Limits / Comments
METHOD	INTEGER	Allows for future use of other methods to calculate COD.	Unitless	0	0 is the only valid input at this time
Ro	Real*8	Outside Radius of Pipe	mm	Defined by the user	Ro > thick
Thick	Real*8	Wall Thickness of Pipe	mm	Defined by the user	Thick > 0
Theta	Real*8	TWC Half-crack angle	radians	Calculated by the Framework	0 < Theta < pi
RO_alpha	Real*8	alpha in the Ramberg-Osgood material stress-strain relation	unitless	Sampled by the Framework	RO_alpha >= 0
RO_sigYS	Real*8	σ_o in the Ramberg-Osgood material stress-strain relation	MPa	Sampled by the Framework	RO_sigYS > 0
RO_epso	Real*8	ε_o in the Ramberg-Osgood material stress-strain relation such that $\sigma_o = E\varepsilon_o$	unitless	Sampled by the Framework	RO_epso > 0
RO_n	Real*8	*n* in the Ramberg-Osgood material stress-strain relation (strain hardening exponent)	unitless	Sampled by the Framework	RO_n >= 0
pressure	Real*8	Internal Pressure	MPa	Supplied by the Framework from input loads	pressure >= 0
BM	Real*8	Applied Bending Moment	N-mm	Supplied by the Framework from input loads	BM >= 0
F_ax	Real*8	Axial Force (other than axial force due to internal pressure)	N	Supplied by the Framework from input loads	F_ax >=0

Table 21. CrCOD module output parameters

Output Variable Name	Type	Description	Units	Value	Limits / Comments
COD_ID	Real*8	COD at ID of pipe wall	mm	Calculated in Module	COD_ID > 0 If COD_ID = -1.0, then error
COD_MID	Real*8	COD at mid-wall of pipe	mm	Calculated in Module	COD_MID > 0 If COD_MID = -1.0, then error
COD_OD	Real*8	COD at OD of pipe wall	mm	Calculated in Module	COD_OD > 0 If COD_OD = -1.0, then error
i_err_code	Integer	Error and Warnings Flag	-	Set in Module	Values based on warning or error Value is 300 for no error / warning

**Note: Real is defined as a “kind” type in FORTRAN as selected_real_kind (P=13, R=300)

Table 22. Error and warning flags used in the CrCOD module

i_err_code value	Error / Warning	COD Reported	Description
300	N / A	As Calculated	Valid Solution - COD reported as calculated
101	Error	-1	Invalid Pipe Geometry
102	Error	-1	Invalid Crack Length
103	Error	-1	Invalid Material Properties
104	Error	-1	Applied Pressure or Bending < 0
105	Error	-1	Invalid Analysis Method Specified
106	Warning	As Calculated	Ramberg-Osgood n>10, calculations performed at 10
107	Warning	As Calculated	theta/pi > 0.90, calculations performed at 0.90
108	Warning	As Calculated	Mean-Radius / thickness < 2, calculation performed at 2
109	Warning	As Calculated	Mean-Radius / thickness > 20, calculation performed at 20
110	Warning	As Calculated	Ramberg-Osgood n<2, calculations performed at 2
201	Error	-1	At least one output was positive infinity
202	Error	-1	At least one output was negative infinity
203	Error	-1	At least one output was positive infinity and at least one output was negative infinity
204	Error	-1	At least one output was not-a-number
205	Error	-1	At least one output was not-a-number and at least one output was positive infinity
206	Error	-1	At least one output was not-a-number and at least one output was negative infinity
207	Error	-1	One output was not-a-number and one output was positive infinity and one output was negative infinity

The specific input and output variables used by the AxCOD Module are described in Table 23 and Table 24, respectively. The module relies on the xLPR Framework to sample any random variables and pass them to the module as input arguments.

Table 23. AxCOD module input parameters

Input Variable Name	Type	Description	Units	Value	Limits / Comments
Method	Integer	Method selection flag	unitless	0	Method = 0
Ro	Real	Outside radius of the pipe	mm	Defined by the user	2 <= Rm/thick<= 10, where Rm = Ro-thick/2
Thick	Real*	Pipe thickness	mm	Defined by the user	2 <= Rm/thick<= 10, where Rm = Ro-thick/2
RO_alpha	Real	Ramberg-Osgood parameter: strength coefficient	unitless	Sampled by the Framework	RO_alpha ≥ 0
RO_sigYS	Real	Ramberg-Osgood parameter: reference stress	MPa	Sampled by the Framework	RO_sigYS >0
RO_epso	Real	Ramberg-Osgood parameter: $\sigma_o = \sigma_{YS}/E$	unitless	Sampled by the Framework	RO_epso > 0
RO_n	Real	Ramberg-Osgood parameter: strain hardening exponent	unitless	Sampled by the Framework	2 ≤ RO_n ≤ 10
Pressure	Real	Internal pressure	MPa	Supplied by the Framework from input loads	0 ≤ Pressure/Po ≤ 0.6, where Po is the limit pressure
Sigh_WRS	Real	Hoop weld residual stress averaged through-wall	MPa	Sampled by the Framework	N/A
C	Real	Half crack length for an axial crack	mm	Calculated by the Framework	0.5 <= C/sqrt(Rm*thick) <= 3, where Rm = Ro-thick/2

*Note: Real is defined as a “kind” type in FORTRAN as selected_real_kind (P=13, R=300)

Table 24. AxCOD module output parameters

Output Variable Name	Type	Description	Units	Value	Limits / Comment
COD_ID	Real	Axial crack COD at inside surface	mm	Calculated in Module	COD_ID ≥ 0 If COD_ID = -1 then errors
COD_MID	Real	Axial crack COD at mid-wall	mm	Calculated in Module	COD_MID ≥ 0 If COD_MID = -1 then errors
COD_OD	Real	Axial crack COD at outside surface	mm	Calculated in Module	COD_OD ≥ 0 If COD_OD = -1 then errors
i_err_code	Integer	Error and Warnings Flag	-	Set in Module	Values will be based on the error. Value is 300 for no error / warning

3.3 Module Verification and Validation

This section summarizes the results from the Verification and Validation (V&V) exercises carried out on the CrCOD and AxCOD modules. Further details of the V&V activities can be found in the Software Test Plans (STP) [24, 25], Software Test Results Reports (STRR) [26, 27], and Module Validation Reports (MVR) [28, 29] for the CrCOD and AxCOD modules, respectively.

3.3.1 CrCOD Module Verification

The verification of the CrCOD module is documented in detail in the STRR for the CrCOD module [26]. The testing activity described in the STRR was intended to verify that the requirements specified in the CrCOD Software Requirements Document (SRD) were met [1]. The STRR covers 1,967 dynamic test cases referred to in the CrCOD Software Test Plan (STP) [24], plus additional dynamic and static tests created by the tester. Some of the requirements in the SRD [1] are applicable to the Framework and thus, verification of those requirements is addressed by the xLPR Framework STP.

The results from the independent verification of the CrCOD module, as documented in the STRR for CrCOD [26] are summarized next:

Performance of STP test cases – Cases 1 to 1,967: These test cases were created by the code developer, along with expected results. The tester independently compiled the CrCOD Fortran code and saved the output in a .csv file. The expected results provided by the code developer in a separate .csv file were then compared to the tester's results in an Excel Spreadsheet. The tester found no anomalies during this testing phase.

Independent calculation of COD – Case 1,968: The tester created an independent Excel spreadsheet, based solely upon the circumferential crack COD equations described in the SDD [7], to calculate COD. The tester then compared the results of the spreadsheet calculations to

the corresponding code output. The tester found that the spreadsheet and code calculations agreed, within round-off error, for the plastic COD calculations, but not the elastic COD calculations. After examining the code and the SDD, the tester consulted with the code developer. The code developer determined that the equations in the SDD required updating, while the coded equations were correct. The tester created JIRA issue XLPR-426, "Update SDD Equations to Include F_ax Contribution to Elastic COD," to address this issue. The SDD was corrected and this JIRA issue was subsequently closed.

Check Analysis Method Input – Case 1,969: The CrCOD code requires an input for the analysis method. If METHOD = 0, then the code performs the COD calculation. Otherwise, the code is required by the requirement RCCOD-5 to report an error of i_err_code = 105 and stop execution. The tester created test case 1,969 to verify this requirement. No anomalies were found during this test.

Check Analysis Method Input – Case 1,970: The CrCOD code requires an input for RO_n, a material property parameter. If RO_n < 2, then the code is required by RCCOD-5 to report a warning of i_err_code = 110, set RO_n = 2, and perform the COD calculation. The tester created test case 1,970 to verify this requirement. No anomalies were found during this test.

Additional static testing: The tester examined the software requirements listed in the SRD to ensure that all requirements were tested and to determine appropriate static testing to be performed. The static testing involved examination of the code and documentation to verify that the listed requirements were met. The tester performed the static testing in conjunction with Test Cases 1 to 1,967, as provided by the code developer.

Static Test 3 verified that Tables 1 and 2 in the SRD contained all the required inputs and outputs. The tester discovered that the input METHOD was missing from Table 1 in the SRD. The tester consulted with the code developer and created JIRA issue XLPR-427 to track this matter, which was subsequently closed. No other anomalies were found during the static testing.

The tester created Static Test 9 to verify that the coded elastic (V_1) and plastic (h_2) influence function coefficients were consistent with those listed in the SDD (see Table 7 in the SDD). The tester discovered five cases where the elastic influence function coefficients in the code were inconsistent with those documented in the SDD [7]. The code developer determined that only one case required an update to the code and SDD. In this instance, digits were transposed. For the other four cases, the inconsistency was rooted in the use of tension versus crack face pressure V_1 influence coefficients for the crack face pressure case. After discussion with the tester, it was agreed that no changes to the code were necessary because the V_1 influence coefficients for tension and crack face pressure are identical within the tolerance of the finite element model meshing and nonlinear convergence criterion (the tension and crack face pressure V_1 influence coefficients differ by less than 0.37%). The tester created JIRA issue XLPR-428, "Update Code and SDD Influence Coefficient," to track this matter. This issue was resolved and subsequently closed.

3.3.2 AxCOD Module Verification

The verification of the AxCOD module is documented in detail in the STRR for the AxCOD module [27]. The testing activity described in the STRR was intended to verify that the requirements specified in the AxCOD Software Requirements Document (SRD) were met [2]. This STRR covers 28 numerical test cases described in the AxCOD Software Test Plan (STP) [25], plus a set of 11 static tests generated by the developer as part of the STP. Some of the requirements

in the SRD [2] are applicable to the Framework and thus, verification of these requirements is addressed by the Framework STP.

Inputs for Test Cases 1 thru 28 created by the code developer are contained in Table 1 of the STP [27]. Expected outputs for the test cases are contained in the output file "Standard_Out.csv", provided by the developer. Running these test cases independently confirms that the code can be successfully compiled and produces the expected results, as specified by the code developer.

Below are summaries of the testing activities performed. Each summary includes a description of any JIRA issues recorded as a result of this activity.

Performance of STP test cases – Cases 1 to 28: These test cases were created by the code developer, along with the expected results. The tester compiled the Fortran code "CALC_AxCOD_V2" using both 32- and 64-bit Intel compilers (i.e., CALC_AxCOD_V2_32bit and CALC_AxCOD_V2_64bit, respectively). Prior to actually running the test cases, the input files for all 28 test cases were compared with the input data specified in Table 1 of the STP [25]. The input file provided by the developer (Test_In.txt) agreed exactly with the input data shown in Table 1 of the STP. The 28 test cases were run by the tester using both the 32- and 64-bit compiled versions of the AxCOD module. The output results obtained by the tester for both versions were then compared with the results obtained by the developer using the file comparison utility Beyond Compare 3 [30]. The agreement between the developer's output file (Standard_Out.csv) and the tester's output files (Standard _Out_STRR_32bit.csv and Standard_Out_STRR_64bit.csv)) was exact.

Additional static testing: The tester examined the software requirements listed in the SRD for AxCOD [2] to ensure that all requirements were tested and to determine appropriate static testing to be performed. The static testing involved examination of the source code and documentation to verify that all of the listed requirements were met. Some of the elements of the verification process do not involve running the "CALC_AxCOD_V2" code to verify that it meets requirements. Rather, these cases involve issues such as: Is the code portable?, Can it be turned into a DLL?, Are there any nonstandard input units considerations?, etc. Most of these cases are handled simply by inspection of the source code and associated documentation. To formalize the traceability of requirements to the Requirements Traceability Matrix (RTM), eleven "static" test cases were developed in the Axial Crack COD STP. Verification that "CALC_AxCOD_V2" meets these requirements simply required looking at the source code and/or associated documentation, e.g., SRD or SDD.

In addition, as another check, the tester calculated the inner, mid-thickness, and outer surface COD values for Test Case 28 using the Section 4.1.1 equations from the SDD [8], coded into an Excel spreadsheet (Check of AxCOD source code against Excel spreadsheet for Test Condition 28.xlsx) and got exact agreement with the inner, mid-thickness, and outer surface CODs shown in Table 2 of the AxCOD STP [25]. The tester also ran Test Case 28 using the AxCOD source code using both SI and equivalent US Customary units to demonstrate that the code would calculate an equivalent value for the COD regardless of the units chosen, as long as the units were consistent.

3.3.3 CrCOD Module Validation

The validation of the CrCOD module is documented in detail in the MVR for the CrCOD module [28]. This MVR documents the validation activities that characterize the predictive capability of

the CrCOD Module over a prescribed range of applicability. The module was validated by comparing the outputs of the module with existing full-scale experimental pipe fracture COD data.

The test specimens for these experiments were sections of nuclear grade piping of various sizes and materials. The experiments evaluated a number of different loading conditions and crack geometries.

- Pipe sizes: 2- to 42-inch nominal diameter, with wall thicknesses up to approximately 90 mm (3.5 inches)

- Materials: carbon steels (including representative weld processes), stainless steels (including representative weld processes), and dissimilar metal welds joining sections of carbon and stainless steel pipe

- Loading conditions: simple quasi-static four-point bending, combined pressure and four-point bending, dynamic, cyclic, and combined dynamic/cyclic pipe system experiments.

- Crack geometries: simple through-wall cracked pipe.

In total there were approximately 140 pipe fracture experiments conducted at Battelle over the years. Included in this overall set of pipe fracture experiments, 57 evaluated circumferential through-wall cracked pipes subjected to a variety of loading conditions. Of these 57 circumferential through-wall cracked pipe experiments, 36 of the representative data files had the necessary crack centerline COD data at crack initiation, and as such were included in the final validation matrix for CrCOD.

Table 25 is a summary of those 36 experiments.

In order to validate the CrCOD module against the existing full-scale pipe fracture experimental data set, an executable version of the CrCOD module (calc_cod_v2) was used. Individual input files for each of the 36 through-wall cracked pipe tests used for validation were created. A file-of-files input file was then created so as to run each of the 36 test cases in batch mode.

The results of the Validation analysis for the CrCOD module are provided in Table 26. The analysis of each experiment resulted in a valid solution (i_err_code value = 300). The only warning codes were for Experiments 4111-3 and 4111-4, which had a warning code of 109 (Mean-Radius / thickness > 20, calculation performed at 20). These were two large diameter, thin-walled pipe experiments for which the Rm/t ratio was much greater than 20. The far right hand column in Table 26 presents the ratio of the predicted COD at crack initiation from the CrCOD module to the experimental COD at crack initiation for each of the 36 individual pipe experiments evaluated in this validation exercise. The COD values are the COD values at the crack centerline. Furthermore, with two exceptions, Experiments 1-7 and 1-8 which had their COD measuring devices on the inside pipe surface, the predicted COD values used in this ratio of the predicted to experimental COD values was the COD value on the OD pipe surface. For Experiments 1-7 and 1-8 the predicted COD values used in the ratio of predicted to experimental COD values was the COD value on the ID pipe surface.

A value for the ratio of the predicted-to-experiment COD greater than 1.0 means that the CrCOD module overpredicted the experimental COD while a value less than 1.0 means that the CrCOD module underpredicted the experimental COD. The red font values in Table 26 highlight those experiments for which the CrCOD module either overpredicted or underpredicted the experimental COD value by a factor of two or more. The most significant overprediction of COD is for Experiment 1.2-9 (predicted-to-experimental COD of 3.85) while the most significant underprediction of COD is for Experiment 1.2-2. (predicted-to-experimental COD of 0.42). The loading conditions for both of these experiments was cyclic four-point bending. Because the CrCOD module was developed assuming quasi-static, monotonic loading, this degree of error is not unexpected for these cyclically loaded pipe experiments. When the seven cyclically loaded experiments from Table 26 are excluded from the analysis, the level of agreement between the predicted COD values and the experimental COD values improves from 1.23 (on average) to 1.17 (on average) with the standard deviation improving as well, from 0.75 to 0.54. However, because the CrCOD module will be used for both monotonic loading (i.e., normal operating conditions) as well as cyclic loading (i.e., seismic loading), one should include all of the experiments in assessing the level of uncertainty in the CrCOD module.

If the stress-strain data used in the analyses is obtained from dynamically loaded tensile specimens instead of quasi-statically loaded tensile specimens, one sees a significant improvement in the agreement between the analyses and the experiments for the dynamically loaded pipe experiments, see Table 27. The resultant level of agreement between the predicted COD values and the experimental COD values for the eight dynamically loaded pipe experiments improves from 1.47 (on average) to 1.13 (on average) with the standard deviation improving as well, from 1.12 to 0.37, when one uses dynamic stress-strain data instead of quasi-static data in analyzing these eight dynamically loaded pipe experiments[1]. Unfortunately, in most cases the end user of xLPR will not have such dynamic (or cyclic) loaded tensile data available for use in their analyses. As a result, one must recognize the level of uncertainty that might exist in

[1] Note, there was no dynamic stress-strain data available for pipe material DP2-F23 used for Experiment 1-7 so it was not possible to analyze this experiment using dynamic stress-strain data

analyzing dynamic, cyclic type events, such as an earthquake, when using quasi-static, monotonic stress-strain data.

For all of the analyses mentioned above, the COD values were the predicted and experimental COD values at crack initiation. The moment values used in the analyses were the moment values at crack initiation. As a check on the broader applicability of the analysis methodology, the COD at maximum moment, after an amount of crack growth had occurred in the experiments, was assessed, see Table 28.

Table 28 indicates that there were a number of experiments for which no crack growth data were available so that we were not able to determine the crack angle (θ) at maximum moment for these experiments. Accordingly, we were not able to make a relative comparison of the predicted to experimental COD values at maximum moment for these experiments. In addition, there were a couple of experiments for which the COD measuring device had saturated by the time maximum moment was attained so that we were also not able to make a relative comparison of the predicted to experimental COD values at maximum moment for these experiments. For the remaining 23 experiments for which we had both crack growth and COD data at maximum moment, the average value of the predicted to experimental COD value was 1.41, with a standard deviation of 0.80, see Table 28

Table 28 indicates slightly worse results than the agreement between the predicted and experimental results at crack initiation shown in Table 26. One of the issues with making comparisons at maximum moment (instead of at crack initiation) is that for many of the carbon steel pipe experiments, the crack grew significantly out of the original circumferential plane of the crack (see Figure 50) once it initiated making it difficult to ascertain what the real experimental COD would be if the crack had remained in the circumferential plane.

Table 25. Validation Matrix for CrCOD Module

Experiment Number	Program(1)	Material/ Crack Location	Loading Conditions (2)	Outside Radius, mm	Wall Thickness, mm	Half Crack Length, (3) radians
4111-1	DP3-II	CS Base	4-Point Bend	57.15	8.89	1.1624
4111-2	DP3-II	CS Base	4-Point Bend	355.60	23.62	1.1624
4111-3	DP3-II	SS Base	4-Point Bend	533.40	7.11	1.1624
4111-4	DP3-II	CS Base	4-Point Bend	533.40	15.88	1.1624
4111-5	DP3-II	SS Weld	4-Point Bend	359.79	30.20	1.1624
4111-6	DP3-II	CS Base	4-Point Bend	455.04	72.85	1.1624
4141-1	DP3-II	SS Weld	4-Point Bend	84.14	14.27	1.1655
4141-3	DP3-II	SS Weld	4-Point Bend	206.76	26.19	1.1530
4141-5	DP3-II	SS Weld	4-Point Bend	83.88	14.10	1.2030
4141-7	DP3-II	CS Weld	4-Point Bend	466.47	86.61	1.1624
1.2-1	IPIRG-1	SS Base	4-Point Bend	84.49	13.89	1.1938
1.2-7	IPIRG-1	CS Base	4-Point Bend	83.82	13.97	1.1310
1.2-8	IPIRG-1	CS Base	4-Point Bend	83.72	13.69	1.1687
1.2-12	IPIRG-1	CS Base	4-Point Bend	83.71	13.77	1.1718
4.2-1	IPIRG-2	CS Base	4-Point Bend	84.14	14.50	0.5236
1.1.1.21	Short Cracks	CS Base	4-Point Bend	355.60	22.68	0.1963
1.1.1.23	Short Cracks	SS Weld	4-Point Bend	355.60	30.23	0.1963
1.1.1.24	Short Cracks	CS Weld	4-Point Bend	306.07	31.34	0.2482
1.1.1.26	Short Cracks	SS Base	4-Point Bend	53.12	8.31	0.7665
4.3-1	IPIRG-2	CS Base	4-Point Bend	381.76	38.18	0.5215
EPRI-6T	EPRI	SS Base	4-Point Bend	30.16	6.02	0.7194
4131-1	DP3-II	SS Base	Pressure + Bend	83.22	13.41	1.1624
4131-3	DP3-II	CS Base	Pressure + Bend	137.07	18.69	1.1624
1-8	IPIRG-2	CS Base	Pressure + Bend	199.64	26.16	0.3770
DMW-6	DMW	DMW	4-Point Bend	108.45	21.25	0.6362
DMW-9	DMW	DMW	4-Point Bend	108.975	21.85	1.17
DMW-11	DMW	DMW	4-Point Bend	108.125	21.2	1.1838
DMW-13	DMW	DMW	4-Point Bend	108.8	21.2	1.1811
1.1.1.28	Short Cracks	DMW	4-Point Bend	463.55	85.85	1.1278
1.2-2	IPIRG-1	CS Base	QS, Cyclic Bend (R=0)	83.82	13.97	1.131
1.2-3	IPIRG-1	SS Base	QS, Cyclic Bend (R=0)	84.33	13.97	1.131
1.2-9	IPIRG-1	SS Base	Dyn, Cyclic Bend (R = -1)	84.30	14.12	1.2032
1.2-10	IPIRG-1	CS Base	Dyn, Cyclic Bend (R = 0)	83.68	13.06	1.1624
4.2-2	IPIRG-2	CS Base	Dyn, Cyclic Bend (R = -1)	82.80	14.50	0.5236
4.2-3	IPIRG-2	CS Weld	Dyn, Cyclic Bend (R = -1)	83.12	14.38	0.5236
1-7	IPIRG-2	CS Base	Dyn, Cyclic Pipe System Expt.	199.90	26.39	0.377

(1) DP3-II – Degraded Piping Program Phase II; IPIRG – International Piping Integrity Research Group program; Short Cracks – Short Cracks in Piping and Piping Welds program; DMW – Dissimilar Metal Weld Pipe Fracture program

(2) 4-Point Bend tests are for quasi-static, monotonic loading conditions

(3) Half crack length at beginning of the experiment, i.e., half crack length at the instant of crack initiation

Table 26. Results of CrCOD validation analysis (crack initiation)

Experiment Number	Experimental COD at Crack Centerline, mm	CrCOD predicted COD on OD surface, mm	CrCOD predicted COD at mid wall thickness, mm	CrCOD predicted COD at ID surface, mm	Predicted COD / Experimental COD
Quasi-static monotonic 4-point bending without internal pipe pressure					
4111-1	4.47	3.35	3.03	2.71	0.750
4111-2	5.59	6.70	6.33	5.90	1.199
4111-3	11.94	11.98	11.49	10.76	1.004
4111-4	11.18	10.18	9.75	9.07	0.910
4111-5	9.03	5.90	5.53	5.14	0.654
4111-6	6.17	8.99	8.11	7.23	1.457
4141-1	4.69	11.94	10.70	9.43	2.547
4141-3	1.4	2.11	1.93	1.74	1.506
4141-5	4.32	9.04	8.13	7.20	2.093
4141-7	13.17	11.39	10.18	8.98	0.864
1.2-7	1.63	1.59	1.43	1.27	0.977
1.1.1.21	3.1	2.89	2.58	2.30	0.931
1.1.1.23	12	10.93	9.69	8.57	0.911
1.1.1.24	2.85	2.09	1.84	1.61	0.734
1.1.1.26	7.95	4.76	4.24	3.73	0.599
1.1.1.28	15.48	11.49	10.25	9.02	0.742
DMW-6	4.8	5.30	4.56	3.85	1.105
DMW-9	3.96	4.15	3.68	3.20	1.047
DMW-11	6.71	9.02	8.02	7.02	1.344
DMW-13	7.23	7.49	6.63	5.77	1.036
4.3-1	10.43	6.71	5.93	5.16	0.643
EPRI-6T	4.7	4.60	3.98	3.38	0.979
Dynamic monotonic 4-point bending without internal pipe pressure					
1.2-1	11.39	27.36	24.59	21.80	2.402
1.2-8	1.49	1.29	1.16	1.04	0.865
1.2-12	1.12	1.37	1.24	1.10	1.227
4.2-1	3.87	1.83	1.58	1.35	0.473
Quasi-static monotonic 4-point bending with internal pipe pressure					
4131-1	8.84	16.51	14.88	13.24	1.867
4131-3	3.34	5.98	5.45	4.92	1.789
1-8	1.93	3.02	2.63	2.26	1.171(1)
Quasi-static cyclic experiments					

1.2-2	2.37	1.00	0.90	0.80	0.423
1.2-3	8.18	10.90	9.75	8.58	1.332
Dynamic cyclic experiments					
1.2-9	3.48	13.40	12.04	10.67	3.851
1.2-10	1.12	1.02	0.92	0.82	0.912
4.2-2	1.35	1.56	1.35	1.15	1.158
4.2-3	4.29	3.80	3.29	2.82	0.886
1-7	1.11	2.80	2.44	2.09	1.886 (1)
Average (all experiments)					1.23
Standard Deviation (all experiments)					0.75
Average (not considering cyclically loaded experiments)					1.17
Standard Deviation (not considering cyclically loaded experiments)					0.54

For Experiments 1-7 and 1-8 the LVDT used to measure the COD was on the inside pipe surface so that the CrCOD predicted COD values used for this ratio were the COD on the inside pipe surface. For all of the other experiments considered, the COD measuring device was located on the outside pipe surface to that the predicted COD values were for the outside pipe surface.

Table 27. Comparison of results from CrCOD module for dynamic experiments between using quasi-static and dynamic stress-strain data in the analysis

Experiment Number	Experimental COD at Crack Centerline, mm	CrCOD predicted COD on OD surface, mm (quasi-static stress-strain data)	Predicted COD / Experimental COD (quasi-static stress-strain data)	CrCOD predicted COD on OD surface, mm (dynamic stress-strain data)	Predicted COD / Experimental COD (dynamic stress-strain data)
1.2-1	11.39	27.36	**2.402**	12.33	1.082
1.2-8	1.49	1.29	0.865	1.15	0.769
1.2-12	1.12	1.37	1.227	1.20	1.071
4.2-1	3.87	1.83	**0.473**	2.76	0.712
1.2-9	3.48	13.40	**3.851**	4.19	1.205
1.2-10	1.12	1.02	0.912	0.96	0.861
4.2-2	1.35	1.56	1.158	2.27	1.680
4.2-3	4.29	3.80	0.886	6.99	1.629
		Average	1.471	**Average**	1.126
		Standard Deviation	1.115	**Standard Deviation**	0.366

Table 28. Results of CrCOD validation analysis (maximum moment)

Experiment Number	Experimental COD at Crack Centerline, mm	CrCOD predicted COD on OD surface, mm	CrCOD predicted COD at mid wall thickness, mm	CrCOD predicted COD at ID surface, mm	Predicted COD / Experimental COD
Quasi-static monotonic 4-point bending without internal pipe pressure					
4111-1	No crack growth data available from experiment				
4111-2	20.78	31.09	29.59	28.03	1.50
4111-3	33.38	43.01	41.42	39.50	1.29
4111-4	38.1	25.33	24.41	23.10	0.66
4111-5	CMOD device had saturated prior to reaching maximum moment				
4111-6	No crack growth data available from experiment				
4141-1	11.53	31.79	28.64	25.45	2.76
4141-3	11.91	23.58	21.74	19.89	1.98
4141-5	12.06	20.94	18.92	16.88	1.74
4141-7	No crack growth data available from experiment				
1.2-7	3.99	5.30	4.82	4.33	1.33
1.1.1.21	11.77	17.60	15.68	13.74	1.50
1.1.1.23	32.19	40.31	35.17	30.12	1.25
1.1.1.24	21.83	16.35	14.38	12.47	0.75
1.1.1.26	10.67	6.99	6.25	5.51	0.65
1.1.1.28	25.35	19.36	17.41	15.44	0.76
DMW-6	13.92	13.48	11.67	9.90	0.97
DMW-9	8.85	7.76	6.91	6.06	0.88
DMW-11	12.68	16.71	14.93	13.14	1.32
DMW-13	14.62	13.63	12.16	10.67	0.93
4.3-1	74.97	62.25	56.30	50.31	0.83
EPRI-6T	No COD data provided in data file				
Dynamic monotonic 4-point bending without internal pipe pressure					
1.2-1	21.73	51.61	46.91	42.16	2.38
1.2-8	3.47	2.94	2.67	2.40	0.85
1.2-12	4.47	5.79	5.29	4.78	1.30
4.2-1	11.83	7.94	6.95	5.96	0.67
Quasi-static monotonic 4-point bending with internal pipe pressure					
4131-1	17.77	38.73	35.18	31.60	2.18
4131-3	6.48	25.50	23.52	21.52	3.94
1-8	Limited range on LVDT (+6.35 mm); LVDT saturated at maximum moment				
Quasi-static cyclic experiments					
1.2-2	No crack growth data available from experiment				
1.2-3	No crack growth data available from experiment				
Dynamic cyclic experiments					
1.2-9	No crack growth data available from experiment				
1.2-10	No crack growth data available from experiment				
4.2-2	No crack growth data available from experiment				
4.2-3	No crack growth data available from experiment				
1-7	No crack growth data available from experiment				
Average (all experiments)					**1.41**
Standard Deviation (all experiments)					**0.80**

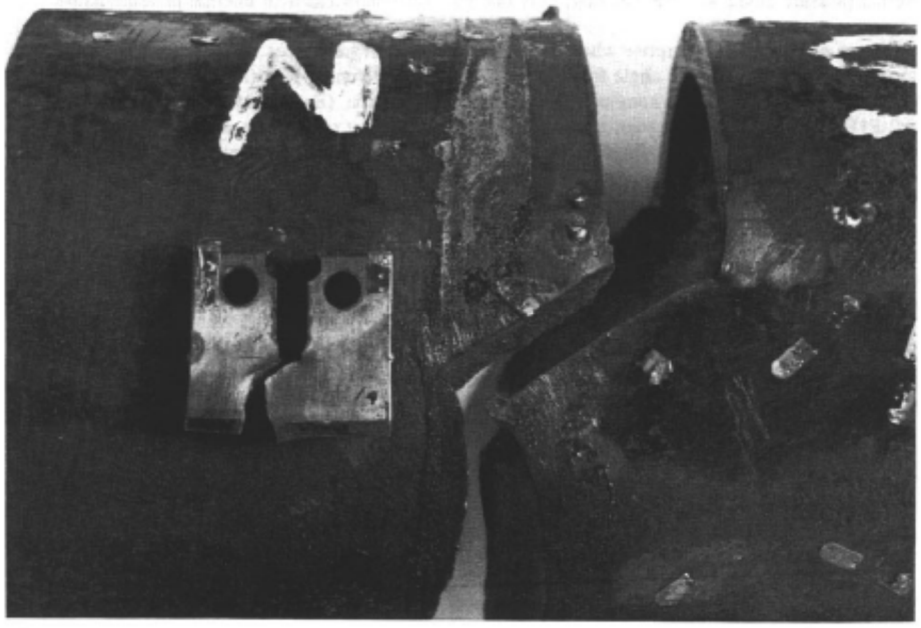

Figure 50. Post-test photograph of the fracture for a representative carbon steel TWC pipe experiment showing significant out-of-plane crack growth

3.3.4 AxCOD Module Validation

Details of the validation efforts conducted for the AxCOD module can be found in the Axial Crack COD MVR [29]. The validation work set forth in the MVR consists of two parts: comparison of model predictions to finite element results and engineering judgment. Validation against FEA describes how well the model actually predicts the finite element results. Validation with engineering judgment involves comparison of model parameters with similar work found in the literature.

3.3.4.1 Comparison of the AxCOD Module Results with Laboratory Data

The AxCOD author performed a literature review to determine if laboratory COD data existed for axial cracks in cylinders. Only one reference [31] presented data for tubes, but was limited to R_m/t = 25, which is too large to validate this model. Therefore, validation with laboratory data requires additional research.

3.3.4.2 Comparison of the AxCOD Module Results with FEA Results

This section presents details related to the validation of the AxCOD module against finite element analyses results. While the AxCOD model is itself derived from FEA results, this validation work shows the degree to which the model actually predicts the FEA solutions. ABAQUS FE analyses were conducted to determine the necessary elastic influence functions (V_1-functions) and plastic influence functions (h_2-functions) for the analytical formulation of COD [8, 32, 33, 34]. An extensive matrix of FE analyses were conducted to determine V_1 as a function of R_m/t ratio, normalized crack length, and three different locations through the pipe wall thickness (inside

surface, mid-wall, and outside surface). In a similar fashion, an extensive matrix of non-linear FEA were conducted to determine the plastic influence functions (denoted as h_2) for the analytical formulation of COD. These plastic influence functions are a function of the strain hardening exponent (n) as well as the R_m/t ratio and normalized crack size.

To illustrate the fidelity of the influence functions, Figure 51 (taken from Reference 8) shows a comparison of the analytically predicted COD values with the COD values from the non-linear finite element analyses. The prediction is good for R_m/t = 5, mid-thickness location, and n=5 if the ratio of p/p_L is less than 0.6.

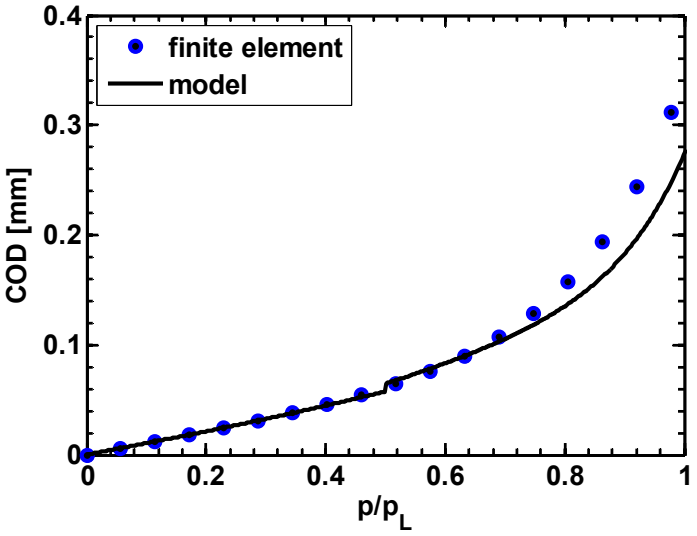

Figure 51. Comparison of finite element results with AxCOD analytical model predictions

Section 7 of the AxCOD MVR [29] shows similar plots to Figure 51 that demonstrate the agreement between the model and the finite element analyses for a broader range of parameters. Based on these comparisons the following conclusions can be made:

- The limitation of $p/p_L \leq 0.6$ is appropriate for the model.
- The agreement between the model and the finite element analyses improves for a larger range of p/p_L for certain combinations of R_m/t ratios, strain hardening exponents (n), and normalized crack lengths (ρ).

3.3.4.3 Validation of the AxCOD Module through Engineering Judgment

Engineering judgment describes a range of validation activities not covered by validation against the FEA results. In validating the AxCOD module, "engineering judgment" involves comparing the elastic (V_1) and plastic (h_2) influence functions determined during the model development process to previous work reported in the literature [22]

Figure 52 shows a comparison of plastic influence functions (h_2) from the AxCOD development process with those from the literature [22] for R_m/t = 5 and n = 7. The results compare well for the mid-thickness location, and the trends are similar for the ID and OD locations. Overall, as part of this comparison with existing solutions from the literature, it was found that the elastic (V_1) and

plastic (h_2) influence functions determined as part of the AxCOD development process compare reasonably well with the values reported by Kim *et al.* [22].

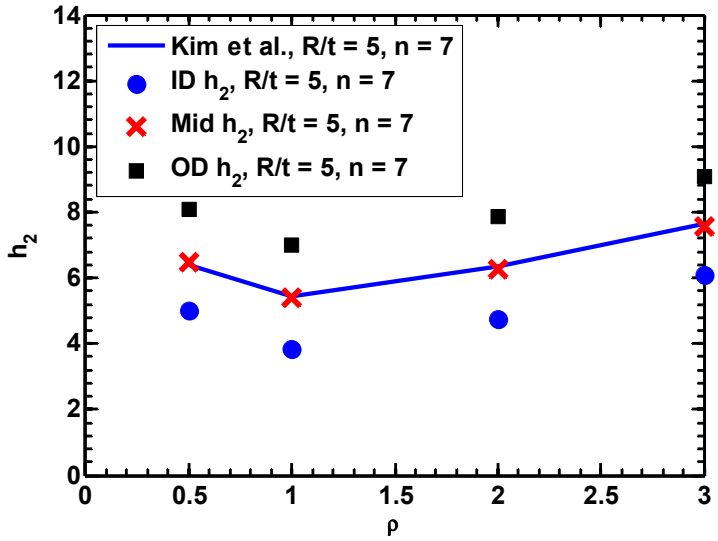

Figure 52. Plastic influence functions (h_2) from AxCOD development process compared with literature values [22]

As a final engineering judgment consideration for validation of AxCOD, it is important to note that the underlying technical basis and model methodology for AxCOD are identical to the underlying technical basis and underlying methodology for the companion circumferential through-wall crack COD module, CrCOD. CrCOD, when compared with a set of 36 experiments showed an average ratio of predicted COD to experimental COD of 1.23 with a standard deviation of 0.75 for COD at crack initiation, and for a subset of 23 of those experiments at maximum moment when there has been significant crack growth, an average ratio of predicted COD to experimental COD of 1.41 with a standard deviation of 0.80. It can be argued that AxCOD should show similar agreement to measured behavior as CrCOD does, because they are rooted in an identical analytical approach.

3.4 Limitations with the COD Modules

Many of the limitations associated with the COD module for xLPR Version 1.0 have been addressed as part of the Version 2.0 COD development process. The Version 2.0 enhancements include:

- xLPR Version 1.0 did not include a model for axial crack COD. It only included a COD model for circumferential cracks. xLPR Version 2.0 includes models for both axial and circumferential cracks.

- For the Version 1.0 CALC_COD module, the pressure and bending loads were applied concurrently whereas for the Version 2.0 CrCOD module, the bending loads are applied subsequent to the application of the tension loads from the internal pipe pressure and crack face pressure.

- For the Version 1.0 CALC_COD module, a single value of COD was obtained and applied uniformly across the crack face. For the Version 2.0 CrCOD module, three

values of COD (ID surface, mid-thickness, and OD surface) are obtained and output to the Framework for consideration in the Leak Rate module.

- The Version 1.0 CALC_COD module did not account for crack face pressure whereas the Version 2.0 CrCOD module does.

- The design space for Version 2.0 has been expanded to include a wider range of R_m/t ratios (2 to 20 for Version 2.0 versus 10 to 20 for Version 1.0) and a wider range of normalized crack sizes (θ/π values up to 0.9 for Version 2.0 versus 0.5 for Version 1.0).

Regardless of these enhancements, there still remain a few limitations associated with the Version 2.0 COD module. Those limitations include:

- The COD modules assume a planar through-wall crack. With this assumption, the cracks are an idealized representation of PWSCC cracks. Actual PWSCC cracks are not planar and do not have a simple leak path for through-wall cracks. Thus, for a given leak rate, a PWSCC crack system would be more diffuse than a planar crack system. PWSCC cracks are characterized by a distributed, connected network of cracks in 3D rather than a single, idealized 2D planar crack. A model for COD of diffuse and connected (i.e. flow through porous media) set of cracks is very different from the ideal crack case used in xLPR 2.0. The effect of this assumption is to over-predict both crack opening displacement and the subsequently calculated leak rate but at present there is no available data for quantification of this over prediction.

- Prior research [35, 36] has shown that the assumption of free rotations at the ends of the pipes results in an overprediction of the circumferential crack COD, when compared with the reality of restrained ends due to the restraint supplied by the rest of the piping system. This effect has not been considered in the Version 2.0 COD module.

- Prior research [35, 36] has shown that the weld residual stresses can cause the crack faces to rotate such that the resultant CODs for circumferential cracks will be greater than predicted on the ID pipe surface and less than predicted on the OD pipe surface. This effect has not been accounted for in the Version 2.0 COD module.

- The current version of AxCOD handles the contribution of weld residual stresses to the overall axial crack COD in a simplistic manner by incorporating an effective pressure term based on the summation of the pressure induced hoop stress and the weld residual stresses. A more rigorous handling of the contributions due to the weld residual stresses based on the inclusion of the weld residual stresses directly into the finite element analyses may be warranted.

- Validation of the AxCOD module is weak. There is no plant experience or laboratory data to make a numerical assessment of the methodology, and this is decidedly unsatisfying.

- The axial crack COD model considers the crack to be in a homogeneous pipe material. In the case of an axial crack in a dissimilar metal weld, if the crack is long enough, the modulus mismatch between the three materials of the weld may influence the COD.

4. RECOMMENDATIONS FOR VERSION 3.0 MODIFICATIONS

A factor not considered in the development of the CrCOD module is the effect of restraint of pressure induced bending on the COD of a circumferential through-wall crack in a piping system. The loads applied to the finite element model used during the development of the CrCOD module were combined pressure and bending, see Figure 3. Furthermore, as discussed previously and as illustrated in Figure 3, the boundary conditions assumed that the pipe is not restrained at the ends, i.e., the ends were free to rotate. However, pipe segments in piping systems are, indeed, restrained. Assuming free rotations, as was the case during the CrCOD development process, introduces an induced bending moment equal to the axial force due to the internal pipe pressure times the eccentricity between the neutral axis of the cracked pipe section and the centerline of the pipe. It has been demonstrated in past studies [35, 36] that this restraint of pressure induced bending due to the rest of the piping system results in a reduction in COD when compared with analyses for which free end boundary conditions are assumed, as was the case for CrCOD. These overestimations comprise one of the major uncertainties in an LBB analysis, as it leads to an under-prediction of the leakage-size-crack length of a postulated leaking TWC for a prescribed leakage detection limit in a plant, and thus, results in a non-conservative estimation of the crack stability from an LBB perspective. To address this limitation, the NRC is currently funding research at Battelle to develop an improved COD module which accounts for this effect. This enhanced module should be incorporated into later versions of xLPR when available.

Another factor affecting COD predictions is the effect of weld residual stresses. The axial weld residual stress distribution for cracks in heavy wall pipes, typically used in nuclear power plants, is tension on the inside pipe surface and compression on the outside pipe surface. As a result, the crack faces of a circumferential through-wall crack in a pipe subject to this weld residual stress distribution would tend to rotate such that the actual COD may be slightly greater than predicted on the inside pipe surface and slightly less than predicted on the outside pipe surface. This effect, which was previously investigated as part of References 35 and 36, was not included during the CrCOD development process because there is no way to include the effect of an arbitrary WRS profile, which can be input into xLPR, without performing case-specific FE runs during an xLPR simulation as a TWC grows. Embedded FE runs within xLPR to calculate COD with WRS could reduce throughput to less than a realization per day on a desktop computer. Currently, the NRC is funding research to develop an improved COD module which accounts for this effect. This enhanced module should be incorporated into later versions of xLPR when available.

The current version of the axial crack COD model (AxCOD) includes the effects of weld residual stresses on the axial crack COD in a somewhat simplistic manner by incorporating an effective pressure term based on the combined pressure induced hoop stress and weld residual stresses. A more rigorous handling of the contributions due to the weld residual stresses based on the inclusion of the weld residual stresses directly into the finite element analyses may be warranted.

5. LESSIONS LEARNED

At the beginning of the CrCOD development process, the initial analyses appeared to be straightforward based on previous published work [10, 11, 18, 37, 38]. However, as the CrCOD development process progressed, there were significant details uncovered that were not discussed in the previously published works. These details included the assumptions of small strains and the requirement that the plastic influence functions be developed at large moments such that the elastic portion of the COD was small compared with the plastic portion. Other unknowns going into the analyses were the boundary and constraint conditions used by the published work. Once these unknown assumptions were resolved through discussions and trial-and-error methods, the analyses for the pure bending solution were developed in relative short order with excellent results.

The following list provides the significant findings from the CrCOD development process:

- All calculations, including the work in References 10 and 18, were based on small strain theory, such that non-linear geometry effects were not considered (i.e. NLGEOM was not invoked in ABAQUS). For COD analyses, small strain theory is an appropriate assumption for developing analytical solutions from finite analyses [16].

- For free-end pipes, the follower-force option is an appropriate assumption for these analyses.

- Rather than using a kinematic constraint for free-end pipes under the loading conditions applied during the CrCOD development process, the use of a continuum distributed coupling constraint on the free-ends of the pipe is a more appropriate constraint condition.

- Based on the analysis methods used and the future use of the calculations performed in this study, the use of a plastic zone correction factor for the elastic component of COD is not recommended when using the results of this study.

- The results obtained are independent of absolute pipe size (i.e. diameter), but are dependent on the standard non-dimensional parameters previously discussed in the open literature, which are mean radius-to-thickness (R_m/t) ratio, strain hardening exponent (n), and normalized crack length (θ/π).

Initially, a kinematic coupling constraint was used to apply the axial load and the bending moment via a reference node at the non-cracked end of the pipe. However, during the analyses, it was determined that this constraint was not behaving as required. This was determined to be a limitation in the constraints which provided a means to constrain displacements, rather than providing a means to distribute forces. Thus, based on the information provided in Reference 13, a continuum distributed coupling constraint was applied to the non-cracked end of the pipe to allow for the proper force transmission and proper pipe-end shape development. Figure 10 displays the application of this constraint to the model.

As regards the lessons learned from the AxCOD development, all of the insight gleaned from the CrCOD development process was subsequently applied here.

6. ASSUMPTIONS AND IMPLICATIONS

The major assumptions and the implications of those assumptions made during the CrCOD and AxCOD development processes are presented in Table 29.

Table 29. List of assumptions and implications of those assumptions made during the CrCOD and AxCOD development processes

Assumptions	Implications
Both CrCOD and AxCOD make the GE-EPRI assumption that COD can be separated into elastic and plastic components and that these components can be characterized using elastic and plastic influence functions based on finite element analyses results.	The results are only as good as the FEA assumptions / boundary conditions. Additional validation to test results should be considered.
Elastic influence functions (V_1) are based on R_m/t ratio and normalized crack size (θ/π). Plastic influence functions (h_2) are based on R_m/t ratio, normalized crack (θ/π) size, and strain hardening exponent (n). Design space for parametric parameters are: • $0.05 \leq \theta/\pi \leq 0.9$ • $2 \leq R_m/t \leq 20$ • $2 \leq n \leq 10$ If the crack or pipe geometry or material properties are outside these ranges, it is assumed that influence functions at limits of range adequately capture the COD behavior.	Design space should cover almost all possible combinations of pipe/crack geometries and pipe materials used in primary systems in nuclear power plants. Some secondary side piping systems may be fabricated from larger diameter, thinner wall pipe for which the R_m/t ratio is greater than 20. Some practical applications require n>10 (i.e., 11-14), but this is judged to be a minor influence on the results because the stress-strain curves become very flat beyond n=10. Once θ/π ratios are beyond 0.9, the rate of leakage is considered to be large compared to detection limits.
Both CrCOD and AxCOD assume linear interpolation of influence functions between discrete finite element result values. Discrete values used in FEA for determining influence functions were: • R_m/t: 2, 5, 10, and 20 • θ/π: 0.05, 0.10, 0.25, 0.50, 0.75, and 0.90 • n: linear elastic, 2, 3, 5, 7, and 10	Curvatures of the functions are judged to be modest, such that, linear interpolation is justified.
A Ramberg-Osgood material representation for an isotropic, homogeneous material was assumed during the development process of both CrCOD and AxCOD. As such, the resultant material inputs required by both models are the necessary Ramberg-Osgood parameters, i.e., yield or reference stress, reference strain, strain hardening exponent (n), and alpha (α)	The choice of tensile data to use in the analyses can have a significant effect on the predictions. It was shown that there were significant differences in the stress-strain curves between quasi-statically loaded tensile specimens and dynamically loaded tensile specimens. As such, when analyzing dynamically loaded pipe experiments with quasi-static stress-strain data an additional level of uncertainty was introduced. It is felt that it may not be possible to specify to the end user of the code which stress-strain curve to use since they may not have dynamic data available. However,

Assumptions	Implications
	since leak rate calculations are most likely to be done under normal operating conditions, at quasi-static loading rates, this may not be an issue. Since both CrCOD and AxCOD were developed assuming isotropic, homogeneous materials, cracks in welds should be analyzed assuming the base metal tensile properties, much like is done for crack stability analyses. For cracks in dissimilar metal welds, the mixture percentage approach should be used to establish the appropriate stress-strain properties. The fit of the Ramberg-Osgood parameters to the tensile data was conducted using "best engineering judgement", such that the range of stress-strain data considered was between 0.1percent strain and the strain corresponding to 80 percent of the ultimate strength using engineering stress – engineering strain curves. It should be noted that not all materials conform to the Ramberg-Osgood material behavior. Results may vary based on actual materials used.
It is assumed that elastic and plastic portions of COD can be based on physical crack size not effective crack size as was done for the original GE/EPRI method	The FEA contains the plastic zone size when calculating the h-functions, there is no reason to re-count this in the analytical representation.
It was assumed that the plastic influence functions (h_2) for the bending term for CrCODcan be made at an applied bending moment of 4 times the collapse moment (M_0).	The basis of the GE/EPRI solution that the elastic and plastic effects can be separated requires an asymptotic plastic solution. The choice of the reference limit moment is arbitrary, so there is no impact on the calculated COD because the influence functions ars simply scaled by collapse moment.
It was assumed that the h_2 values for the tension term for CrCOD can be made at a tension equivalent to either 8 or 10 times the collapse tension (P_0).	The basis of the GE/EPRI solution that the elastic and plastic effects can be separated requires an asymptotic plastic solution. The choice of the reference limit moment is arbitrary, so there is no impact on the calculated COD because the influence functions ars simply scaled by collapse moment.
CrCOD and AxCOD assume small scale yielding behavior around the crack tip. Assumes J is a valid parameter for calculating the stress-strain field around the crack tip.	Inherent assumption for J-theory. In practice, CrCOD loads applied are on the order of 0.6 times the limit load or less. For AxCOD, the loads are much smaller than net-section yield.
CrCOD assumes thin shell theory	Assumption only affects influence functions and does not introduce errors into the code.
CrCOD includes contributions from tension, bending, and crack face pressure (CFP) loadings. Axial load due to internal pipe pressure and crack face pressure are applied concurrently. Crack face pressure is assumed proportional to the	The inclusion of the crack face pressure term is an improvement over past COD methodologies. Prior methodologies applied moment and tension loads concurrently. Applying bending loads

Assumptions	Implications
internal pipe pressure and applied as a constant pressure on the crack faces at 0.5 times the internal pressure. Moments are applied subsequent to axial loads in analyses.	subsequent to tensile loads is thought to be more representative of actual plant behavior. Thermal Hydraulic condition through the pipe wall is complex and unknown, thus, the simplified assumption of an average value was made. This assumption then leads to the effect of 0.5 times the internal pressure being the crack face pressure. Overall the addition of crack face pressure is a small influence on COD. Experiments should be considered to understand this effect better.
It is assumed that in the AxCOD module, sthe only driving froce is from contributions from pressure and weld residual stress loadings. It is also assumed that weld residual stress contribution can be accounted for through an effective pressure term.	It is known that weld residual stresses can change COD from opening to pinched shut. Inclusion of a weld residual stress term, however simplistic, is viewed as an improvement over not including this effect. Future efforts to develop a more technically, rigorous approach may be warranted.
It is assumed that pressure can be limited to 60 percent of the pressure at the limit load for AxCOD calculations.	If the pressure is beyond to 60 percent of the limit pressure, the pressure loading is beyond credible.
It is assumed that the efffort to calculate COD at the inside surface (ID), mid-thickness, and outside surface (OD) is valuable. (Prior versions of COD only calculated a single value for COD.)	Crack faces tend to rotate due to bending loads so CrCOD should result in a better prediction of the crack opening as input to leak rate calculations. Leak rate calculations have inputs for all three locations through the pipe wall thickness.
CrCOD analysis assumes that the ends of the pipe are free to rotate. Effects of restraint of pressure induced bending and system stiffness are not included in any version of CrCOD.	The loads applied to the finite element model used during the development of the CrCOD module were combined pressure and bending. The boundary conditions assume that the pipe is not restrained at the ends, i.e., the ends were free to rotate. However, pipe segments in piping systems are, indeed, restrained. Assuming free rotations introduces an induced bending moment equal to the axial force due to the internal pipe pressure times the eccentricity between the neutral axis of the cracked pipe section and the centerline of the pipe. It has been demonstrated in past studies [36, 39] that this restraint of pressure induced bending due to the rest of the piping system results in a reduction in COD when compared with analyses for which free end boundary conditions are assumed. These overestimations comprise one of the major uncertainties in an LBB analysis, as it leads to an under-prediction of the leakage-size-crack length of a postulated leaking TWC for a prescribed leakage detection limit in a plant, and thus, results in a non-conservative estimation of the crack

Assumptions	Implications
	stability from an LBB perspective. However, it leads to a conservative assumption when discussing applied stress intensity factors. It is judged that this phenomenon has one of the largest effects on uncertainty in xLPR in general. Studies should be undertaken to examine plant models and experiments that incorporate and quantify this effect.
It is assumed that the effect of weld residual stresses on COD in CrCOD cannot be handled within the context of the very general xLPR treatment of WRS. Accordingly, CrCOD is a very simple model that captures only first-order effects.	The effect of weld residual stress on COD is quite variable, ranging from causing additional COD to pinching flow off altogether. The driver for this is the specific WRS profile, pipe/weld geometry and subsequent TWC, and the only way to capture all of the inherent xLPR analysis input possibilities is to perform case-specific finite element analyses. This would be time/cost prohibitive because an FE analysis of the type needed would take days per run. As a consequence, CrCOD has been desgined to only capture the effects of applied load on COD, ignoring WRS. Work has been conducted to show a simplified model using a restrained plate solution to estimate the effect of WRS on COD might be able to be adapted to the current CrCOD results; however, this model was judged “too late” to be incorporated into xLPR v2.0. It is judged that this has a large effect on COD uncertainty in xLPR.
COD is calculated at the crack centerline assuming an idealized flaw shape. Framework must assume an appropriate crack shape, i.e., elliptical, rectangular, or diamond for leak rate calculations.	The choice of crack shape will affect crack opening area and thus the resultant leak rate. Sensitivity studies should be performed to understand which geometry (if any) drives calculated leak/leak detection probabilities.
An empirical correction term (f_4 = 1.15) was applied to the CrCOD solutions so that the solutions would agree better with a limited data set of experiments used to access the accuracy of the model during the development process. The assumption was made that this factor is suitable for any xLPR analysis case.	The data set that can be used to validate CrCOD is limited. A subset of the data was used to find f_4 = 1.15 to make the model agree with the experimental data the best. Subsequent application of CrCOD to a larger set of comparisons in the validation testing has shown that f_4 = 1.15 is a reasonable choice, although some selected COD predictions can be off by more that a factor of two larger or smaller than the experiments. The impact is very case-specific.
The COD modules assume a planar through-wall crack. With this assumption, the cracks are an idealized representation of PWSCC cracks. Actual PWSCC cracks are not planar and do not have a simple leak path for through-wall cracks. Thus, for a given leak rate, a PWSCC crack system would be more diffuse than a planar crack	The effect of this assumption is to over-predict both crack opening displacement and the subsequently calculated leak rate but at present there is no available data for quantification of this over prediction. It is judged that this has a large effect on COD uncertainty in xLPR.

Assumptions	Implications
system. PWSCC cracks are characterized by a distributed, connected network of cracks in 3D rather than a single, idealized 2D planar crack. A model for COD of diffuse and connected (i.e. flow through porous media) set of cracks is very different from the ideal crack case used in xLPR 2.0.	

7. SUMMARY

Modules for predicting the crack-opening displacements (COD) of both circumferential (CrCOD) and axial (AxCOD) cracks in pipes have been developed as part of xLPR Version 2.0. Both models are formulated using the same approach as the prior GE/EPRI solutions, where the total COD is the summation of the elastic and plastic contributions to COD. As was the case for the GE/EPRI solutions, elastic (V_1) and plastic (h_2) influence functions have been developed, based on FEA. Whereas the original GE/EPRI solutions were developed using shell elements, the new solutions developed as part of Version 2.0 are based on more rigorous 3-D continuum brick elements. Furthermore, only a single value of COD to be applied uniformly across the pipe wall thickness was obtained from the original GE/EPRI COD solutions, whereas the new Version 2.0 models output COD values at three locations across the pipe wall thickness, i.e., at the ID surface, at the mid-thickness location, and at the OD surface. In addition, the design space for the new Version 2.0 model has been greatly expanded when compared with the original GE/EPRI solutions:

- GE/EPRI does not have an axial crack solution
- Solutions are available for R_m/t ratios of 2 to 20 for the Version 2.0 model, whereas the original GE/EPRI solutions were only available for R_m/t ratios of 10 to 20
- For the circumferential crack case, the normalized crack lengths (θ/π) considered is now up to 0.9, whereas previously the limit on the normalized crack length was only 0.5.

Verification of the CrCOD and AxCOD models, as documented in the CrCOD STRR [26] and AxCOD STRR [27] have shown that all of the requirements specified in the CrCOD SRD [1] and AxCOD SRD [2] have been satisfied, except those that pertain to the xLPR Framework and will be addressed as part of its verification testing. .

Validation of the CrCOD model through comparison with full-scale pipe fracture experimental data, as documented in the CrCOD MVR [28], has shown that the CrCOD model does a very credible job of predicting the COD for circumferentially oriented through-wall cracks under both bending and combined pressure and bending loading conditions. Overall, when the results from all of the experiments are considered, the CrCOD model overpredicts the experimental COD by about 23 percent, i.e., average ratio of the predicted COD to the experimental COD is 1.23 with a standard deviation of 0.75. Part of this uncertainty can be attributed to analyzing dynamic, cyclic experiments with quasi-static, monotonic stress-strain data. If the dynamic, cyclic experiments are eliminated from the validation matrix or dynamic and/or cyclic stress-strain data are used to analyze these dynamic and/or cyclic loaded pipe experiments, then the agreement between predictions and experimental data improves somewhat.

Validation of the AxCOD model against FE analysis is documented in the MVR for the AxCOD model [29]. As documented in this MVR, the comparison of the analytically predicted COD values agrees quite well with the COD values extracted from non-linear FEA. In addition, it was shown that the elastic (V_1) and plastic (h_2) influence functions, determined as part of the AxCOD development process, compare favorably with the values reported previously in the literature by Kim *et al.* [22]. Finally, it is important to note that the underlying technical basis and model methodology for AxCOD are identical to the underlying technical basis and underlying methodology for the companion circumferential through-wall crack COD module, CrCOD. From

an engineering perspective, it can be argued that AxCOD should show similar agreement to measured behavior as CrCOD does, because they are rooted in an identical analytical approach.

Without question, the largest consideration in the overall scope of the CrCOD modules is that they are a very simplified abstraction of the COD behavior of an actual leaking PWSCC crack. PWSCC, at some level, can be imagined as 3D distributed damage with leak behavior resembling flow through a porous media. CrCOD and AxCOD, on the other hand, assume that the crack is planar with two continuous and mostly parallel faces. For CrCOD and AxCOD, application of greater driving loads always causes the crack faces to rotate and to open and this, consequently, leads to greater leak rates. For real PWSCC, one can only imagine that the volume of open space changes under increasing load, but it is not obvious that the leak rate will, necessarily increase. Accordingly, CrCOD and AxCOD can only be viewed as being crude approximations of PWSCC crack opening behavior.

The general sense is that CrCOD and AxCOD will overestimate the COD of a real PWSCC crack and this will make subsequent leak detection much easier because the leak rate is overestimated. From a regulatory perspective, this is non-conservative because it suggests that cracking will be detected when cracks are small. To offset this, the COD from CrCOD and AxCOD could be scaled down. The difficulty with this is that the appropriate scaling factor is unknown without conducting complex tests. Sensitivity studies could be performed to see the effect of a much reduced COD on leak and rupture probabilities, but the value of doing this can only be realized by "doing something" with the crack stability modules: They too assume that the cracks are planar with two continuous and mostly parallel faces.

As a final comment, within the bounds of the continuous and mostly parallel face crack geometry assumption, CrCOD and AxCOD do quite a good job of capturing very complex behavior in simple engineering models. As one moves to more realistic conditions such as, crack growth out of plane, restraint of pressure-induced bending effects, and PWSCC cracks, the models are being used beyond, and sometimes well beyond their regions of validity.

8. REFERENCES

1. xLPR SRD COD, xLPR Software Requirements Description for Circumferential Through-Wall Crack Combined Tension and Bending COD, Version 3.0, October 2014.

2. xLPR-SRD-AxCOD, xLPR Software Requirements Description for Axial Through-Wall Crack Crack Opening Displacement Module, Version 2.0, June 2014.

3. B. A. Young, R. Olson, and M. Kerr, "Advances in COD Modeling: Circumferential Through-Wall Cracks", ASME International, PVP 2012, PVP2012-78181, Toronto, ON, Canada, July 2012.

4. B. A. Young, R.J. Olson, and P. M. Scott, "Advances in COD Modeling – Multiple Loading Modes: Concurrent Axial and Crack Face Pressure with a Subsequent Applied Bending Moment," abstract submitted for publication, Structural Mechanics in Reactor Technology (SMiRT) 22, San Francisco, CA, August 2013.

5. A. Cox, B. A. Young, and P.M. Scott, "Advances in COD Modeling: Validation of an Analytical Model to Experimental Results," abstract submitted for publication, Structural Mechanics in Reactor Technology (SMiRT) 22, San Francisco, CA, August 2013.

6. Paul T. Williams and Hilda B. Klasky (2010), Recommended Programming Practices for the xLPR Pilot Project.

7. xLPR-SDD-CrCOD, xLPR Software Design Description for the Circumferential Through-Wall Crack Combined Tension and Bending COD Module, Version 2.0, October 2014.

8. xLPR-SDD-AxCOD, xLPR Software Design Description for the Axial Through-Wall Crack Crack Opening Displacement Module, Version 1.0, June 2014.

9. xLPR MODELS Crack Opening Displacement Models Subgroup Work Plan Rev. 2, xLPR Crack Opening Displacement Models Subgroup, December 31, 2012.

10. Kumar, V. and German, M. D., "Elastic-Plastic Fracture Analysis of Through-Wall and Surface Flaws in Cylinders," EPRI Report NP-5596, Research Project 1237-5, January 1988.

11. Rudland, D.L., Wang, Y. Y., and Wilkowski, "Comparison of crack-opening predictions for LBB applications," International Journal of Pressure Vessels and Piping, Vol. 79 (2002), pp. 209-217.

12. Martin, M., Watson, C., and Wright, K., "Review of ASME III Code Case for the Application of Finite Element Based Limit Load Analysis", PVP2011-57138, ASME PVP Conference, July 17-21, 2011, Baltimore, MD.

13. ABAQUS/Answers, "Answers to Common ABAQUS Questions," Summer 1999.

14. Kanninen, M. F. and Popelar, C. H., "Advanced Fracture Mechanics," Oxford University Press, New York, NY, pp. 299-312, 1985.

15. Anderson, T. L., “Fracture Mechanics Fundamentals and Applications,” 3rd Edition, CRC Press, pp. 111-113, 2005.

16. Private discussion between F. W. Brust of Engineering Mechanics Corporation of Columbus and B. A. Young of Battelle Memorial Institute, December 2011.

17. D. Rudland and C. Harrington, xLPR Pilot Study Report, NUREG-2110, U.S. Nuclear Regulatory Commission, Rockville, MD, May 2012 (Adams accession no. ML12145A470).

18. Rahman, S. et al., “Crack-opening-area analyses for circumferential through-wall cracks in pipes Part I: analytical models,” International Journal of Pressure Vessels and Piping, Vol 75 (1998), pp. 357-373.

19. Wilkowski, G. M., and others, “Short Cracks in Piping and Piping Welds,” NUREG/CR-4599 Vol. 4, No. 1, January 1995.

20. Kim, Y. -J., Huh, N. -S., and Y. -J. Kim, "Enhanced reference stress-based J and crack opening displacement estimation method for leak-before-break analysis and comparison with GE/EPRI method", Fatigue and Fracture of Engineering Materials and Structures, Volume 24, pp. 243-254, 2001.

21. Kim, Y. J. and others, "Reference stress based elastic-plastic fracture analyses for circumferential through-wall cracked pipes under combined tension and bending," Engineering Fracture Mechanics, Volume 69, pp 367-388, 2002.

22. Y.-J Kim, N.-S Huh, Y.-J. Park, and Y.-J. Kim, “Elastic-Plastic J and COD Estimates for Axial Through-Wall Cracked Pipes,” International Journal of Pressure Vessels and Piping, 79, pp. 451-464, 2002.

23. “Structural Integrity Assessment Procedures for European Industry: SINTAP, Final Report,” July 1999, Report No. BE95-1426/FR/7.

24. xLPR-STP-CrCOD, xLPR Software Test Plan for the Circumferential Through-Wall Crack Combined Tension and Bending COD Module, Version 1.0, October 2014.

25. xLPR-STP-AxCOD, xLPR Software Test Plan for the Axial Through-Wall Crack Crack Opening Displacement Module, Version 1.0, June 2014.

26. xLPR-STRR-CrCOD, xLPR Software Test Results Report for CrCOD Module, Version 1.0, October 2014.

27. xLPR-STRR-AxCOD, xLPR Software Test Results Report for AxCOD Module, Version 1.0, October 2014.

28. xLPR-MVR-CrCOD, xLPR Module Validation Report for Circumferential Through-Wall Crack Combined Tension and Bending COD Module (CrCOD). Version 1.0, November 2014

29. xLPR-MVR-AxCOD, xLPR Module Validation Report for Axial Crack COD Model (AxCOD), Version 1.0, November

30. Beyond Compare 3, Scooter Software, http://www.scootersoftware.com

31. G. D. Fearnehough and B. Watkins, “Application of the Crack Opening Displacement Approach to the Prediction of Pressurized Tube Failure,” Int. J. Fracture Mechanics, Vol. 4, No. 3, September 1968, 233-243.

32. M. L. Benson, B. A. Young, D.-J. Shim, and F. W. Brust, “Crack Opening Displacement Model for Through-Wall Axial Cracks in Cylinders,” PVP2013-98008, Proceedings of the 2013 ASME Pressure Vessels and Piping Conference, July 14-18, 2013, Paris, France.

33. Kumar, V., German, M., and Shih, C., “An Engineering Approach for Elastic-Plastic Fracture Analysis,” EPRI Report No. NP-1931, July 1981.

34. Kumar, V., German, M., Wilkening, Andrews, W., deLorenzi, H., and Mowbray, D., “Advances in Elastic-Plastic Analysis, ” EPRI Final Report NP-3607, August 1984.

35. Ghadiali, N., Rahman, S., Choi, Y., and Wilkowski, G., “Deterministic and Probabilistic Evaluations for Uncertainty in Pipe Fracture Parameters in Leak-Before-Break and In-Service Flaw Evaluations,” NUREG/CR-6443, June 1996.

36. Scott, P., and others, “The Battelle Integrity of Nuclear Piping (BINP) Program Final Report,” NUREG/CR-6837, Vols. 1 and 2, June 2005.

37. Rahman, S. et al., “Crack-opening-area analyses for circumferential through-wall cracks in pipes – Part II: model validations,” International Journal of Pressure Vessels and Piping, Vol 75 (1998), pp. 375-396.

38. Rahman, S. et al., “Crack-opening-area analyses for circumferential through-wall cracks in pipes – Part III: off-center cracks, restraint of bending, thickness transitions and weld residual stresses,” International Journal of Pressure Vessels and Piping, Vol. 79 (2002), pp. 209-217.

39. Ghadiali, N., and others, “Deterministic and Probabilistic Evaluations for Uncertainty in Pipe Fracture Parameters in Leak-Before-Break and In-Service Flaw Evaluations,” NUREG/CR-6443, June 1996.